creative commons

COMMONS DEED

저작자표시-비영리-변경금지 2.0 대한민국

이용자는 아래의 조건을 따르는 경우에 한하여 자유롭게

- 이 저작물을 복제, 배포, 전송, 전시, 공연 및 방송할 수 있습니다.

다음과 같은 조건을 따라야 합니다:

저작자표시. 귀하는 원저작자를 표시하여야 합니다.

비영리. 귀하는 이 저작물을 영리 목적으로 이용할 수 없습니다.

변경금지. 귀하는 이 저작물을 개작, 변형 또는 가공할 수 없습니다.

- 귀하는, 이 저작물의 재이용이나 배포의 경우, 이 저작물에 적용된 이용허락조건을 명확하게 나타내어야 합니다.
- 저작권자로부터 별도의 허가를 받으면 이러한 조건들은 적용되지 않습니다.

저작권법에 따른 이용자의 권리는 위의 내용에 의하여 영향을 받지 않습니다.

이것은 이용허락규약(Legal Code)을 이해하기 쉽게 요약한 것입니다.

Disclaimer

dCollection

Master's Thesis

Numerical Studies of Self-Modulation Instability in the Beam-Driven Plasma Wakefield Experiments

Kook-Jin Moon

Department of Physics

Graduate School of UNIST

2017

ULSAN NATIONAL INSTITUTE OF SCIENCE AND TECHNOLOGY

Numerical Studies of Self-Modulation Instability in the Beam-Driven Plasma Wakefield Experiments

Kook-Jin Moon

Department of Physics

Graduate School of UNIST

ULSAN NATIONAL INSTITUTE OF SCIENCE AND TECHNOLOGY

Numerical Studies of Self-Modulation Instability in the Beam-Driven Plasma Wakefield Experiments

A thesis submitted to
the Graduate School of UNIST
in partial fulfillment of the
requirements for the degree of
Master of Science

Kook-Jin Moon

1. 19. 2017 of submission
Approved by

Advisor
Moses Chung

ULSAN NATIONAL INSTITUTE OF SCIENCE AND TECHNOLOGY

Numerical Studies of Self-Modulation Instability in the Beam-Driven Plasma Wakefield Experiments

Kook-Jin Moon

This certifies that the thesis of Kook-Jin Moon is approved.

1/19/2017

signature

Advisor: Moses Chung

signature

typed name: Hae-June Lee

signature

typed name: Min-Sup Hur

ULSAN NATIONAL INSTITUTE OF SCIENCE AND TECHNOLOGY

Abstract

The plasma wakefield accelerator is one of promising and advanced particle accelerator models. It can make particle accelerator more compact and cheaper. A beam bunch propagating through plasma excites the plasma wakefield at some conditions. The optimum wake is obtained for $k_p\sigma_z = 2^{\frac{1}{2}}$ and $k_p\sigma_r \leq 1$. Where k_p is plasma wave number and σ_z (or σ_r) is RMS beam length (or RMS beam radius). But we are interested in using CERN's long and high-energy proton beams. The CERN's proton beams are much longer (~ 12 cm) than the optimum driving beam length (in order of plasma wavelength λ_p). Here we focus on the instability which occurs based on the interaction between beam and plasma electrons. By this instability, the long driving beam is modulated along the propagation direction, so it makes the beam satisfy the optimum size for excitation of plasma waves. What we should know is that the plasma oscillation which is initially and axi-symmetrically excited by beam head will seed self-modulation of driving beam. Therefore, we first study fundamental theories of excitation of plasma waves by the charged particle beam. It's about the response of plasma electrons to driving beam. The driving beam doesn't interact with and only affects plasma. Here excited plasma wakefields should be considered. As the next step, the dynamics of plasma wakefield accelerator is introduced. Evolution of beam envelope in time could result in beam centroid offset or radius pinching. Where the two phenomena, centroid offset and radius pinching of the beam in plasma are called 'Self-modulation instability' and 'Hose instability'. Those two instabilities compete each other. As the last step, the parameters of Injector Test Facility (ITF) at Pohang Accelerator Laboratory (PAL) is used to demonstrate the self-modulation instability.

ULSAN NATIONAL INSTITUTE OF SCIENCE AND TECHNOLOGY

Contents

1. Introduction

1.1 Interaction of a relativistic electron bunch with a Plasma ---------- 2

1.2 Beam-plasma instabilities ---------- 4

2. Particle-In-Cell Method

2.1 Electrostatics and electromagnetics ---------- 5

2.2 Computational cycles for Particle-In-Cell simulations ---------- 6

2.3 Staggering in time and space ---------- 8

2.4 Difference equations ---------- 10

3. Plasma Wakefields of a Short Beam Bunch in Plasmas

3.1 Energy transfer in co-linear wakefield accelerator ---------- 16

3.2 Blowing-out and sucking in of plasma electrons by the charged particle bunch's field ------ 17

3.3 Nonlinear one dimensional relativistic plasma ---------- 22

3.4 Simulations of a short beam-driven plasma wakefields using WARP ---------- 26

4. Self-Modulation Instability of a Long Beam Bunch in Plasmas

4.1 Analytical approach on the beam-envelope equation ---------- 29

4.2 Numerical solution of beam envelope equation ---------- 32

4.3 Coupled beam hose and self-modulation instabilities and their growth rates ---------- 34

4.4 Transverse equilibrium and stability of the primary beam in plasma ---------- 36

4.5 Simulations of a long beam-driven plasma wakefields using WARP ---------- 37

5. Summary and Future Works ---------- 43

6. Appendix

6.1 Fundamental equations ---------- 44

6.2 Derivation and solving of differential equations from the body ---------- 45

6.3 Script of WARP for plasma wakefield acceleration---------- 56

7. References ---------- 64

ULSAN NATIONAL INSTITUTE OF SCIENCE AND TECHNOLOGY

List of Figures

Fig. 1.1. A short electron beam which propagates in plasma wakes the plasma waves. Here the excited plasma waves have no group velocity and their amplitudes are very small. The density variation of plasma electron is quite exaggerated to provide a simple picture of the beam-driven plasma wakefield concept. ---------- 2

Fig. 2.1. After loading charged particles, charge and current depositions should be interpolated. Then from Gauss's law, electric potential and field can be calculated. Before the step for integrating equation of motion of particles, fields which are calculated on grids around the particles should be interpolated. Once integrating the equation of motion of particles, updated charge depositions are calculated. Same steps are repeated. ---------- 6

Fig. 2.2. After loading charged particles, charge and current depositions should be interpolated. And next, electromagnetic fields in recent time can be calculated updating two fields of coupled differential equations in time. Before the step for integrating equation of motion of particles, fields which are calculated on grids around the particles should be interpolated. Once integrating the equation of motion of particles, updated charge and current depositions are calculated. Same steps are repeated. ---------- 7

Fig. 2.3. Staggering in time between momentum and position, current and charge, and magnetic and electric fields are depicted. Each field is on the same time step with its source. But each of electric and magnetic fields alternate with each other in time. Magnetic field is on the half integer of upper index 'n', whereas electric field is on the integer of upper index 'n'. ---------- 8

Fig. 2.4. Staggering in space of rectangular coordinates between current and charge and magnetic and electric fields are depicted. The Yee grid is proper for calculating $\nabla\times$. ---------- 9

Fig. 2.5. Scheme of 2-dimensional linear weighting. The s'th particle is at (x_s, y_s), $i\Delta x \le x_s \le (i+1)\Delta x$, $j\Delta y \le y_s \le (j+1)\Delta y$. The specific position of the particle is expressed by $x_s = (i+\delta_x)\Delta x$ and $y_s = (j+\delta_y)\Delta y$ (note that $0 \le \delta_x \le 1$ and $0 \le \delta_y \le 1$). ---------- 11

Fig. 3.1. The electric fields induced by disc-shaped electron beam within $r < a$ are plotted. The relative coordinate of driving beam position $y = v_b t - z$ increases in opposite direction of beam propagation. Note that there exist phase differences between plasma response and wakefields. ---------- 21

Fig. 3.2. The normalized velocity of plasma electron at the end of the driving beam (the second turning point of $x(\tau)$ $[x'(\tau) = 0]$. At $\alpha = 1/2$, β reaches -1. In the region where it is not satisfied that $|\beta| \ll 1$ or $|\alpha| \ll 1$, the system has nonlinearity. It is the reason that we should have investigated the nonlinearity of the plasma oscillation. The region which is enough to be linearized would be within $|\alpha| \ll 1$. ---------- 24

ULSAN NATIONAL INSTITUTE OF SCIENCE AND TECHNOLOGY

Fig. 3.3. Inhomogeneous solution at $\alpha = 1/2$. Each of (a) $eE_0/mc\omega_p$ and (b) n_1/n_0 asymptotically reaches -1 and -0.5. It lasts until the end of the beam, i.e., $\alpha = 0$. The pictures behind the beam are listed in Refs. [2] and [6], but it is not our interest. ---------- 25

Fig. 3.4. Plasma wakefield driven by a short electron beam at $n_b/n_0 \ll 1$. (a) Longitudinal component of wakefield has trigonometric-like curve along the propagation axis of the beam. (b) By this transverse wakefields, the rear part of the negatively charged driving beam will be focused. ---------- 26

Fig. 3.5. The plasma wakefield driven by a short electron beam at $n_b/n_0 = 0.35$. (a) The longitudinal component of the wakefield has the sawtooth-like curve along the propagation axis of the beam. And the periodicity of the wake is about λ_p. (b), (c) Charge density ρ is depicted. Background plasma electrons are pulled out by repulsive force of the electron beam. Magnitudes of plasma density peaks are very high compared with the equilibrium plasma electron density n_0. ---------- 27

Fig. 3.6. The plasma wakefield driven by a short proton beam at $n_b/n_0 = 0.01$. (a) The longitudinal component of the wakefield has the trigonometric-like curve along the propagation axis of the beam. (b) By this transverse wakefields, the rear part of the positively charged driving beam will be focused. ---------- 28

Fig. 4.1 Dispersion relation of the SMI: (a) For $\mathrm{Im}(\delta\omega) \to \infty$, k has real roots (Curves are symmetric in the second quadrant.). So the instability is convective. (b) In $\sqrt{3} < \delta\omega < 2$, k has complex roots (Curves are symmetric in the four'th quadrant.). Only when k is in the upper half of complex plane, the SMI grows. ------ 31

Fig. 4.2 A brief picture for the numerical study of beam envelope equation: The beam is initially cylinder-shaped and has a uniform beam profile. As time goes, it goes through radius evolution. ---------- 32

Fig. 4.3 The beam radius evolution in time with beam-envelope equation: The time and beam position coordinates are normalized as beam-envelope equation was. The self-modulation instability grows as time goes and in the direction which ξ increases. The beam length is $62.8 \approx 10\times2\pi$ and the number of modulated beam peaks is 10. ---------- 33

Fig. 4.4. The hose instability of smooth electron beam with ATF beam parameters: Here plasma electron density is $n_0 = 4.2e+22\ [m^{-3}]$, beam energy is 58 MeV $(\gamma_0 = 114)$, rms transverse momentum spread is $\sqrt{\langle p_\perp^2\rangle}/m_b c = 8.6\times10^{-3}$, transverse rms beam size is $\sigma_r = 120\ \mu m$, longitudinal rms beam size is $\sigma_z = 960\ \mu m$, beam density profile is $n_b = n_{b0}\left[1+\cos\left(\sqrt{\frac{\pi}{2}}\frac{z+\sigma_z\sqrt{2\pi}}{\sigma_z}\right)\right]e^{-\frac{r^2}{2\sigma_r^2}}$, initial beam density peak is $n_{b0} = 3.6e+18\ [m^{-3}]$, beam length is $L_b = 2\sigma_z\sqrt{2\pi}$, and total beam charge is $Q = 250$ pC. ---------- 37

ULSAN NATIONAL INSTITUTE OF SCIENCE AND TECHNOLOGY

Fig. 4.5. The self-modulation instability of half-cut electron beam with ATF beam parameters: Here plasma electron density is $n_0 = 4.2e + 22\ [m^{-3}]$, beam energy is 58 MeV $(\gamma_0 = 114)$, rms transverse momentum spread is $\sqrt{\langle p_\perp^2 \rangle}/m_b c = 8.6\times10^{-3}$, transverse rms beam size is $\sigma_r = 120\ \mu m$, longitudinal rms beam size is $\sigma_z = 960\ \mu m$, beam density profile is $n_b = n_{b0}\left[1 + \cos\left(\sqrt{\frac{\pi}{2}}\frac{z+\sigma_z\sqrt{2\pi}}{\sigma_z}\right)\right] e^{-\frac{r^2}{2\sigma_r^2}}$, initial beam density peak is $n_{b0} = 3.6e + 18\ [m^{-3}]$, beam length is $L_b = \sigma_z\sqrt{2\pi}$, and total beam charge is $Q = 125$ pC. ---------- 38

Fig. 4.6. The self-modulation instability of half-cut electron beam with ATF beam parameters in varying plasma densities: The number of modulated bunches increases as increasing plasma density. Here plasma electron density is $n_0 = 1.8e + 21\ [m^{-3}] \sim 4.2e + 22\ [m^{-3}]$, $\frac{L_b}{\lambda_{pe}} =$ (a) 3, (b) 6, (c) 9, (d) 12, (e) 15, beam energy is 58 MeV $(\gamma_0 = 114)$, rms transverse momentum spread is $\sqrt{\langle p_\perp^2 \rangle}/m_b c = 8.6\times10^{-3}$, transverse rms beam size is $\sigma_r = 120\ \mu m$, longitudinal rms beam size is $\sigma_z = 960\ \mu m$, beam density profile is $n_b = n_{b0}\left[1 + \cos\left(\sqrt{\frac{\pi}{2}}\frac{z+\sigma_z\sqrt{2\pi}}{\sigma_z}\right)\right] e^{-\frac{r^2}{2\sigma_r^2}}$, initial beam density peak is $n_{b0} = 3.6e + 18\ [m^{-3}]$, beam length is $L_b = \sigma_z\sqrt{2\pi}$, and total beam charge is $Q = 125$ pC. ---------- 39

Fig. 4.7 The self-modulation instability of half-cut proton beam with ATF beam parameters: Here plasma electron density is $n_0 = 4.2e + 22\ [m^{-3}]$, beam energy is 24 GeV $(\gamma_0 = 25)$, rms transverse momentum spread is $\sqrt{\langle p_\perp^2 \rangle}/m_b c = 4.5\times10^{-3}$, transverse rms beam size is $\sigma_r = 120\ \mu m$, longitudinal rms beam size is $\sigma_z = 960\ \mu m$, beam density profile is $n_b = n_{b0}\left[1 + \cos\left(\sqrt{\frac{\pi}{2}}\frac{z+\sigma_z\sqrt{2\pi}}{\sigma_z}\right)\right] e^{-\frac{r^2}{2\sigma_r^2}}$, initial beam density peak is $n_{b0} = 3.6e + 18\ [m^{-3}]$, beam length is $L_b = \sigma_z\sqrt{2\pi}$, and total beam charge is $Q = 125$ pC. ---------- 40

Fig. 4.8. The self-modulation instability of half-cut electron beam with ATF beam parameters: Here plasma electron density is $n_0 = 4.2e + 22\ [m^{-3}]$, beam energy is 58 MeV $(\gamma_0 = 114)$, rms transverse momentum spread is $\sqrt{\langle p_\perp^2 \rangle}/m_b c = 8.6\times10^{-3}$, transverse rms beam size is $\sigma_r = 120\ \mu m$, longitudinal rms beam size is $\sigma_z = 960\ \mu m$, beam density profile is $n_b = n_{b0}\left[1 + \cos\left(\sqrt{\frac{\pi}{2}}\frac{z+\sigma_z\sqrt{2\pi}}{\sigma_z}\right)\right] e^{-\frac{r^2}{2\sigma_r^2}}$, initial beam density peak is $n_{b0} = 3.6e + 18\ [m^{-3}]$, beam length is $L_b = \sigma_z\sqrt{2\pi}$, and total beam charge is $Q = 125$ pC. ---------- 41

Fig. 4.9. The self-modulation instability of half-cut electron beam with ITF beam parameters: Here plasma electron density is $n_0 = 2.5e + 22\ [m^{-3}]$, beam energy is 60 MeV $(\gamma_0 = 114)$, rms transverse momentum spread is $\sqrt{\langle p_\perp^2 \rangle}/m_b c = 2.4\times10^{-3}$, transverse rms beam size is $\sigma_r = 318\ \mu m$, longitudinal rms beam size is $\sigma_z = 637\ \mu m$, beam density profile is $n_b = n_{b0}\left[1 + \cos\left(\sqrt{\frac{\pi}{2}}\frac{z+\sigma_z\sqrt{2\pi}}{\sigma_z}\right)\right] e^{-\frac{r^2}{2\sigma_r^2}}$, initial beam density peak is $n_{b0} = 3.6e + 18\ [m^{-3}]$, beam length is $L_b = \sigma_z\sqrt{2\pi}$, and total beam charge is $Q = 580$ pC. ---------- 42

ULSAN NATIONAL INSTITUTE OF SCIENCE AND TECHNOLOGY

Chapter 1. Introduction: Why Self Modulation Instability?

As particle physics community gets on a step for the new discovery, a teraelectronvolt-scale electron-positron collider (for example, the International Linear Collider) is needed for the next large-scale project for high-energy particle physics. Due to the energy loss by synchrotron radiation it should be built as a one pass linear collider, so it will be huge in machine size (~ 30 km long) and very expensive for construction. In this circumstance, investigating new schemes based on the plasma wakefield acceleration, which would be compact in size, might be one of the promising alternative approaches for the realization of the electron-positron collider [1]. To reach for the new energy frontier of electron acceleration using plasma wakefield accelerator, how parameters of driving beam and plasma should be determined must be discussed.

Since Tajima and Dawson proposed plasma wakefield generation by a short (pulse length $L_p < \lambda_{pe}$) laser pulse for electron acceleration in 1979 [2], various methods and associated theories to excite plasma waves have been proposed and developed by many brilliant researchers. Pisin Chen introduced the interaction of a bunched electron beam with a plasma in 1985 [3]. In this paper, to resonantly excite the plasma waves the driver beam should be shorter than plasma wavelength λ_{pe} [3]. As another important work, R. D. Ruth et al. proposed that for an axisymmetric charged particle beam, the transformer ratio is generally given by $R = E_+/E_- \leq 2 - N_{witness}/N_{drive}$ in 1984 [4]. (Here, E_+ and E_- are the maximum accelerating and decelerating fields induced by the driving beam, and $N_{witness}$ and N_{drive} are the number of witness and driving beam particles, respectively.) From the transformer ratio argument, we would think that to reach for the TeV energy range in a single stage (a few tens of meters long) of the beam-driven plasma acceleration, the TeV proton bunch from the CERN LHC can be used as a driver beam. However, the TeV proton bunch from the SPS (injector for the LHC) would usually be about 12-centimeter long. Based on the previous theoretical works, we note that it is too long to resonantly excite the plasma waves. This is a critical issue to be addressed.

Generating short drivers which are of the order of a plasma wavelength long has been one of the key technical challenges in both laser and charged particle beam communities. Various methods to excite plasma wakefields using long laser pulse or long charged particle beam have been proposed to overcome the technical limits. In this study, we particularly focus on the Self-Modulation Instability (SMI) of a long charged particle beam in plasma. In this chapter, we first review fundamental theories of beam-plasma interactions, which will form the basis of the numerical studies on the SMI given in this study.

ULSAN NATIONAL INSTITUTE OF SCIENCE AND TECHNOLOGY

1.1 Interaction of a relativistic electron bunch with a plasma

The scheme of linearized plasma system makes it possible to determine the frequencies of oscillation and to discuss the part played by temperature effects, which turn out in general to be unimportant, even more so in the study of plasma oscillations in electron beams, where the temperature is practically zero [6]. There could be numerous ways of basic interpretation of the excitation of plasma waves by a charged particle beam though, in this study we introduce two well-known methods. The first method is from the paper of Pisin Chen (1985) [2]. Another one will be covered in Chapter 3.

We first consider that a negatively charged relativistic particle beam with $\beta_0 = v_b/c \lesssim 1$ goes through a cold, uniform plasma along the z axis. The beam is assumed to be a bunch of q electrons, and thus the total beam charge is $Q = qe$. Here, the beam is treated as a single particle with the magnitude of charge $Q = qe$. To describe the small amplitudes and nonrelativistic plasma oscillations, we use linearized equations, such as equation of motion and continuity equation for the cold, non-relativistic background plasma. All the equations of electromagnetism which are used in this study are expressed in the Gaussian unit.

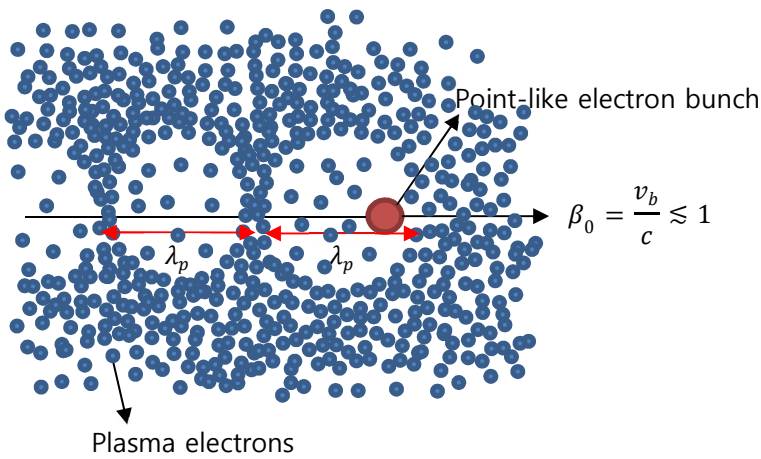

Fig. 1.1. A short electron beam which propagates in plasma wakes the plasma waves. Here the excited plasma waves have no group velocity and their amplitudes are very small. The density variation of plasma electron is quite exaggerated to provide a simple picture of the beam-driven plasma wakefield concept.

$$\frac{\partial n_p}{\partial t} + \nabla \cdot (n_p \mathbf{v}_p) = \frac{\partial (n_{p0} + n_{p1})}{\partial t} + \nabla \cdot \left((n_{p0} + n_{p1})(\mathbf{v}_{p0} + \mathbf{v}_{p1}) \right),$$
$$\frac{\partial n_{p1}}{\partial t} + n_{p0} \nabla \cdot \mathbf{v}_{p1} = 0, \tag{1.1}$$

$$\frac{d\mathbf{v}_p}{dt} = \frac{\partial \mathbf{v}_p}{\partial t} + (\mathbf{v}_p \cdot \nabla)\mathbf{v}_p = -\frac{e}{m}\left((\mathbf{E}_{p1} + \mathbf{E}_{b1}) + (\mathbf{v}_{p0} + \mathbf{v}_{p1}) \times (\mathbf{B}_0 + \mathbf{B}_1) \right),$$
$$\frac{\partial \mathbf{v}_{p1}}{\partial t} \simeq -\frac{e}{m}(\mathbf{E}_{p1} + \mathbf{E}_{b1}) = -\frac{e}{m}\mathbf{E}_1. \tag{1.2}$$

ULSAN NATIONAL INSTITUTE OF SCIENCE AND TECHNOLOGY

Here, n_{p0} is the background plasma electron density $(\partial n_{p0}/\partial t = 0)$ and n_{p1} is the density perturbed by the driving beam $(n_{p0} \gg n_{p1})$. The elementary charge is defined by $e \equiv |e| = 1.602\times10^{-19}$ C. Note that the definition of the elementary charge 'e'. It could be defined in a little different way that $e \equiv -|e| = -1.602\times 10^{-19}$ C. Originally plasma has no net flow and external magnetic field is zero $(\mathbf{v}_{p0} = \mathbf{B}_0 = 0)$. We only kept linear terms. For the driving-electron bunch, the charge and current densities are

$$\text{Net charge density,} \qquad \rho(\mathbf{x}) = -en_{p1}(\mathbf{x}) - Q\delta(\mathbf{x} - \mathbf{x}_0), \tag{1.3}$$

$$\text{Net current density,} \qquad \mathbf{j}_1(\mathbf{x}) = -en_{p0}\mathbf{v}_{p1}(\mathbf{x}) - Q\mathbf{v}_b\delta(\mathbf{x} - \mathbf{x}_0). \tag{1.4}$$

Here $\mathbf{x} = \rho\mathbf{e}_1 + z\mathbf{e}_3$ in cylindrical coordinates and $\mathbf{x}_0$ is position of the bunch. Each density contains both contributions from the plasma and the driving beam. As remarked above, in this study we will discuss the features of the plasma wave for being used as the ion cavity accelerating charged particles. Because the electric field is calculated from magnetic vector potential $\mathbf{A}$ and electric potential V as

$$\mathbf{E}_1 = -\frac{1}{c}\frac{\partial \mathbf{A}_1}{\partial t} - \nabla V_1, \tag{1.5}$$

we will derive two differential equations for obtaining $\mathbf{A}$ and V induced by plasma wave. Here we define ζ as relative coordinate from the driving beam position.

$$\zeta \equiv z - v_b t \leq 0. \tag{1.6}$$

Applying chain rule on ζ and assuming $\beta_0 \approx 1$, we get the interaction formula between longitudinal electric field and two types of potentials.

$$\begin{gathered} \partial_z = \partial_\zeta \partial_z \zeta = \partial_\zeta, \\ \partial_t = \partial_\zeta \partial_t \zeta = -v_b \partial_\zeta, \\ [\mathbf{E}_1]_z = -\left[\frac{1}{c}\frac{\partial \mathbf{A}_1}{\partial t} + \nabla V_1\right]_z = \beta_0 \partial_\zeta A_{1z} - \partial_\zeta V_1 \simeq \partial_\zeta(A_{1z} - V_1). \end{gathered} \tag{1.7}$$

We should obtain the solutions of Poisson equation and inhomogeneous wave equation for the magnetic vector potential.

$$\nabla^2 V_1 = -4\pi\rho_1, \tag{1.8}$$

$$\nabla_\perp^2 \mathbf{A}_1 - \frac{1}{c^2}\frac{\partial^2 \mathbf{A}_1}{\partial t^2} = -\frac{4\pi}{c}\mathbf{j}_1 - \frac{1}{c}\nabla\frac{\partial V_1}{\partial t}. \tag{1.9}$$

ULSAN NATIONAL INSTITUTE OF SCIENCE AND TECHNOLOGY

Here because the relativistic factor γ_0 is approximately constant, the second term of the left hand side in Eq. (1.9) is removed. Then now we can derive two differential equations and obtain two solutions of them. (see Appendix. 1)

$$\left(\partial_\zeta^2 + k_p^2\right)V_1 = -Q\,\partial_\zeta^2\left(\frac{1}{|\mathbf{x}-\mathbf{x}_0|}\right), \tag{1.10}$$

$$V_1(\zeta) = -\frac{2\pi Q}{\lambda_p}\left\{\frac{1}{k_p|\zeta|} + k_p\int_\zeta^\infty d\zeta'\,\frac{\sin k_p(\zeta'-\zeta)}{k_p|\zeta'|}\right\}, \tag{1.11}$$

$$\left(\nabla_\perp^2 - \beta_0^2 k_p^2\right)A_{1z} = -\beta_0 Q\nabla_\perp^2\left(\frac{1}{|\mathbf{x}-\mathbf{x}_0|}\right), \tag{1.12}$$

$$A_{1z}(\zeta) = -\frac{2\pi Q}{\lambda_p}\beta_0^2\int_0^\infty d\rho' K_1(\beta_0 k_p \rho')\frac{\rho'}{[\rho'^2+\zeta^2]^{\frac{3}{2}}}. \tag{1.13}$$

Here, $\lambda_p = 2\pi/k_p$. The maxima of E_{1z} are at $|\zeta| = \left(n+\frac{1}{2}\right)\lambda_p$, where n is any nonnegative integer, and the contribution to the maximum E_{1z} comes predominantly from the scalar potential. This treatment ignores nonlinear plasma effects and self-consistency effects that act to slow the driving bunches. It is only valid **i)** if the electric field does not approach the cold wave-breaking amplitude, and **ii)** if the electric energy is small compared to the free energy of the driving bunches. The first condition provides an upper limit on the maximum allowed energy gradient, i.e., maximum $\varepsilon \simeq (n_{p0})^{\frac{1}{2}}$ eV/cm $\simeq 3.2$ GeV/m. The second condition requires that $(E_{1z}^2/8\pi)L < q\gamma_0 mc^2/A$, where L is the length of the beam plasma interaction region and A is the beam area. ||

1.2 Beam-plasma instabilities

The bunch transverse dimensions must be on the order of, or smaller than the cold plasma collisionless skin depth ($\sigma_r \approx c/\omega_p$) to avoid transverse bunch filamentation. In this case, the relation between the primary beam and plasma becomes

$$\sigma_r \approx \frac{c}{\omega_p} = c\sqrt{\frac{m_e\varepsilon_0}{n_0 e^2}} \propto n_0^{-\frac{1}{2}}. \tag{1.14}$$

The hose instability (HI) can occur in the limit, $\sigma_z > \lambda_p$. We consider the electron beam in an equilibrium state where the plasma electrons have been expelled from the region of the beam by the beam space charge. When the beam suffers a small transverse displacement, the plasma electrons at $r = r_n$ are also displaced in such a way that the interaction is unstable. It makes the driving beam twisted (or go wrong). Based on the similar physics, transverse two-stream instability (TTSI) can occur. When the beam envelope symmetrically evolves by the transverse wakefields induced by the beam head in the collisionless ($n_b \ll n_0$) region, it is called self-modulation instability (SMI). Analytical approaches of the self-modulation instability and hose instability are given at Chapter 4.

ULSAN NATIONAL INSTITUTE OF SCIENCE AND TECHNOLOGY

Chapter 2. Particle-In-Cell (PIC) Method

This work is based on the computer simulation. Especially Particle-In-cell (PIC) code WARP [17] is used to demonstrate the physics process in the charged particle beam and plasma system. In this chapter, fundamental concepts of the PIC method are briefly explained.

2.1 Electrostatics and Electromagnetics

The physical system we will study could be electrostatic or electromagnetic. The differences of the two limits are explained here. For the electrostatics,

$$\frac{\partial \mathbf{B}}{\partial t} \approx 0, \tag{2.1}$$

$$\nabla \cdot \mathbf{E} = 4\pi\rho. \tag{2.2}$$

Magnetic fields vary slowly and only external magnetic fields are considered. Thus, self-induced magnetic fields are neglected. Fast evolutions such as radiation, retardation and beam envelope evolution effects are also neglected. The particles are slow compared to c. The fields change adiabatically and depend only on the instantaneous positions of the particles. This system is considerably simplified and requires only two equations to get the solution of the problem. But for the electromagnetics, we need

$$\nabla \times \mathbf{E} = -\frac{1}{c}\frac{\partial \mathbf{B}}{\partial t}, \tag{2.3}$$

$$\nabla \times \mathbf{B} = \frac{4\pi}{c}\mathbf{J} + \frac{1}{c}\frac{\partial \mathbf{E}}{\partial t}. \tag{2.4}$$

The four Maxwell's equations are fully satisfied, but only the above two equations are enough to get the solution of the system. Above two equations already satisfy other two equations with continuity equation. This system self-consistently includes magnetic fields generated by the beams or plasmas and supports fast evolution of fields, radiation, retardation and beam envelope evolution effects. The particles move close to c and accelerate abruptly. So, the fields depend on the history of the particles, which means that the radiation effects should be considered. We are interested in the evolution of beam envelope in plasma. Therefore, the limit we are interested in is in electromagnetics.

2.2 Computational cycles for Particle-In-Cell simulations

The Particle-In-Cell method is one of the first principle methods. The fundamental theories of electrodynamics are used. Basically, PIC simulation repeatedly calculates the specific computational cycles. The loops are listed below for the two cases of electrostatics and electromagnetics.

The PIC loop in electrostatics

For the PIC loop in electrostatics, only position of particle is used to obtain the source ρ. So, only electric field is calculated during the simulation steps. Magnetic field exists only externally.

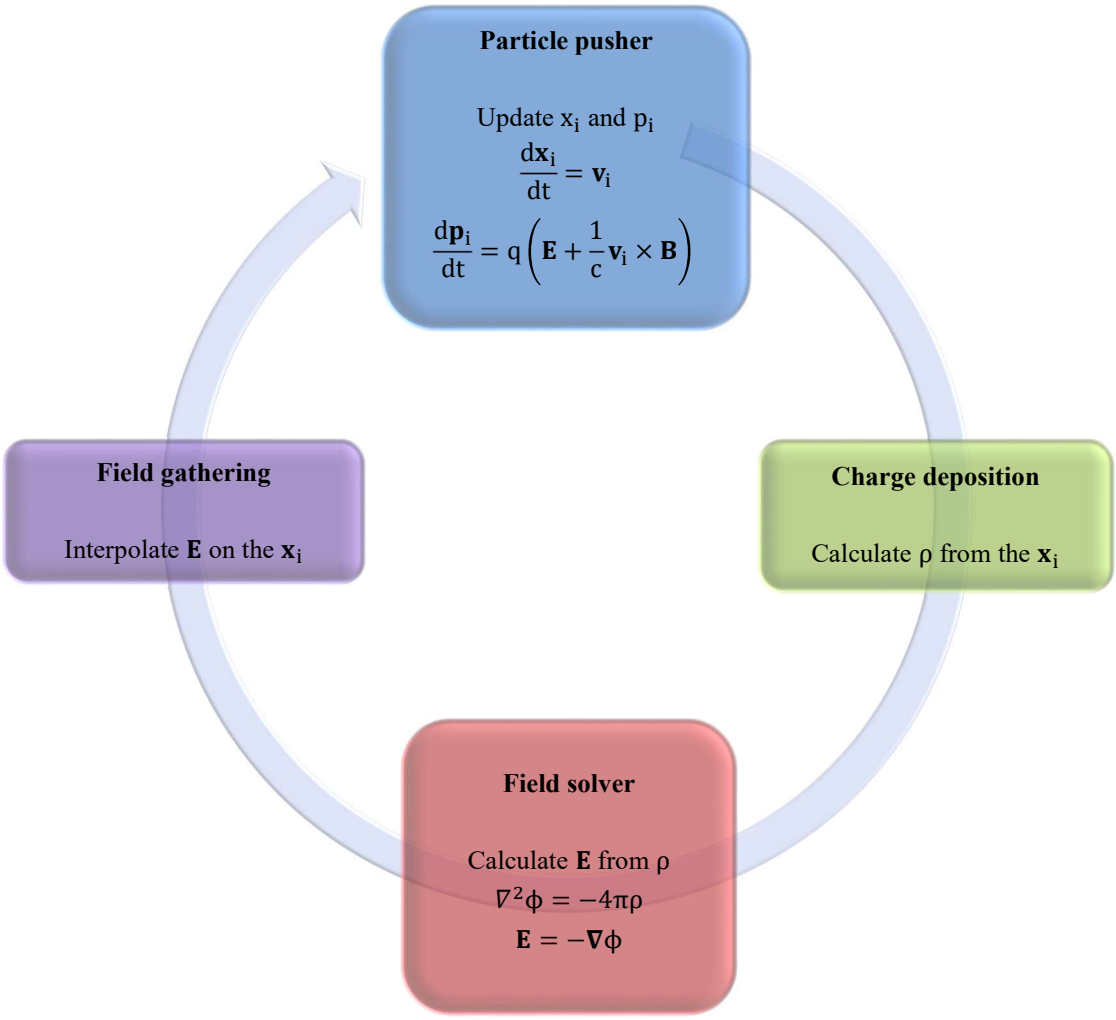

Fig. 2.1. After loading charged particles, charge and current depositions should be interpolated. Then from Gauss's law, electric potential and field can be calculated. Before the step for integrating equation of motion of particles, fields which are calculated on grids around the particles should be interpolated. Once integrating the equation of motion of particles, updated charge depositions are calculated. Same steps are repeated.

The PIC loop in electromagnetics

For the PIC loop in electromagnetics, position and momentum of particle is used to obtain the charge and current densities. So, electromagnetic fields can be calculated from electromagnetic field solver. Magnetic field can be induced in the system.

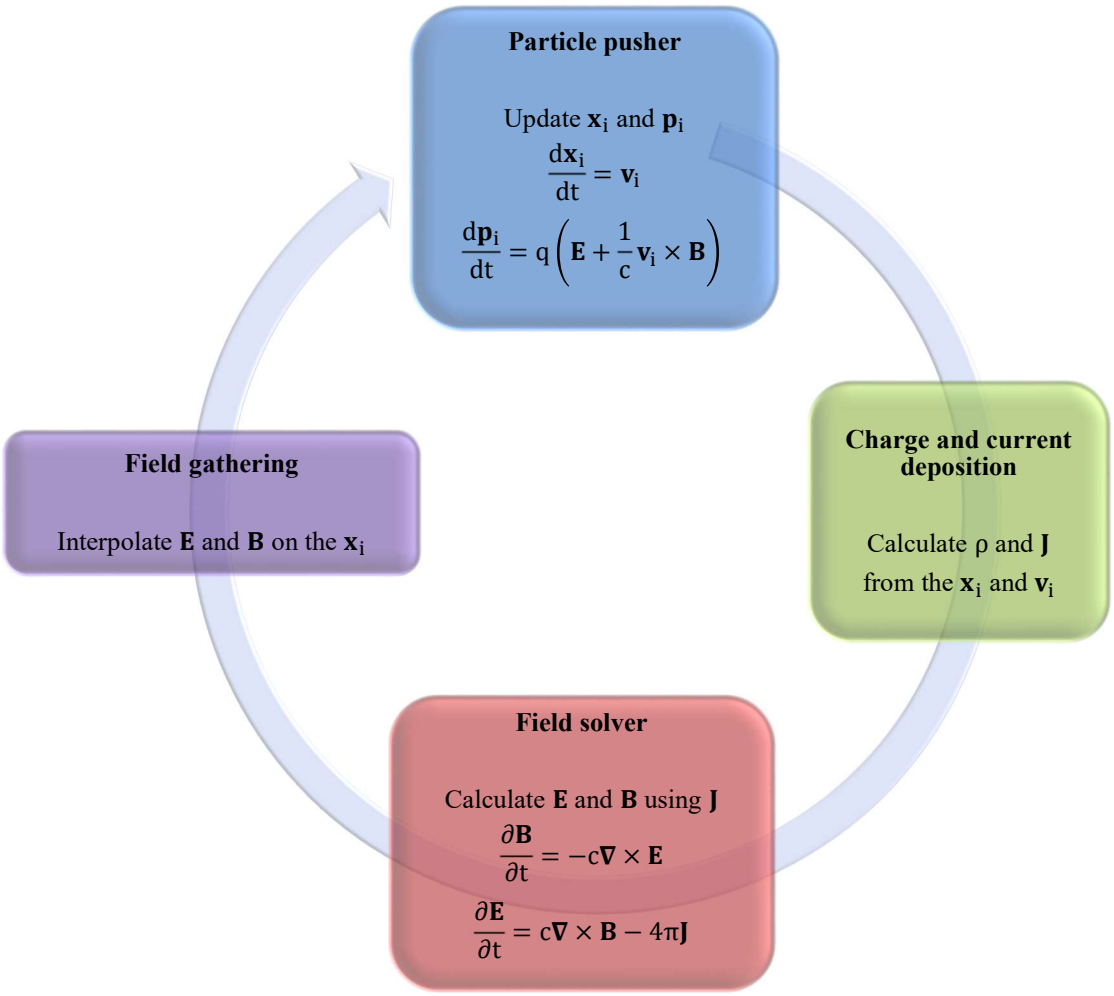

Fig. 2.2. After loading charged particles, charge and current depositions should be interpolated. And next, electromagnetic fields in recent time can be calculated updating two fields of coupled differential equations in time. Before the step for integrating equation of motion of particles, fields which are calculated on grids around the particles should be interpolated. Once integrating the equation of motion of particles, updated charge and current depositions are calculated. Same steps are repeated.

2.3 Staggering in time and space

$$\frac{\partial \mathbf{B}}{\partial t} = -c\nabla\times\mathbf{E}, \tag{2.5}$$

$$\frac{\partial \mathbf{E}}{\partial t} = c\nabla\times\mathbf{B} - 4\pi\mathbf{J}. \tag{2.6}$$

In the electromagnetic field solver from Maxwell's equations, electric and magnetic fields are coupled to each other and derivatives of fields with respect to both time and space show up in the two equations above. Each component of two fields should exist in different memories from each other to realize the coupling with derivatives in time and space. In other words, the indices of fields (and other arguments for particle) alternately show up with respect to temporal and spatial grids. They are staggered at each step of both time and space to each other.

Staggering in time

Magnetic and electric fields should be staggered in time to perform time derivatives in Faraday's law and Ampere's law. Each field is on the same time step with its source. Momentum of particle corresponds to magnetic field in time, while position of particle corresponds to electric fields in time. Each of electric and magnetic fields alternate with each other in time. Magnetic field is on the half integer of upper index 'n', while electric field is on the integer of upper index 'n'.

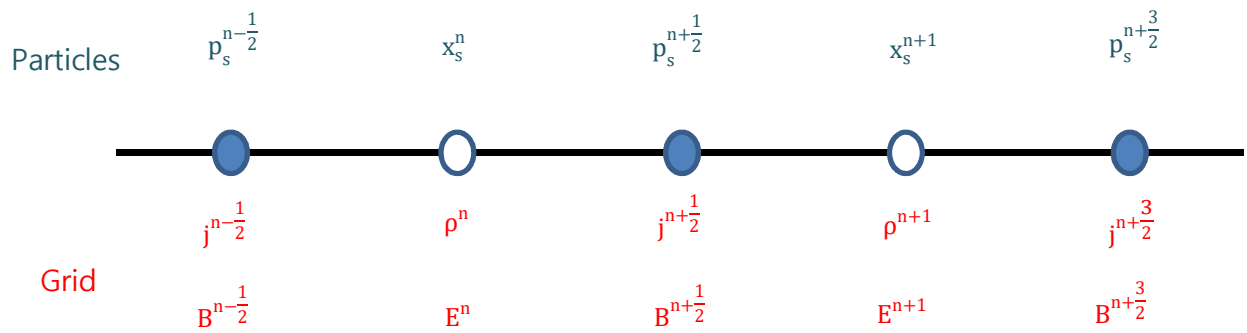

Fig. 2.3. Staggering in time between momentum and position, current and charge, and magnetic and electric fields are depicted. Each field is on the same time step with its source. But each of electric and magnetic fields alternate with each other in time. Magnetic field is on the half integer of upper index 'n', whereas electric field is on the integer of upper index 'n'.

ULSAN NATIONAL INSTITUTE OF SCIENCE AND TECHNOLOGY

Staggering in space: The Yee grid (Rectangular coordinates)

Staggering in space of rectangular coordinates between current and charge, magnetic and electric fields are depicted here. The Yee grid [18] is proper for calculating $\nabla\times$. Each component of electric field is always on the grid which is parallel to that component and has half integer of index in that direction. On the other hand, each component of magnetic field is always among grids which are perpendicular to that component and has half integer of index in other directions.

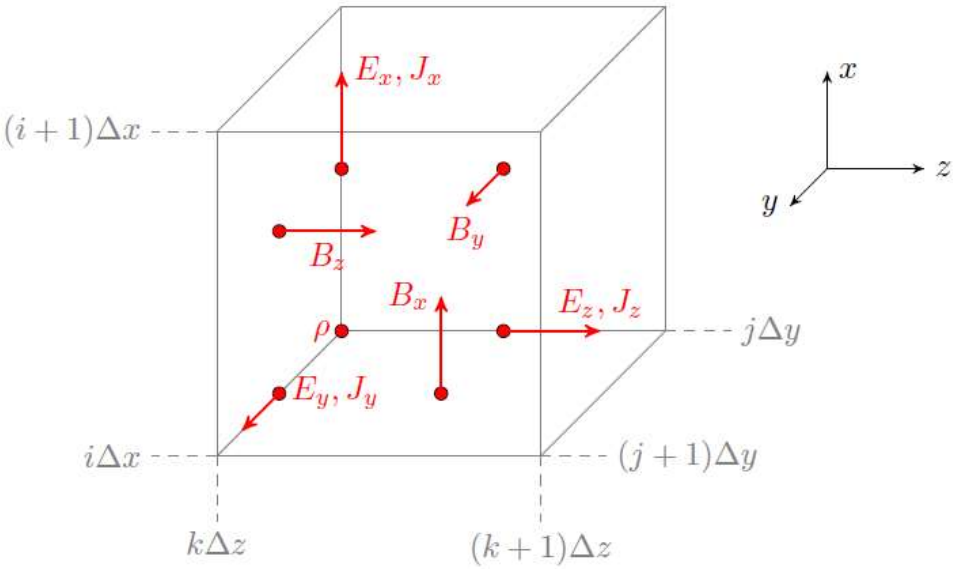

Fig. 2.4. Staggering in space of rectangular coordinates between current and charge and magnetic and electric fields are depicted. The Yee grid is proper for calculating $\nabla\times$.

ULSAN NATIONAL INSTITUTE OF SCIENCE AND TECHNOLOGY

2.4 Difference equations

The four procedures contained in the PIC loop of electromagnetics are described in rectangular coordinates with numerical notations. Staggering in time and space is considered. The PIC scheme repeatedly updates the values for the particle and fields from initial to final time, step by step using these equations.

Field solver

Faraday and Ampere's equations are used to calculate fields. We call those equations 'field solver' here.

$$\left.\frac{\partial \mathbf{B}}{\partial t}\right|^{n} = -c\nabla\times\mathbf{E}^{n}, \tag{2.7}$$

$$\begin{aligned}
\frac{B_{x_{i,j+\frac{1}{2},k+\frac{1}{2}}}^{n+\frac{1}{2}} - B_{x_{i,j+\frac{1}{2},k+\frac{1}{2}}}^{n-\frac{1}{2}}}{\Delta t} &= -c\left[\frac{E_{z_{i,j+1,k+\frac{1}{2}}}^{n} - E_{z_{i,j,k+\frac{1}{2}}}^{n}}{\Delta y} - \frac{E_{y_{i,j+\frac{1}{2},k+1}}^{n} - E_{y_{i,j+\frac{1}{2},k}}^{n}}{\Delta z}\right],\\
\frac{B_{y_{i+\frac{1}{2},j,k+\frac{1}{2}}}^{n+\frac{1}{2}} - B_{y_{i+\frac{1}{2},j,k+\frac{1}{2}}}^{n-\frac{1}{2}}}{\Delta t} &= +c\left[\frac{E_{x_{i+\frac{1}{2},j,k+1}}^{n} - E_{x_{i+\frac{1}{2},j,k}}^{n}}{\Delta z} - \frac{E_{z_{i+1,j,k+\frac{1}{2}}}^{n} - E_{z_{i,j,k+\frac{1}{2}}}^{n}}{\Delta x}\right],\\
\frac{B_{z_{i+\frac{1}{2},j+\frac{1}{2},k}}^{n+\frac{1}{2}} - B_{z_{i+\frac{1}{2},j+\frac{1}{2},k}}^{n-\frac{1}{2}}}{\Delta t} &= -c\left[\frac{E_{y_{i+1,j+\frac{1}{2},k}}^{n} - E_{y_{i,j+\frac{1}{2},k}}^{n}}{\Delta x} - \frac{E_{x_{i+\frac{1}{2},j+1,k}}^{n} - E_{x_{i+\frac{1}{2},j,k}}^{n}}{\Delta y}\right],
\end{aligned} \tag{2.8}$$

and

$$\left.\frac{\partial \mathbf{E}}{\partial t}\right|^{n+\frac{1}{2}} = c\nabla\times\mathbf{B}^{n+\frac{1}{2}} - 4\pi\mathbf{J}^{n+\frac{1}{2}}, \tag{2.9}$$

$$\begin{aligned}
\frac{E_{x_{i+\frac{1}{2},j,k}}^{n+1} - E_{x_{i+\frac{1}{2},j,k}}^{n}}{\Delta t} &= c\left[\frac{B_{z_{i+\frac{1}{2},j+\frac{1}{2},k}}^{n+\frac{1}{2}} - B_{z_{i+\frac{1}{2},j-\frac{1}{2},k}}^{n+\frac{1}{2}}}{\Delta y} - \frac{B_{y_{i+\frac{1}{2},j,k+\frac{1}{2}}}^{n+\frac{1}{2}} - B_{y_{i+\frac{1}{2},j,k-\frac{1}{2}}}^{n+\frac{1}{2}}}{\Delta z}\right] - 4\pi J_{x_{i+\frac{1}{2},j,k}}^{n+\frac{1}{2}},\\
\frac{E_{y_{i,j+\frac{1}{2},k}}^{n+1} - E_{y_{i,j+\frac{1}{2},k}}^{n}}{\Delta t} &= c\left[\frac{B_{x_{i,j+\frac{1}{2},k+\frac{1}{2}}}^{n+\frac{1}{2}} - B_{x_{i,j+\frac{1}{2},k-\frac{1}{2}}}^{n+\frac{1}{2}}}{\Delta z} - \frac{B_{z_{i+\frac{1}{2},j+\frac{1}{2},k}}^{n+\frac{1}{2}} - B_{z_{i-\frac{1}{2},j+\frac{1}{2},k}}^{n+\frac{1}{2}}}{\Delta x}\right] - 4\pi J_{y_{i,j+\frac{1}{2},k}}^{n+\frac{1}{2}},\\
\frac{E_{z_{i,j,k+\frac{1}{2}}}^{n+1} - E_{z_{i,j,k+\frac{1}{2}}}^{n}}{\Delta t} &= c\left[\frac{B_{y_{i+\frac{1}{2},j,k+\frac{1}{2}}}^{n+\frac{1}{2}} - B_{y_{i-\frac{1}{2},j,k+\frac{1}{2}}}^{n+\frac{1}{2}}}{\Delta x} - \frac{B_{x_{i,j+\frac{1}{2},k+\frac{1}{2}}}^{n+\frac{1}{2}} - B_{x_{i,j-\frac{1}{2},k+\frac{1}{2}}}^{n+\frac{1}{2}}}{\Delta y}\right] - 4\pi J_{z_{i,j,k+\frac{1}{2}}}^{n+\frac{1}{2}}.
\end{aligned} \tag{2.10}$$

When there are no sources of fields such as charge or current, fields can be updated only by these two equations. Electromagnetic wave in vacuum is one of those examples. But when there are movable charged particles in the system, fields are affected by position and current of the particles, not only by previous fields.

ULSAN NATIONAL INSTITUTE OF SCIENCE AND TECHNOLOGY

Field gathering (Linear weights of fields)

Because particles are not on the grids, the fields which are fixed on the grids should be interpolated to the places where the particles are located. Here only the linearly weighted fields are introduced. The linear interpolation is one of the most common weighting methods. It has the error whose size is in the order of $\sim\Delta x^2$ and is fast in calculation time.

In Fig. 2.4. the s'th particle is at (x_s, y_s), $i\Delta x \le x_s \le (i+1)\Delta x$, $j\Delta y \le y_s \le (j+1)\Delta y$. The specific position of the particle is expressed by $x_s = (i+\delta_x)\Delta x$ and $y_s = (j+\delta_y)\Delta y$ (note that $0 \le \delta_x \le 1$ and $0 \le \delta_y \le 1$.). Then the interpolated field $\mathbf{W}(x_s, y_s)$ in 2-dimensional space is expressed by

$$\mathbf{W}(x_s, y_s) = (1-\delta_x)(1-\delta_y)\mathbf{W}_{i,j} + \delta_x(1-\delta_y)\mathbf{W}_{i+1,j} + (1-\delta_x)\delta_y\mathbf{W}_{i,j+1} + \delta_x\delta_y\mathbf{W}_{i+1,j+1}. \tag{2.11}$$

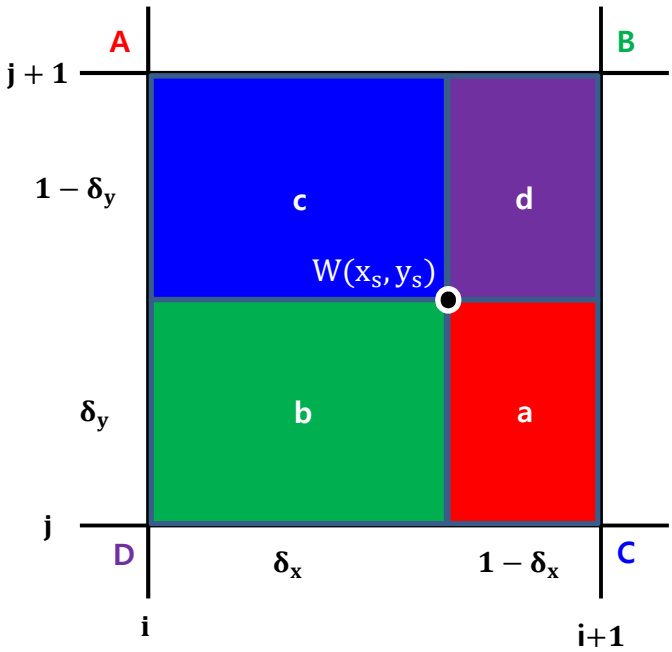

Fig. 2.5. Scheme of 2-dimensional linear weighting. The s'th particle is at (x_s, y_s), $i\Delta x \le x_s \le (i+1)\Delta x$, $j\Delta y \le y_s \le (j+1)\Delta y$. The specific position of the particle is expressed by $x_s = (i+\delta_x)\Delta x$ and $y_s = (j+\delta_y)\Delta y$ (note that $0 \le \delta_x \le 1$ and $0 \le \delta_y \le 1$).

ULSAN NATIONAL INSTITUTE OF SCIENCE AND TECHNOLOGY

The interpolated electric field at s'th particle (x_s, y_s, z_s) in 3-dimensional rectangular Yee grid is expressed by

$$
\begin{aligned}
\overline{E}_x(\mathbf{x}_s^n) = &\left(1 - \frac{\left|\left(i+\frac{1}{2}\right)\Delta x - x_s\right|}{\Delta x}\right)\left(1 - \frac{|j\Delta y - y_s|}{\Delta y}\right)\left(1 - \frac{|k\Delta z - z_s|}{\Delta z}\right) E_{x_{i+\frac{1}{2},j,k}}^{\ n} \\
&+ \frac{\left|\left(i+\frac{1}{2}\right)\Delta x - x_s\right|}{\Delta x}\left(1 - \frac{|j\Delta y - y_s|}{\Delta y}\right)\left(1 - \frac{|k\Delta z - z_s|}{\Delta z}\right) E_{x_{i+\frac{3}{2},j,k}}^{\ n} \\
&+ \left(1 - \frac{\left|\left(i+\frac{1}{2}\right)\Delta x - x_s\right|}{\Delta x}\right)\frac{|j\Delta y - y_s|}{\Delta y}\left(1 - \frac{|k\Delta z - z_s|}{\Delta z}\right) E_{x_{i+\frac{1}{2},j+1,k}}^{\ n} \\
&+ \left(1 - \frac{\left|\left(i+\frac{1}{2}\right)\Delta x - x_s\right|}{\Delta x}\right)\left(1 - \frac{|j\Delta y - y_s|}{\Delta y}\right)\frac{|k\Delta z - z_s|}{\Delta z} E_{x_{i+\frac{1}{2},j,k+1}}^{\ n} \\
&+ \frac{\left|\left(i+\frac{1}{2}\right)\Delta x - x_s\right|}{\Delta x}\frac{|j\Delta y - y_s|}{\Delta y}\left(1 - \frac{|k\Delta z - z_s|}{\Delta z}\right) E_{x_{i+\frac{3}{2},j+1,k}}^{\ n} \\
&+ \frac{\left|\left(i+\frac{1}{2}\right)\Delta x - x_s\right|}{\Delta x}\left(1 - \frac{|j\Delta y - y_s|}{\Delta y}\right)\frac{|k\Delta z - z_s|}{\Delta z} E_{x_{i+\frac{3}{2},j,k+1}}^{\ n} \\
&+ \left(1 - \frac{\left|\left(i+\frac{1}{2}\right)\Delta x - x_s\right|}{\Delta x}\right)\frac{|j\Delta y - y_s|}{\Delta y}\frac{|k\Delta z - z_s|}{\Delta z} E_{x_{i+\frac{1}{2},j+1,k+1}}^{\ n} \\
&+ \frac{\left|\left(i+\frac{1}{2}\right)\Delta x - x_s\right|}{\Delta x}\frac{|j\Delta y - y_s|}{\Delta y}\frac{|k\Delta z - z_s|}{\Delta z} E_{x_{i+\frac{3}{2},j+1,k+1}}^{\ n}.
\end{aligned}
\tag{2.12}
$$

Here, s'th particle in the cell is defined in the region $i + 1/2 \le x_s/\Delta x \le i + 3/2$, $j \le y_s/\Delta y \le j + 1$ and $k \le z_s/\Delta z \le k + 1$ at the time $n\Delta t$, in which each of $\left|\left(i+\frac{1}{2}\right)\Delta x - x_s\right|/\Delta x$, $|j\Delta y - y_s|/\Delta y$ and $|k\Delta z - z_s|/\Delta z$ corresponds to δ_x, δ_y and δ_z in Fig. 2.5, respectively.

ULSAN NATIONAL INSTITUTE OF SCIENCE AND TECHNOLOGY

The interpolated magnetic field at s'th particle (x_s, y_s, z_s) in 3-dimensional rectangular Yee grid is expressed by

$$
\begin{aligned}
\overline{B}_x\left(\mathbf{x}_s^{n+\frac{1}{2}}\right) = {} & \left(1-\frac{|\Delta x - x_s|}{\Delta x}\right)\left(1-\frac{\left|\left(j+\frac{1}{2}\right)\Delta y - y_s\right|}{\Delta y}\right)\left(1-\frac{\left|\left(k+\frac{1}{2}\right)\Delta z - z_s\right|}{\Delta z}\right) B_{x_{i,j+\frac{1}{2},k+\frac{1}{2}}}^{n+\frac{1}{2}} \\
& + \frac{|\Delta x - x_s|}{\Delta x}\left(1-\frac{\left|\left(j+\frac{1}{2}\right)\Delta y - y_s\right|}{\Delta y}\right)\left(1-\frac{\left|\left(k+\frac{1}{2}\right)\Delta z - z_s\right|}{\Delta z}\right) B_{x_{i+1,j+\frac{1}{2},k+\frac{1}{2}}}^{n+\frac{1}{2}} \\
& + \left(1-\frac{|\Delta x - x_s|}{\Delta x}\right)\frac{\left|\left(j+\frac{1}{2}\right)\Delta y - y_s\right|}{\Delta y}\left(1-\frac{\left|\left(k+\frac{1}{2}\right)\Delta z - z_s\right|}{\Delta z}\right) B_{x_{i,j+\frac{3}{2},k+\frac{1}{2}}}^{n+\frac{1}{2}} \\
& + \left(1-\frac{|\Delta x - x_s|}{\Delta x}\right)\left(1-\frac{\left|\left(j+\frac{1}{2}\right)\Delta y - y_s\right|}{\Delta y}\right)\frac{\left|\left(k+\frac{1}{2}\right)\Delta z - z_s\right|}{\Delta z} B_{x_{i,j+\frac{1}{2},k+\frac{3}{2}}}^{n+\frac{1}{2}} \\
& + \frac{|\Delta x - x_s|}{\Delta x}\frac{\left|\left(j+\frac{1}{2}\right)\Delta y - y_s\right|}{\Delta y}\left(1-\frac{\left|\left(k+\frac{1}{2}\right)\Delta z - z_s\right|}{\Delta z}\right) B_{x_{i+1,j+\frac{3}{2},k+\frac{1}{2}}}^{n+\frac{1}{2}} \\
& + \frac{|\Delta x - x_s|}{\Delta x}\left(1-\frac{\left|\left(j+\frac{1}{2}\right)\Delta y - y_s\right|}{\Delta y}\right)\frac{\left|\left(k+\frac{1}{2}\right)\Delta z - z_s\right|}{\Delta z} B_{x_{i+1,j+\frac{1}{2},k++\frac{3}{2}}}^{n+\frac{1}{2}} \\
& + \left(1-\frac{|\Delta x - x_s|}{\Delta x}\right)\frac{\left|\left(j+\frac{1}{2}\right)\Delta y - y_s\right|}{\Delta y}\frac{\left|\left(k+\frac{1}{2}\right)\Delta z - z_s\right|}{\Delta z} B_{x_{i,j+\frac{3}{2},k+\frac{3}{2}}}^{n+\frac{1}{2}} \\
& + \frac{|\Delta x - x_s|}{\Delta x}\frac{\left|\left(j+\frac{1}{2}\right)\Delta y - y_s\right|}{\Delta y}\frac{\left|\left(k+\frac{1}{2}\right)\Delta z - z_s\right|}{\Delta z} B_{x_{i+1,j+\frac{3}{2},k+\frac{3}{2}}}^{n+\frac{1}{2}}
\end{aligned}
\tag{2.13}
$$

$$
\overline{B}_x(\mathbf{x}_s^n) \equiv \frac{\overline{B}_x\left(\mathbf{x}_s^{n+\frac{1}{2}}\right) + \overline{B}_x\left(\mathbf{x}_s^{n-\frac{1}{2}}\right)}{2}. \tag{2.14}
$$

Here s'th particle in the cell is defined in the region $i \le x_s/\Delta x \le i+1$, $j+1/2 \le y_s/\Delta y \le j+3/2$ and $k+1/2 \le z_s/\Delta z \le k+3/2$ at the time $(n \pm 1/2)\Delta t$, in which each of $|i\Delta x - x_s|/\Delta x$, $|(j+1/2)\Delta y - y_s|/\Delta y$ and $|(k+1/2)\Delta z - z_s|/\Delta z$ corresponds to δ_x, δ_y and δ_z in Fig. 2.5, respectively.

Particle pusher (Integration of equation of motion)

Once fields are gathered at the position of a particle, the equation of motion can be updated in time.

$$\left.\frac{d\mathbf{p}_s}{dt}\right|^n \equiv \frac{\mathbf{p}_s^{n+\frac{1}{2}} - \mathbf{p}_s^{n-\frac{1}{2}}}{\Delta t} = q\left[\mathbf{E}(\mathbf{x}_s^n) + \frac{1}{c}\mathbf{v}_s \times \mathbf{B}(\mathbf{x}_s^n)\right], \tag{2.15}$$

$$\begin{aligned}
\frac{p_{s,x}^{n+\frac{1}{2}} - p_{s,x}^{n-\frac{1}{2}}}{\Delta t} &= q\left[\overline{E}_x(x_s^n, y_s^n, z_s^n) + \frac{1}{c}\left[\frac{v_{s,y}^{n+\frac{1}{2}} - v_{s,y}^{n-\frac{1}{2}}}{2}\overline{B}_z(x_s^n, y_s^n, z_s^n) - \frac{v_{s,z}^{n+\frac{1}{2}} - v_{s,z}^{n-\frac{1}{2}}}{2}\overline{B}_y(x_s^n, y_s^n, z_s^n)\right]\right], \\
\frac{p_{s,y}^{n+\frac{1}{2}} - p_{s,y}^{n-\frac{1}{2}}}{\Delta t} &= q\left[\overline{E}_y(x_s^n, y_s^n, z_s^n) - \frac{1}{c}\left[\frac{v_{s,x}^{n+\frac{1}{2}} - v_{s,x}^{n-\frac{1}{2}}}{2}\overline{B}_z(x_s^n, y_s^n, z_s^n) - \frac{v_{s,z}^{n+\frac{1}{2}} - v_{s,z}^{n-\frac{1}{2}}}{2}\overline{B}_x(x_s^n, y_s^n, z_s^n)\right]\right], \\
\frac{p_{s,z}^{n+\frac{1}{2}} - p_{s,z}^{n-\frac{1}{2}}}{\Delta t} &= q\left[\overline{E}_z(x_s^n, y_s^n, z_s^n) + \frac{1}{c}\left[\frac{v_{s,x}^{n+\frac{1}{2}} - v_{s,x}^{n-\frac{1}{2}}}{2}\overline{B}_y(x_s^n, y_s^n, z_s^n) - \frac{v_{s,y}^{n+\frac{1}{2}} - v_{s,y}^{n-\frac{1}{2}}}{2}\overline{B}_x(x_s^n, y_s^n, z_s^n)\right]\right].
\end{aligned} \tag{2.16}$$

Using updated momentum and previous position of the particle, new position can be obtained as follows.

$$\left.\frac{d\mathbf{x}_s}{dt}\right|^{n+\frac{1}{2}} \equiv \frac{\mathbf{x}_s^{n+1} - \mathbf{x}_s^n}{\Delta t} = \frac{\mathbf{p}_s^{n+\frac{1}{2}}}{m\gamma_s^{n+\frac{1}{2}}}, \tag{2.17}$$

$$\begin{aligned}
\frac{x_s^{n+1} - x_s^n}{\Delta t} &= \frac{p_{s,x}^{n+\frac{1}{2}}}{m\gamma_s^{n+\frac{1}{2}}}, \\
\frac{y_s^{n+1} - y_s^n}{\Delta t} &= \frac{p_{s,y}^{n+\frac{1}{2}}}{m\gamma_s^{n+\frac{1}{2}}}, \\
\frac{z_s^{n+1} - z_s^n}{\Delta t} &= \frac{p_{s,z}^{n+\frac{1}{2}}}{m\gamma_s^{n+\frac{1}{2}}}.
\end{aligned} \tag{2.18}$$

Particles are moved by the interpolated constant electromagnetic forces during the time interval Δt at each time step.

Charge and current deposition (Linear weights of sources)

Once a particle moves to a new position, new charge and current densities can be obtained (i.e., weighted) from the information of position and momentum.

$$\text{Linear weights,} \quad S(x-x_s, y-y_s, z-z_s) = \left(1-\frac{|x-x_s|}{\Delta x}\right)\left(1-\frac{|y-y_s|}{\Delta y}\right)\left(1-\frac{|z-z_s|}{\Delta z}\right), \tag{2.19}$$

$$\text{only if } |x-x_s| < \Delta x \text{ and } |y-y_s| < \Delta y \text{ and } |z-z_s| < \Delta z$$

$$\rho^n_{i,j,k} = \frac{1}{\Delta x \Delta y \Delta z}\sum_s q_s S(i\Delta x - x^n_s, j\Delta y - y^n_s, k\Delta z - z^n_s), \tag{2.20}$$

$$j_{x_{i+\frac{1}{2},j,k}}^{n+\frac{1}{2}} = \frac{1}{\Delta x \Delta y \Delta z}\sum_s \frac{q_s p_{s,x}^{n+\frac{1}{2}}}{m\gamma_s^{n+\frac{1}{2}}} S\left(\left(i+\frac{1}{2}\right)\Delta x - \frac{x_s^{n+1}-x_s^n}{2}, j\Delta y - \frac{y_s^{n+1}-y_s^n}{2}, k\Delta z - \frac{z_s^{n+1}-z_s^n}{2}\right),$$

$$j_{y_{i,j+\frac{1}{2},k}}^{n+\frac{1}{2}} = \frac{1}{\Delta x \Delta y \Delta z}\sum_s \frac{q_s p_{s,y}^{n+\frac{1}{2}}}{m\gamma_s^{n+\frac{1}{2}}} S\left(i\Delta x - \frac{x_s^{n+1}-x_s^n}{2}, \left(j+\frac{1}{2}\right)\Delta y - \frac{y_s^{n+1}-y_s^n}{2}, k\Delta z - \frac{z_s^{n+1}-z_s^n}{2}\right), \tag{2.21}$$

$$j_{z_{i,j,k+\frac{1}{2}}}^{n+\frac{1}{2}} = \frac{1}{\Delta x \Delta y \Delta z}\sum_s \frac{q_s p_{s,z}^{n+\frac{1}{2}}}{m\gamma_s^{n+\frac{1}{2}}} S\left(i\Delta x - \frac{x_s^{n+1}-x_s^n}{2}, j\Delta y - \frac{y_s^{n+1}-y_s^n}{2}, \left(k+\frac{1}{2}\right)\Delta z - \frac{z_s^{n+1}-z_s^n}{2}\right).$$

The sources which are interpolated to grids are used to calculate new fields acting on particles. So, procedures are iterated.

ULSAN NATIONAL INSTITUTE OF SCIENCE AND TECHNOLOGY

Chapter 3. Plasma Wakefields of a Short Beam Bunch in Plasmas

In this chapter, initially proposed linear beam-driven plasma wakefield theories of Refs [4] and [6] are introduced. As remarked above, linearly excited plasma wakefield would generates the self-modulation instability. Because the optimum condition for excitation of plasma wakefield is satisfied by a short beam, it is required to understand the physics of a short beam-driven plasma wakefield.

3.1 Energy transfer in co-linear wakefield accelerator

In this section, we discuss a general property of energy transfer in plasma wakefield accelerators. One of promising definitions of plasma wakefield accelerators described in this paper is that the ion cavity for accelerating charged particle in plasma has no stored energy before the driving (or leading) beam arrives. Considering the energy change of the bunch per unit length due to its own wake,

$$\frac{d(N_1E_1)}{dz} = -N_1^2e^2W(0), \tag{3.1}$$

where N_1 is the number of particles in the bunch and E_1 is the energy per particle. $W(0)$ is a wakefield function of the plasma ion cavity structure at $y = 0$ from a elementary charge e. Here we regard bunches as rigid collections of particles which have zero length (i.e., point-like). The energy change of the secondary (or trailing or witness) beam injected at a distance y behind the driving beam is affected by both its own wake and the driving beam's wake. These two effects are linearly superposed as

$$\frac{d(N_2E_2)}{dz} = -N_2^2e^2W(0) - N_1N_2e^2W(y), \tag{3.2}$$

where N_2 and E_2 meant the number of particles and energy per particles of the trailing bunch. Due to energy conservation, the total energy of driving and injected beam does not increase.

$$\frac{d(N_1E_1)}{dz} + \frac{d(N_2E_2)}{dz} = -(N_1^2 + N_2^2)e^2W(0) - N_1N_2e^2W(y) \leq 0 \tag{3.3}$$

Considering that it should be satisfied for all N_1 and N_2 $(N_1 = N_2)$,

$$[-W(y)] \leq 2W(0). \tag{3.4}$$

Then the acceleration gradient seen by a single particle in the witness beam is

$$G \equiv \frac{dE_2}{dz} = -N_2e^2W(0) - N_1e^2W(y) \leq (2N_1 - N_2)e^2W(0). \tag{3.5}$$

ULSAN NATIONAL INSTITUTE OF SCIENCE AND TECHNOLOGY

Assuming the energy of the driving beam will be fully transferred to plasma wave (wakefield), the driving beam will stop in a distance L,

$$L = \frac{E_1}{N_1 e^2 W(0)}. \tag{3.6}$$

As the total charge of the driving beam increase, it makes high accelerating gradient for the secondary beam though, will last for a shorter distance L. Then the energy gain which secondary beam will obtain from the wakefield is

$$\Delta E_2 = GL \leq E_1\left(2 - \frac{N_2}{N_1}\right). \tag{3.7}$$

Therefore, maximum energy gain of the secondary beam from the driving beam is about 2 times of the driving beam energy. Notice that the only assumptions necessary to derive this result are conservation of energy, linear superposition and a rigid point bunch. The inequality can be made for a single mode lossless medium in which the wakefield oscillates with a single frequency behind the driving bunch. Energy transfer efficiency from the driving beam to the secondary beam is

$$\eta \equiv \frac{\Delta(N_2 E_2)}{N_1 E_1} = \frac{N_2}{N_1}\left(2 - \frac{N_2}{N_1}\right). \tag{3.8}$$

In such a case the maximum efficiency is achieved by choosing $N_2 = N_1$. The energy of the leading bunch is then completely transferred to the trailing bunch and no wakefield is left after the trailing bunch.

3.3 Blowing out and sucking in of plasma electrons due to the charged particle bunch's field

In this section, we analyze the response of a cold plasma to a driving bunch by calculating the wakefield for three cases: a one dimensional nonrelativistic plasma, a three-dimensional nonrelativistic plasma, and a one dimensional relativistic plasma. In all 3 cases the plasma is a single frequency medium.
We use three linearized equations.

$$\text{Continuity equation,} \quad \frac{\partial n_1}{\partial t} + n_0(\nabla \cdot \mathbf{v}_p) = 0, \tag{3.9}$$

$$\text{Equation of motion,} \quad \frac{\partial \mathbf{v}_p}{\partial t} = \frac{e\mathbf{E}}{m}, \tag{3.10}$$

$$\text{Gauss's law,} \quad \nabla \cdot \mathbf{E} = 4\pi e(n_1 + n_b). \tag{3.11}$$

Here n_1 is the perturbed background plasma electron density, and n_b is the driving beam density. The elementary charge is defined by $e \equiv -|e| = -1.602\times10^{-19}$ C. Note that this definition of e is different from the one in Chapter 1.1. When the driving beam consists of electrons, it has a negative value. When the driving

ULSAN NATIONAL INSTITUTE OF SCIENCE AND TECHNOLOGY

beam consists of protons, it has a positive value. Thus, the sign of n_b is not explicitly shown by itself. Combining above equations, we get the equation of perturbed plasma electron density.

$$\frac{\partial^2 n_1}{\partial t^2} + n_0\left(\nabla\cdot\frac{\partial \mathbf{v}_p}{\partial t}\right) = \frac{\partial^2 n_1}{\partial t^2} + n_0\left(\nabla\cdot\frac{e\mathbf{E}}{m}\right) = \frac{\partial^2 n_1}{\partial t^2} + \frac{en_0}{m}4\pi e(n_1+n_b) = 0,$$
$$\frac{\partial^2 n_1}{\partial t^2} + \frac{4\pi e^2 n_0}{m}n_1 = -\frac{4\pi e^2 n_0}{m}n_b \quad \Leftrightarrow \quad \frac{\partial^2 n_1}{\partial t^2} + \omega_p^2 n_1 = -\omega_p^2 n_b. \tag{3.12}$$

Here, plasma frequency $\omega_p^2 \equiv 4\pi e^2 n_0/m_e$ and driving beam density $n_b = \sigma\delta(z - v_b t)$ are introduced. Defining the beam frame coordinate $y = v_b t - z$ $(\partial y = v_b\,\partial t)$ and $k \equiv \omega_p/v_b$, differential equation for the density perturbation is

$$\frac{\partial^2 n_1}{\partial y^2} + k^2 n_1 = -k^2\sigma\delta(y) \tag{3.13}$$

Solving the second order differential equation that we obtained in the region, $y > 0$

$$\frac{\partial^2 n_1}{\partial y^2} = -k^2 n_1, \qquad y > 0$$
$$n_1 = A\sin(ky), \qquad y > 0 \tag{3.14}$$
$$(\because n_1(0) = 0.)$$

And integrating our original differential equation for $0_- < y \le 0_+$,

$$\int_{0_-}^{0_+}\frac{\partial^2 n_1}{\partial y'^2}dy' + k^2\int_{0_-}^{0_+} n_1 dy' = -k^2\sigma,$$
$$\left.\frac{\partial n_1}{\partial y}\right|_{y=0_+} - \left.\frac{\partial n_1}{\partial y}\right|_{y=0_-} = -k^2\sigma \tag{3.15}$$
$$\left(\because \int_{0_-}^{0_+} n_1 dy' = A\int_{0_-}^{0_+}\sin(ky)dy' \simeq 0\right)$$

Because the region $y < 0$ is out of our interest, we ignore the first order derivative of n_1 at $y = 0_-$.

$$\left.\frac{\partial n_1}{\partial y}\right|_{y=0_+} = -k^2\sigma. \tag{3.16}$$

Assuming

$$\left.\frac{\partial n_1}{\partial y}\right|_{y=0_+} = \left.\frac{\partial n_1}{\partial y}\right|_{y=0},$$
$$\left.\frac{\partial n_1}{\partial y}\right|_{y=0} = Ak\cos(0) = -k^2\sigma, \tag{3.17}$$
$$A = -k\sigma,$$

ULSAN NATIONAL INSTITUTE OF SCIENCE AND TECHNOLOGY

We have

$$n_1 = \begin{cases} -k\sigma \sin(ky), & y > 0 \\ 0, & y < 0 \end{cases} \tag{3.18}$$

When the driving beam consists of electrons, $\sigma > 0$, and n_1 must be negative within the region $0 < y < \pi$, i.e., in a half of the first period (or plasma wavelength). It means that background electrons are pulled out by Coulomb repulsive force of the driving beam. In the similar way, when the driving beam consists of protons or positrons, $\sigma < 0$, and n_1 must be positive within the region $0 < y < \pi$, i.e., in a half of the first period (or plasma wavelength). It means that background electrons are sucked in by Coulomb attractive force of the driving beam. There is no plasma wave ahead of the driving beam. This is due to the fact that the plasma wave has zero group velocity. It does not propagate in space and therefore does not overtake the driving beam even if the driving beam moves non-relativistically. Mathematically, this is from the absence of spatial derivatives. From Gauss's law, the electric field induced by the perturbed density is

$$E = \begin{cases} -4\pi e\sigma \cos(ky), & y > 0, \\ 0, & y < 0. \end{cases} \tag{3.19}$$

Considering the energy conservation law,

$$\begin{gathered} u_{em}(\text{the energy density of the electric field at the peak}) \\ = \frac{E^2(\text{peak})}{8\pi} = 2\pi e^2\sigma^2 = E(0)e\sigma = -\Delta\text{Energy} \\ \therefore \varepsilon(0) = -2\pi e\sigma \end{gathered} \tag{3.20}$$

Note that there exists a phase retardation while the energy lost by the driving beam is fully deposited at the crest of plasma waves. Here the electric field $\varepsilon(0) = -2\pi e\sigma$ is a half of the peak value. It well satisfies the upper limit of energy transfer efficiency. Here, to satisfy the linearity condition, energy density of the driving beam should be much larger than that of plasma waves.

$$\frac{1}{2}n_0 m v_b^2 \gg \frac{E^2(\text{peak})}{8\pi} = \frac{1}{2}n_0 m v^2(\text{peak}). \tag{3.21}$$

We now consider a cylindrically symmetric leading bunch with density given by

$$n_b = \sigma(r)\delta(z - v_b t) \tag{3.22}$$

ULSAN NATIONAL INSTITUTE OF SCIENCE AND TECHNOLOGY

As in the one-dimensional case, the perturbed density is

$$n_1 = \begin{cases} -k\sigma(r)\sin(ky), & y > 0, \\ 0 \quad , & y < 0. \end{cases} \tag{3.23}$$

Note that the r dependence of n_1 is equal to that of the driving beam. This is again a consequence of zero group velocity. Introducing the electrostatic potential $V = R(r)Z(z)$, we solve

$$\nabla^2 V = 4\pi e(n_1 + n_b)$$
$$\frac{1}{r}\frac{\partial}{\partial r}\left(r\frac{\partial}{\partial r}V\right) + \frac{\partial^2 V}{\partial \phi^2} + \frac{\partial^2 V}{\partial z^2} = 4\pi e(n_1 + n_b) \tag{3.24}$$

Here ϕ dependence doesn't exist. In other words, the driving beam is axisymmetric. Thus, the second term of left hand side should be removed. Specifically, we use a parabolic distribution for the surface charge density of the driving beam.

$$\sigma(r) = \begin{cases} \frac{2N}{\pi a^2}\left(1 - \frac{r^2}{a^2}\right), & r < a \\ 0 \quad , & r > a \end{cases} \tag{3.25}$$

Assuming $Z(z) = A\sin(kz - \omega_p t) \equiv A\sin(ky)$, given partial differential equation becomes

i) $y > 0,\ r < a$

$$\frac{\partial^2 R}{\partial r^2} + \frac{1}{r}\frac{\partial R}{\partial r} - k^2 R = \frac{8eN}{a^2}\left(1 - \frac{r^2}{a^2}\right)k \tag{3.26}$$

ii) $y > 0,\ r > a$

$$\frac{\partial^2 R}{\partial r^2} + \frac{1}{r}\frac{\partial R}{\partial r} - k^2 R = 0 \tag{3.27}$$

Then the potential behind the bunch is given by

$$V = R(r)\sin(ky) \tag{3.28}$$

with (see Appendix 3.1)

$$R(r) = \frac{16eN}{ka^2}\begin{cases} K_2(ka)I_0(kr) + \frac{1}{2} - \frac{2}{(ka)^2} - \frac{r^2}{2a^2}, & r < a \\ I_2(ka)K_0(kr) \quad , & r > a \end{cases} \tag{3.29}$$

ULSAN NATIONAL INSTITUTE OF SCIENCE AND TECHNOLOGY

It yields the electric fields

$$E_z = -kR(r)\cos(ky) \qquad , \qquad r < a$$

$$E_r = -\frac{16eN}{a^2}\left\{K_2(ka)I_1(kr) - \frac{r}{ka^2}\right\}\sin(ky)\,. \qquad r < a \tag{3.30}$$

where I_n and K_n are modified Bessel functions. Here, longitudinal electric field component can accelerate the injected witness beam.

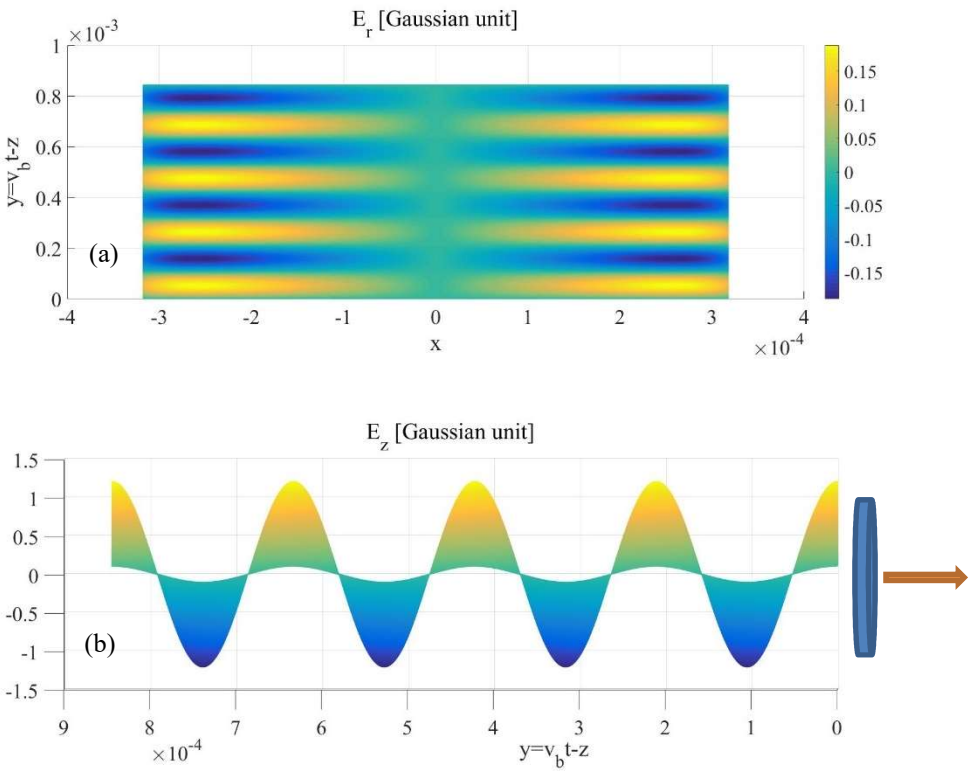

Fig. 3.1. The electric fields induced by disc-shaped electron beam within $r < a$ are plotted. The relative coordinate of driving beam position $y = v_b t - z$ increases in opposite direction of beam propagation. Note that there exist phase differences between plasma response and wakefields.

ULSAN NATIONAL INSTITUTE OF SCIENCE AND TECHNOLOGY

3.5 Nonlinear one dimensional relativistic plasma

For the large amplitudes of plasma oscillations, we can neglect the thermal fluctuations of plasma. This approximation is reasonable even when we are investigating nonlinear oscillations in a high temperature plasma. Under the condition which is nearly in the zero temperature, we don't have to introduce a distribution functions to specify the state of the plasma, but just use the electron density, which depends on the coordinates and time [5]. In this section, we study the nonlinear properties of plasma oscillation in one dimension, which is analytically solvable. The equation governing the nonlinear plasma oscillation in absence of the driving beam along the propagation direction of the plane wave (in one dimension) is (See Appendix 3.2)

$$\frac{d^2}{d\tau^2}\left(\frac{1-\beta u_z}{\sqrt{1-u_z^2}}\right) = \omega_p^2 \frac{\beta^2 u_z}{\beta - u_z}. \tag{3.31}$$

Here, each of β, u_z and ω_p is corresponding to the normalized phase velocity, the velocity of the plasma electrons in z direction and the plasma frequency, respectively. From now on, we follow the story of the paper written by Rosenzwig [6]. Replacing the variable $\tau = t - (\hat{\imath}\cdot\vec{r}/v_{ph})$ with $\tau = \omega_p\left[t - \left(\hat{\imath}\cdot\frac{\vec{r}}{v_{ph}}\right)\right]$ and adding the source of the drive beam in the right-hand side of Eq. (3.31), the differential equation of the nonlinear plasma oscillation driven by the charged particle beam will be

$$\frac{d^2}{d\tau^2}\left(\frac{1-\beta_{ph}\beta}{\sqrt{1-\beta^2}}\right) = \beta_{ph}^2\left(\frac{\beta}{\beta_{ph}-\beta} + \frac{n_b}{n_0}\right). \tag{3.32}$$

Here β and u_z were replaced by β_{ph} and β. Because we are investigating the application for the high-energy physics, we assume the ultra-relativistic driving beam, $\beta_{ph} \approx 1$, and introduce a new variable below

$$x(\tau) = \left(\frac{1-\beta}{1+\beta}\right)^{\frac{1}{2}}. \tag{3.33}$$

Defining $\alpha = n_b/n_0$, our differential equation becomes

$$x''(\tau) = \frac{1}{2}\left(\frac{1}{x^2} - 1 + 2\alpha\right). \tag{3.34}$$

Here, the prime indicates differentiation with respect to τ. Now we consider this equation in the case of an electron beam bunch whose longitudinal profile is constant over the full beam of length l_b.

$$\alpha = \begin{cases} \text{constant}, & 0 \le ct - z \le l_b \\ 0 \quad , & \text{elsewhere} \end{cases} \tag{3.35}$$

ULSAN NATIONAL INSTITUTE OF SCIENCE AND TECHNOLOGY

There is no plasma oscillation for $\tau < 0$, so $\beta = 0$ and the initial conditions are $x(0) = 1$, $x'(0) = 0$. The first integral of Eq. (3.34) is then (see Appendix 3.2)

$$[x'(\tau)]^2 = 2(1-\alpha) - \frac{1}{x} - (1-2\alpha)x. \tag{3.36}$$

Solutions of real number exist for $\alpha < 1/2$, and $x'(\tau) = 0$ at $x = 1,\ 1/(1-2\alpha)$. These points correspond (see Appendix 3.2) to perturbed plasma electron densities of

$$n_1 = n - n_0 = 0, -2n_b(1-\alpha). \tag{3.37}$$

Now that the expression for x' has been found, we may write an equation for the electric field inside the beam as a function of $x(\tau)$ (see Appendix 3.2)

$$E(x) = -\frac{mc\omega_p}{e}(x') = \pm\frac{mc\omega_p}{e}\left[2(1-\alpha) - \frac{1}{x} - (1-2\alpha)x\right]^{\frac{1}{2}}. \tag{3.38}$$

Integrating Eq. (3.36), we have $T/2$.

$$\frac{T}{2} = \int d\tau = (1-2\alpha)^{-\frac{1}{2}}\int_1^{\frac{1}{1-2\alpha}}\left[\frac{x}{(x-1)\left(\frac{1}{1-2\alpha} - x\right)}\right]^{\frac{1}{2}} dx = \frac{2E(\Psi,k)}{\sqrt{1-2\alpha}}, \tag{3.39}$$

where $E(\Psi,k)$ is the incomplete elliptic integral of the second kind and

$$\Psi = \sin^{-1}[(x-1)(1-2\alpha)]^{\frac{1}{2}}, \qquad \text{at } x = \frac{1}{1-2\alpha} \quad (k^2 = 2\alpha). \tag{3.40}$$

The frequency of the driven oscillation is

$$\omega = \frac{2\pi}{T} = \frac{\pi\sqrt{1-2\alpha}}{E(\Psi,k)} = \frac{\pi\sqrt{1-2\alpha}}{2E(k)}\omega_p. \tag{3.41}$$

Here $E(k)$ is the complete elliptic integral of the second kind and k is as defined above. The oscillation frequency ω is smaller than ω_p for larger amplitude excitations, i.e., the larger beam density of the driving beam, n_b makes frequency down shift. Because the plasma electron density n is always less than n_0 inside the driving beam, the nonlinearity in the oscillation is due mainly to the relativistic mass increase of the plasma electrons especially for $\alpha \to 1/2$. It causes the serious frequency downshift as shown from Eq. (3.41) in this limit. It means that plasma electrons become ultra-relativistic for $\alpha \to 1/2$. For the second turning point at $\alpha = 1/2$ (or $n_1 = -n_b$),

ULSAN NATIONAL INSTITUTE OF SCIENCE AND TECHNOLOGY

$$\beta = \frac{1-x^2}{1+x^2} = \frac{(1-2\alpha)^2-1}{(1-2\alpha)^2+1} = -1, \qquad \text{for } \alpha = \frac{1}{2}. \tag{3.42}$$

As n_b goes to $n_0/2$, the plasma electron approaches the ultra-relativistic regime and makes turn at $n_1 = -n_b$. The electric field near the turning point at $n_1 = -n_b$ approaches the linear wave-breaking limit. Substituting $\alpha = 1/2$ and $1/x = 0$ into Eq. (3.38), we obtain the result below.

$$E_0 = \frac{mc\omega_p}{e} \simeq 96\sqrt{n_0(\mathrm{cm}^{-3})} \qquad [\mathrm{V/m}]. \tag{3.43}$$

This is the largest electric field obtainable inside the driving beam in the linear wave limit.

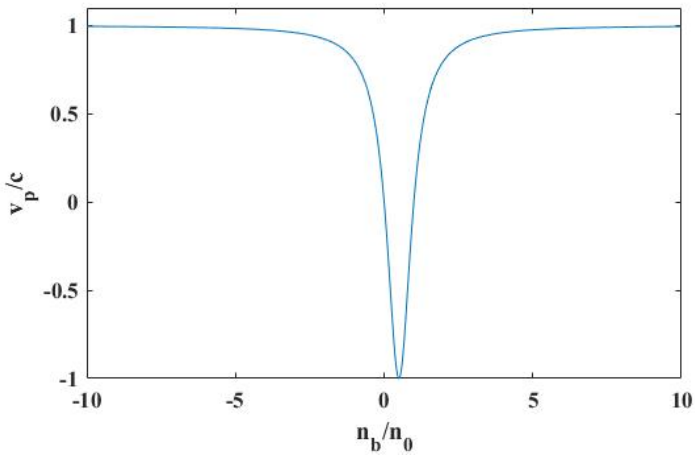

Fig. 3.2. The normalized velocity of plasma electron at the end of the driving beam (the second turning point of $x(\tau)$ $[x'(\tau) = 0]$. At $\alpha = 1/2$, β reaches -1. In the region where it is not satisfied that $|\beta| \ll 1$ or $|\alpha| \ll 1$, the system has nonlinearity. It is the reason that we should have investigated the nonlinearity of the plasma oscillation. The region which is enough to be linearized would be within $|\alpha| \ll 1$.

ULSAN NATIONAL INSTITUTE OF SCIENCE AND TECHNOLOGY

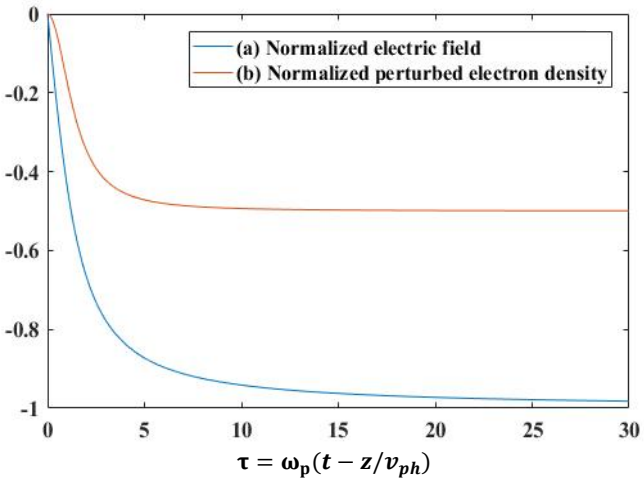

Fig. 3.3. Inhomogeneous solution at $\alpha = 1/2$. Each of (a) $eE_0/mc\omega_p$ and (b) n_1/n_0 asymptotically reaches -1 and -0.5. It lasts until the end of the beam, i.e., $\alpha = 0$. The pictures behind the beam are listed in Refs. [2] and [6], but it is not our interest.

So far, we have investigated the properties of nonlinear oscillation of plasma electron inside the bunch. In the case of the electron beam, when n_b/n_0 goes to $1/2$, β increases up to -1 at the end of the beam. In other words, n_1 reaches $-n_0/2$ and it lasts until the differential equation we have becomes homogeneous, i.e., $0 \leq ct - z \leq l_b$. Behind the beam, solving the homogeneous equation using the continuity of $n_1(\tau)$ and $E(\tau)$, we get the response of plasma behind the beam. However, knowing the response of plasma behind the beam is not our interest. Here what we should note is that $n_1 = -n_0/2$ lasts to the end of the beam. And as remarked above, because the larger beam density causes the more perturbed beam density, the oscillation frequency ω is a function of α and the modulation of the plasma electron density. It can be very unstable in the periodicity. Because we are interested in the condition which SMI will be developed in, then we realize that we don't have to consider the nonlinearity of plasma for our purpose and our study would be in the limit of the linear system. But it is only before the SMI saturates. When the SMI is fully developed, the transition of plasma oscillations into nonlinear regime occurs.

We have assumed the beam density n_b is constant and the time scale of beam envelope evolution is much slower than the responses of plasma (the time scale of ω^{-1}). In Chapter 4, the dynamics of driving beam is briefly discussed, so the self-modulation instability is introduced.

3.6 Simulations of a short beam-driven plasma wakefields using WARP

Referring to Ref. [8] is useful to demonstrate the plasma wakefields driven by the short and charged beams. The optimum condition to resonantly excite the plasma waves is satisfied with $\sigma_r k_p \leq 1$ and $\sigma_z k_p = \sqrt{2}$ of the Gaussian beam profile. But here the former condition $\sigma_r k_p \ll 1$ is not fully satisfied ($\sigma_r k_p \approx 1.4$), where $\sigma_r = \sigma_z = 382$ μm and plasma electron density $n_0 = 3.8\times10^{20}$ m^{-3}.

1) The electron beam driven plasma wakefield at $n_b/n_0 = 0.01$.

When the ratio of driving beam to plasma electron density is $n_b/n_0 \ll 1$, the system is in the linear regime. In this case, the longitudinal component of the wakefield has the trigonometric-like curve along the propagation axis of the beam. And the periodicity of the wake is about λ_p.

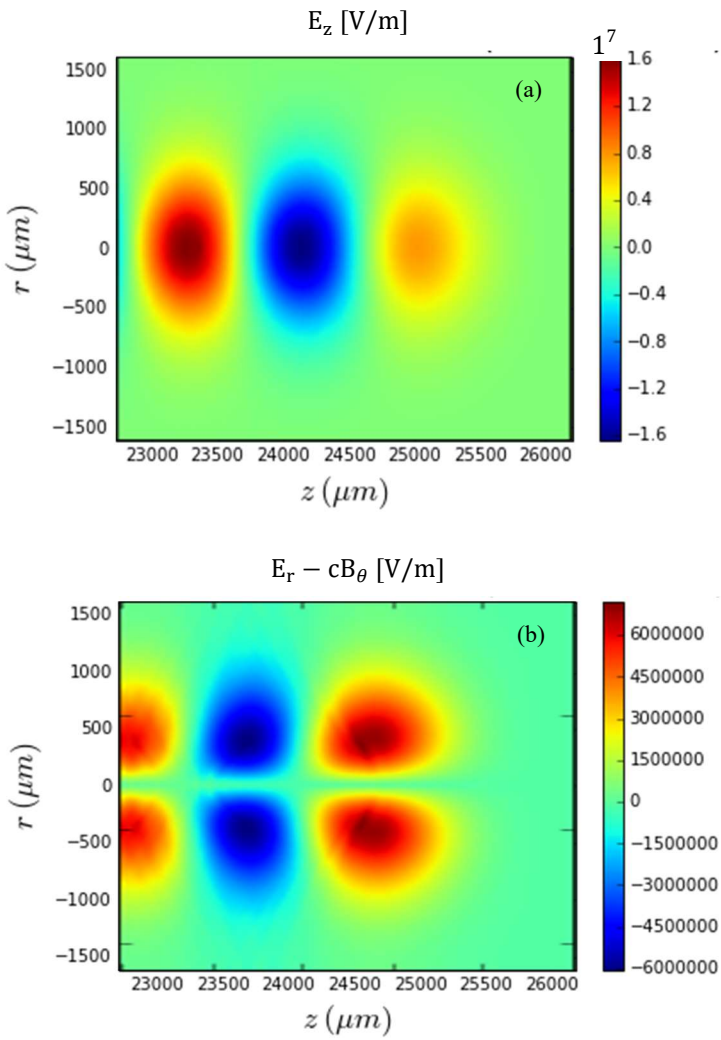

Fig. 3.4. Plasma wakefield driven by a short electron beam at $n_b/n_0 \ll 1$. (a) Longitudinal component of wakefield has trigonometric-like curve along the propagation axis of the beam. (b) By this transverse wakefields, the rear part of the negatively charged driving beam will be focused.

ULSAN NATIONAL INSTITUTE OF SCIENCE AND TECHNOLOGY

2) The electron beam driven plasma wakefield at $n_b/n_0 = 0.35$.

When the ratio of beam density to plasma electron density is $n_b/n_0 = 0.35$, the system is nearly in the nonlinear regime. In this case, we see the steepening of the longitudinal component of the wakefield. It is not like trigonometric curve anymore. 'Plasma bubbles' which are formed by the largely perturbed plasma electrons are observed. Where we call it 'pulling out of the plasma electrons' and in this case the plasma electron density $n = n_0 + n_1$ is not like constant value anymore.

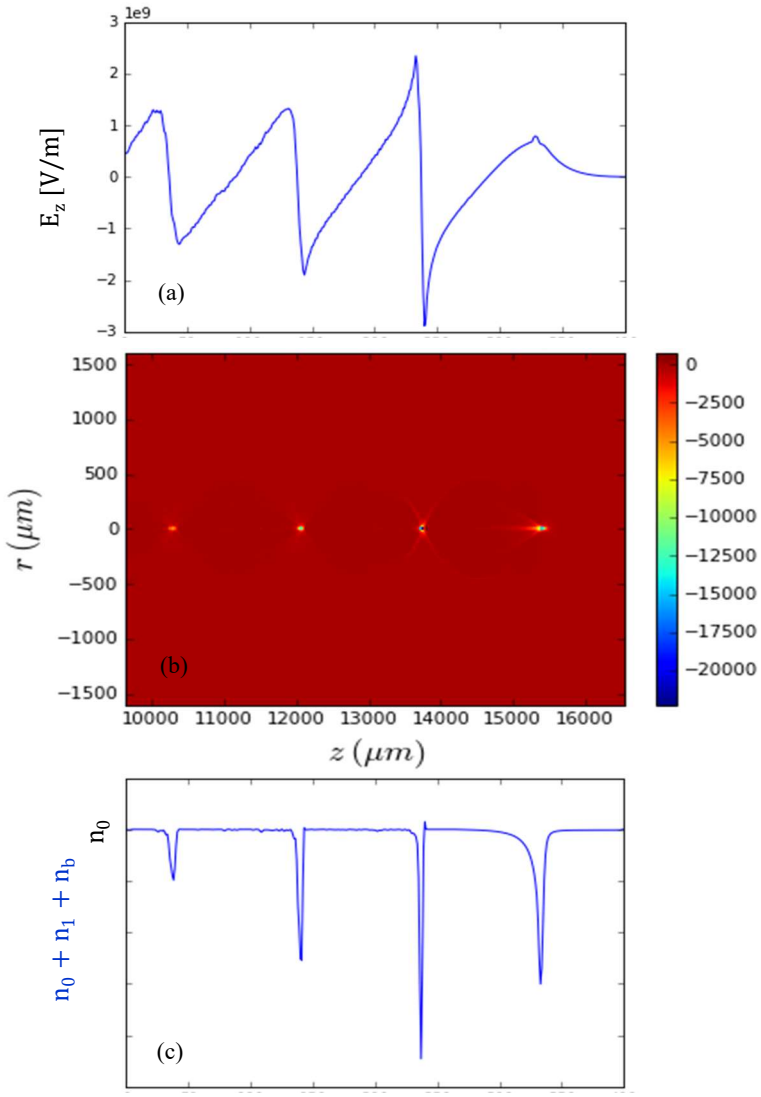

Fig. 3.5. The plasma wakefield driven by a short electron beam at $n_b/n_0 = 0.35$. (a) The longitudinal component of the wakefield has the sawtooth-like curve along the propagation axis of the beam. And the periodicity of the wake is about λ_p. (b), (c) Charge density ρ is depicted. Background plasma electrons are pulled out by repulsive force of the electron beam. Magnitudes of plasma density peaks are very high compared with the equilibrium plasma electron density n_0.

ULSAN NATIONAL INSTITUTE OF SCIENCE AND TECHNOLOGY

4) The proton beam-driven plasma wakefield at $n_b/n_0 = 0.01$.

The proton beam-driven wakefield is analogous to the electron beam-driven case, but here because the driving beam sucks in background plasma electrons, it has phase difference π from the electron beam case. This result corresponds to linear theory of Chapter 3.3.

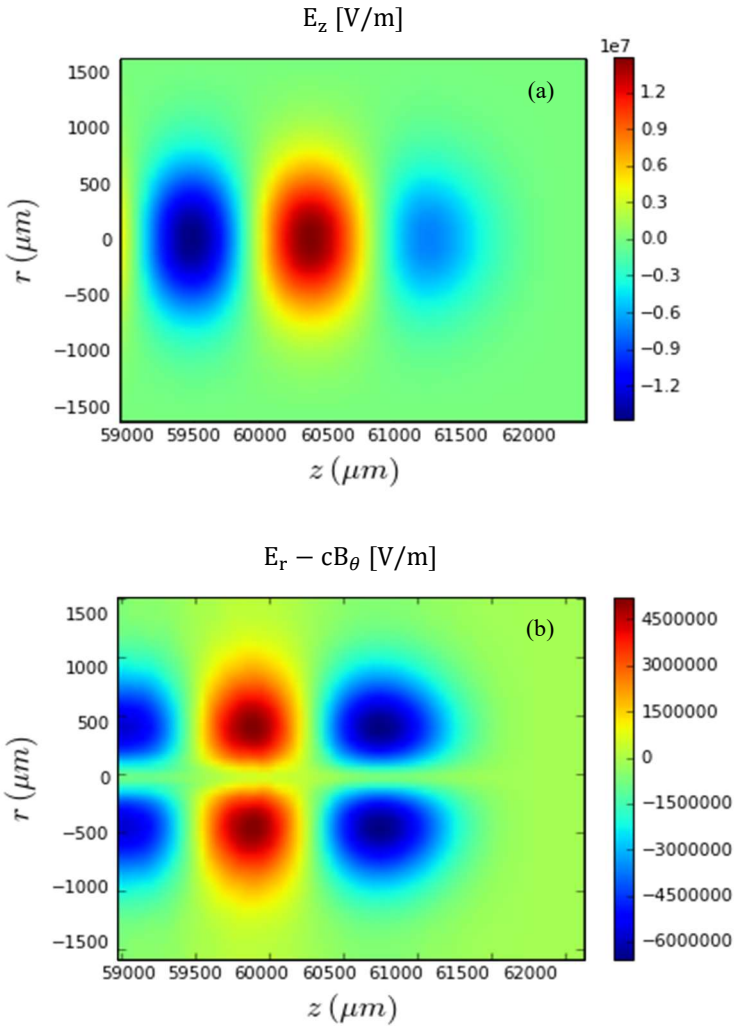

Fig. 3.6. The plasma wakefield driven by a short proton beam at $n_b/n_0 = 0.01$. (a) The longitudinal component of the wakefield has the trigonometric-like curve along the propagation axis of the beam. (b) By this transverse wakefields, the rear part of the positively charged driving beam will be focused.

ULSAN NATIONAL INSTITUTE OF SCIENCE AND TECHNOLOGY

Chapter 4. Self-Modulation Instability of a Long Beam Bunch in Plasmas

The self-modulation of the beam occurs through coupling of the transverse wakefield with the beam radius evolution. Periodic regions of focusing and defocusing modulate the beam density at λ_p, driving a larger plasma density modulation that further focuses the beam periodically. For beams long compared to λ_p, where self-modulation occurs, the instability is enabled by the drive beam dynamics, and therefore the wakefield properties will be strongly affected by the drive beam dynamics [10]. In this chapter, we will see the evolution of the drive beam envelope in time τ and relative beam position ξ. For the analysis, analytical and semi-analytical approaches of the beam-envelope equation are introduced. But the details of derivation of the beam-envelope equation are not explained here. Next, we inspect the coupling of beam centroid offset and radius pinching. These two phenomena are called the hose and self-modulation instability, respectively.

4.1 Analytical approach on the beam-envelope equation

We begin with the analytical theory of the beam self-modulation based on the beam-envelope approach in Ref. [8]. As remarked before, the self-modulation instability or beam radius evolution can arise by the coupling of the transverse wakefield with the beam radius evolution when the drive beam length is longer than plasma wavelength λ_p. Following the approach of Ref. [15], we can write down the two-dimensional expressions for the wakefields of an axisymmetric beam driver of an arbitrary profile by utilizing the Euler variables $\xi = \beta_0 c\tau - z$, where $\beta_0 = v_{b,z}/c$ and $\tau \equiv t$ assuming the quasi-static approximation $(\partial_\tau \simeq 0)$ for the beam driver. Inside the body of a long proton bunch $(0 < \xi < L_b)$, the longitudinal and transverse wakefields are

$$E_z(r,\xi) = 4\pi k_p^2 \int_0^{\xi}\int_0^{\infty} r'dr'\rho(r',\xi')I_0(k_p r_<)K_0(k_p r_>)d\xi' f(\xi')\cos k_p(\xi-\xi') \tag{4.1}$$

and

$$W_\perp(r,\xi) \simeq (E_r - B_\theta)(r,\xi) = 4\pi k_p \int_0^{\xi}\int_0^{\infty} r'dr'\,\partial_{r'}\rho(r',\xi')I_1(k_p r_<)K_1(k_p r_>)d\xi' f(\xi')\sin k_p(\xi-\xi'), \tag{4.2}$$

where $\rho(r,\xi) = \rho_0\psi(r)f(\xi)$ is the beam charge density with the Heaviside step-function profile $\psi(r) = \Theta(r_b - r)$, $I_{0(1)}$ and $K_{0(1)}$ are the modified Bessel functions of order 0(1), $r_< = \min(r,r')$ and $r_> = \max(r,r')$, $k_p = \omega_p/c$ is the background plasma wave number, L_b is the length of the bunch in the $\hat{\mathbf{z}}$ direction, and we have assumed $\beta_0 \approx 1$. Dynamics of the drive beam, especially in ultra-relativistic regime, could be considerably affected by this transverse wakefield $W_\perp$. So, from a precedent study of the general beam-envelope equation theory [16], the equation for the beam envelope for a long proton bunch in the plasma wakefields is written as

ULSAN NATIONAL INSTITUTE OF SCIENCE AND TECHNOLOGY

$$\frac{\partial^2 r_b}{\partial \tau^2} - \frac{\mathcal{M}^2}{r_b^3} = -\frac{\omega_b^2}{\gamma_0}\int_0^{\xi} r_b(\xi')I_1\{k_p r_b(\xi')\}K_1\{k_p r_b(\xi')\}f(\xi')k_p \sin k_p(\xi-\xi')d\xi', \tag{4.3}$$

where $\gamma_0 = (1-\beta_0^2)^{-\frac{1}{2}}$ is the relativistic Lorentz factor of the beam, $\omega_b^2 = 4\pi\rho_0 e/m_b$ is the square of the non-relativistic beam-plasma frequency of the proton bunch, $\rho_0 = n_b e$ is the charge density of the proton bunch, and m_b is the mass of the beam particle. Here $r_b = r_b(\xi)$ is a function of ξ on account of pinching caused by the wakefield on the beam. The constant $\mathcal{M}$ is from the integration of the θ component of the equation of motion for the beam electrons yielding the angular momentum constant, and is associated with the transverse emittance of the beam [16]. For the demonstration of the self-modulation instability of a proton beam, we consider a thin beam $\left[\lim_{k_p r_b \ll 1} I_1\{k_p r_b(\xi')\}K_1\{k_p r_b(\xi')\} \approx 1/2\right]$ with a Heaviside step-function profile $[f(\xi') \equiv \Theta(\xi')]$ and take $\mathcal{M} = \omega_{\beta 0} r_{b0}^2$, where $\omega_{\beta 0}^2 = \omega_b^2/2\gamma_0$ and r_{b0} is the initial radius of the beam. And we normalize the coordinates as $r_b = r_b/r_{b0}$, r_{b0}, , $\tau = \omega_{\beta 0}\tau$, $\xi = k_p\xi$. So, normalized beam-envelope equation is simply written by

$$\frac{\partial^2 r_b(\xi)}{\partial \tau^2} - \frac{1}{r_b^3(\xi)} = -\int_0^{\xi} r_b(\xi')\sin(\xi-\xi')d\xi'. \tag{4.4}$$

Assuming the beam radius is perturbed around the equilibrium radius $[r_b = 1 + \delta r_b]$ and the perturbation term has the phase which corresponds to the plasma wakefields spatially $\left[\delta r_b = \delta\hat{r}_b \exp(i\xi)\right.$ when $\left.|\partial_\xi \delta\hat{r}_b| \ll |\delta\hat{r}_b|\right]$, we get an equation of $\delta\hat{r}_b$ handling the beam-envelope equation (see Appendix. 4.).

$$(\partial_\xi^2 + 1)(\partial_\tau^2 + 3)\delta\hat{r}_b = -\delta\hat{r}_b, \tag{4.5}$$

where we see that $\delta\hat{r}_b$ varies in time and space inside the beam. We assume that there is additional pinching which has any group velocity $\left[\delta\hat{r}_b \sim \exp(i\delta\omega\tau - ik\xi)\right.$, at $\left.k_p \gg k\right]$. So, the dispersion relation of the wave which delivers the pinching inside the beam is obtained as (see Appendix. 4.)

$$D \equiv (k^2 - 1)(\delta\omega^2 - \Delta) = -1, \qquad \Delta \equiv 3. \tag{4.6}$$

For complex $\delta\omega = \delta\omega_r + i\delta\omega_i$, when $\mathrm{Im}(\delta\omega) \to \infty$ [Fig. 4.1(a)], k has real roots.

$$k = \pm \lim_{|\delta\omega|\to\infty} \sqrt{\frac{\delta\omega^2 - (1+\Delta)}{\delta\omega^2 - \Delta}} = \pm 1 \tag{4.7}$$

So, instability is convective $[\delta\hat{r}_b \sim \exp(i\delta\omega\tau \pm i\xi)]$.

ULSAN NATIONAL INSTITUTE OF SCIENCE AND TECHNOLOGY

The dispersion relation gives two complex k roots (one in the upper half and another in the lower half of the complex k plane) for real $\delta\omega = \mathrm{Re}(\delta\omega) = \delta\omega_r$ $\left(\sqrt{\Delta} < \delta\omega < \sqrt{1+\Delta}\right)$ (see Appendix. 4.) [Fig. 4.1(b)]

$$k = ik_i = \pm i\sqrt{\frac{(1+\Delta) - \delta\omega_r^2}{\delta\omega_r^2 - \Delta}}. \tag{4.8}$$

When k is in the upper half of complex plane, the perturbation grows spatially in the $\xi > 0$ direction and when k is in the lower half of complex plane, the perturbation grows spatially in the $\xi < 0$ direction.

$$\delta\hat{r}_b \sim \exp(i\delta\omega\tau - ik\xi) \sim \exp(i\delta\omega\tau - ik_r\xi)\exp(k_i\xi) \text{ with } k_i = \pm\sqrt{\frac{(1+\Delta) - \delta\omega_r^2}{\delta\omega_r^2 - \Delta}}. \tag{4.9}$$

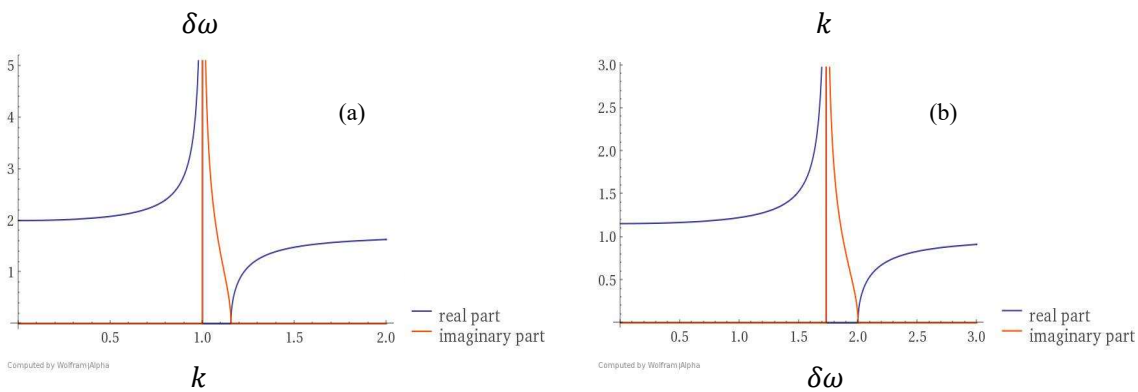

Fig. 4.1 Dispersion relation of the SMI: (a) For $\mathrm{Im}(\delta\omega) \to \infty$, k has real roots (Curves are symmetric in the second quadrant.). So the instability is convective. (b) In $\sqrt{3} < \delta\omega < 2$, k has complex roots (Curves are symmetric in the four'th quadrant.). Only when k is in the upper half of complex plane, the SMI grows.

In this section, the self-modulation instability has been treated as a wave inside the beam. So, it has its own group velocity, and by inspecting the dispersion relation of the instability, we found that the instability could grow up.

ULSAN NATIONAL INSTITUTE OF SCIENCE AND TECHNOLOGY

4.2 Numerical solution of beam envelope equation

Let's assume the beam envelope for a long cylinder-shaped beam density profile. In normalized coordinates, the longitudinal point $k_p\xi = 0$ indicates the beam's head and $k_p\xi = k_pL_b$ indicates the beam's tail. The initial radius of the beam is $r_{b0} = 1$. As remarked before, the normalized envelope equation we have is for the thin beam $[k_p r_b \ll 1]$. Then the boundary conditions are $r_b(\xi, 0) = 1$ and $\partial_\tau r_b(\xi, 0) = 0$.

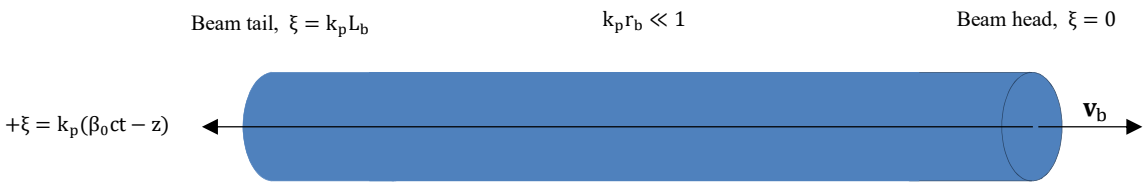

Fig. 4.2 A brief picture for the numerical study of beam envelope equation: The beam is initially cylinder-shaped and has a uniform beam profile. As time goes, it goes through radius evolution.

Reminding (A.4.2),

$$\frac{d^2y(\xi,\tau)}{d\xi^2} + y(\xi,\tau) = r_b(\xi,\tau),$$
$$\frac{\partial^2 r_b(\xi,\tau)}{\partial\tau^2} + \frac{1}{r_b^3(\xi,\tau)} = -y(\xi,\tau), \qquad \text{(A.4.2)}$$

we solve the beam envelope-equation numerically. As remarked above, the Self-modulation instability becomes larger as increasing ξ and τ. Because we normalized the coordinates, the distance between nearest two peaks should be about 2π. Here the beam length is $62.8 \approx 10\times 2\pi$ and the number of modulated beam peaks is 10. The numerical result of radius evolution in time is listed below.

ULSAN NATIONAL INSTITUTE OF SCIENCE AND TECHNOLOGY

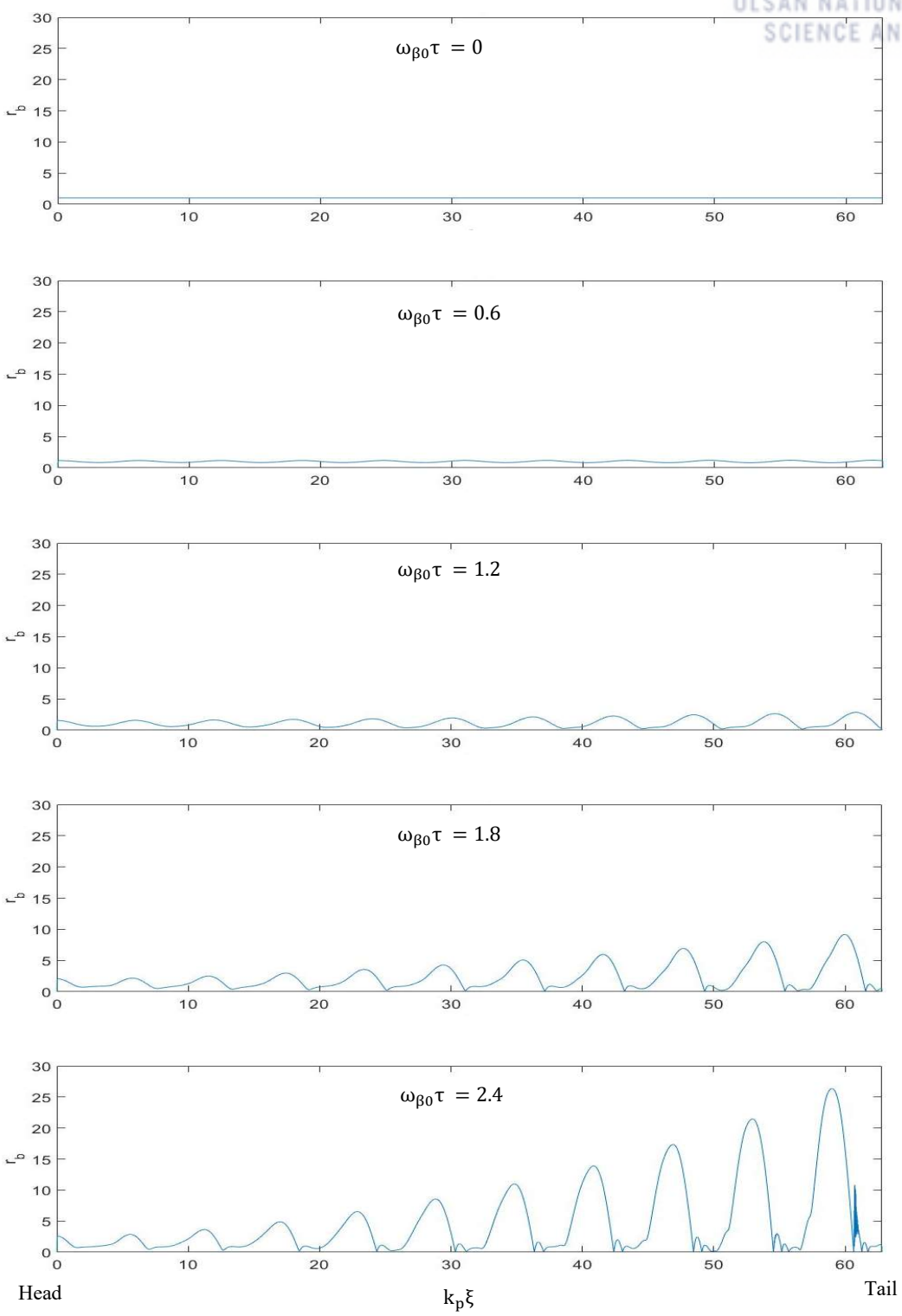

Fig. 4.3 The beam radius evolution in time with beam-envelope equation: The time and beam position coordinates are normalized as beam-envelope equation was. The self-modulation instability grows as time goes and in the direction which ξ increases. The beam length is $62.8 \approx 10\times 2\pi$ and the number of modulated beam peaks is 10.

ULSAN NATIONAL INSTITUTE OF SCIENCE AND TECHNOLOGY

4.3 Coupled beam hose and self-modulation instabilities and their growth rates

As we have seen, transverse stability of the drive beam is critical to plasma wakefield accelerators. A long, relativistic particle beam propagating in an overdense plasma is subject to beam envelope modulation and centroid displacement instabilities. The beam envelope modulation is about the self-modulation instability. The latter one is called hose instability. Referring to Refs. [9,10], the equation for the centroid displacement instability is

$$\frac{d^2x_c}{dz^2} = \frac{k_b^2}{\gamma}\frac{I_1(r_b)}{r_b}\int_{\infty}^{\zeta} d\zeta' \sin(\zeta-\zeta')\frac{r_{b0}^2}{r_b(\zeta')}K_1\big(r_b(\zeta')\big)[x_c(\zeta')-x_c(\zeta)], \tag{4.10}$$

and similarly, the equation for the beam envelope modulation instability is

$$\frac{d^2r_b}{dz^2} - \frac{\epsilon^2}{r_b^3} = -\frac{k_b^2}{\gamma}\frac{4I_2(r_b)}{r_b}\int_{\infty}^{\zeta} d\zeta' \sin(\zeta-\zeta')\frac{r_{b0}^2}{r_b(\zeta')}K_1\big(r_b(\zeta')\big), \tag{4.11}$$

where $\zeta = k_p(z-\beta_b t)$ is the normalized comoving variable with the plasma wavenumber $k_p = \frac{\omega_p}{c}$ and $\beta_b = \frac{v_b}{c}$, x_c is the averaged centroid offset of any slice of the beam, $k_b^2 = \frac{4\pi\hat{n}_b e^2}{M_b c^2}$ is the square beam wavenumber, M_b is the mass of the beam particle, γ is Lorentz factor, $I_{1(2)}$ and K_1 are modified bessel function, r_b is the beam radius, and ϵ is the geometric emittance. Note that here the beam-envelope equation is not exactly same as Eq. (4.3) and the beam radius evolution couples to the centroid evolution. Obviously, the centroid evolution at any slice ζ is affected by the radius evolution. From these theories, assuming a slowly varying envelope $\left[r_1 = \frac{\hat{r}\exp(ik_p\zeta)}{2} + \text{c.c. with } |\partial_\zeta \hat{r}| \ll |k_p\hat{r}|\right]$ and the strongly coupled regime where the growth length of the instability is short compared to $\sqrt{\gamma}k_b^{-1}$ $[|\partial_{\hat{z}}\hat{r}| \gg 2\kappa|\hat{r}|]$, the asymptotic solution of the beam envelope modulation is written by

$$r_1 = \delta r\left[\frac{3^{\frac{1}{4}}}{\sqrt{8\pi}}\right]\frac{e^{N_{smi}}}{\sqrt{N_{smi}}}\cos\left(\frac{\pi}{12} - k_p\zeta - \frac{N_{smi}}{\sqrt{3}}\right), \tag{4.12}$$

where the number of e-folds of the self-modulation instability is

$$N_{smi} = \frac{3^{\frac{3}{2}}}{4}\left(\nu\frac{n_{b0}m_e}{n_0 M_b\gamma}\zeta z^2\right)^{\frac{1}{3}}, \tag{4.13}$$

where $\nu = 4I_2(k_p r_0)K_2(k_p r_0)$, n_{b0} is the initial beam peak density, and n_0 is the equilibrium background plasma density.

ULSAN NATIONAL INSTITUTE OF SCIENCE AND TECHNOLOGY

Again, assuming the beam envelope is non-evolving $[r_b = r_0 = \text{constant}]$, i.e., for a rigid beam approximation, the asymptotic solution of the centroid evolution is written by

$$x_c = \delta x_c \left[\frac{3^{\frac{1}{4}}}{\sqrt{8\pi}}\right] \frac{e^{N_h}}{\sqrt{N_h}} \cos\left(\frac{\pi}{12} - k_p\zeta - \frac{N_h}{\sqrt{3}}\right), \tag{4.14}$$

where the number of e-folds of the hose instability is

$$N_h = \frac{3^{\frac{3}{2}}}{4}\left(\mu \frac{n_{b0} m_e}{n_0 M_b \gamma} \zeta z^2\right)^{\frac{1}{3}}, \tag{4.15}$$

where $\mu = 2I_1(k_p r_0)K_1(k_p r_0)$. So, comparing the hosing growth rate to the self-modulation instability growth rate,

$$\frac{N_h}{N_{smi}} = \left(\frac{\mu}{2\nu}\right)^{\frac{1}{3}} \sim 1, \tag{4.16}$$

and in the narrow beam limit $[k_p r_0 \ll 1]$,

$$\frac{N_h}{N_{smi}} \sim 0.8. \tag{4.17}$$

We note that **i)** both of the two instabilities exponentially grow in the direction $\zeta > 0$. **ii)** Eq. (4.10) indicates that a beam tilt or non-uniform head-to-tail displacement with respect to the beam propagation direction $x_c(\zeta) \neq x_c(\zeta')$ is required for the hose instability. **iii)** Seeding of the self-modulation instability interrupts the growth of the hose instability [10].

Note that the envelope equation is defined in a little different form by Refs. [8,9] and their growth rates are not exactly same to each other.

ULSAN NATIONAL INSTITUTE OF SCIENCE AND TECHNOLOGY

4.4 Transverse equilibrium and stability of the primary beam in plasma

When the driving beam propagates in plasmas, beam space charge, self-induced magnetic field, background plasma ions and electrons affect the transverse dynamics of the driving beam. For $n_b < n_0$, the plasma electrons neutralize the beam space charge $[E_r = 0 \text{ with } k_p r_b < 1]$. Referring to Ref. [11], transverse equilibrium and stability of the primary beam in over-dense plasma is written by

$$R_{eq}^2 = \frac{4\epsilon_{n,RMS}^2}{\beta\gamma_b}\frac{mc^3}{e|I_b|}\left\{1 - 2\left(\frac{R_{eq}\omega_p}{c}\right)^2\left[1 - \exp\left(-\frac{c^2}{\omega_p^2 R_{eq}^2}\right)\right]\right\}^{-1}, \tag{4.18}$$

and for the narrow beam $[k_p r_b \ll 1]$,

$$R_{eq} = 2\epsilon_{n,RMS}\left(\frac{mc^3}{\beta\gamma_b e|I_b|}\right)^{\frac{1}{2}}. \tag{4.19}$$

Equations (4.18) and (4.19) describe a balance between the focusing of the self-magnetic field of the beam and the beam emittance, with the result that R_{eq} decreases as $|I_b|$ increases. The beam density can vary significantly versus both the beam position coordinates ζ and time τ as a result of the radial mismatch oscillations. The mismatched beam which damps to an approximate equilibrium state would produce a smaller wakefield than a matched beam with larger radius and emittance. In other words, the wakefield is reduced by the temporal and spatial fluctuations in the beam density. To circumvent the radial mismatch oscillations, we should be able to control the emittance of the beam. For an ultra-relativistic beam passing through a plasma in z direction, (assuming $\beta_0 \simeq 1$), the invariant of transverse momentum is

$$\begin{aligned} p_{x,lab} = \gamma_0 m_0 v_{x,lab} = p_{x,beam} = m_0 v_{x,beam}, \\ \gamma_0 v_{x,lab} = v_{x,beam}, \end{aligned} \tag{4.20}$$

and the relation between transverse temperature and emittance [12] is

$$\begin{aligned} k_b T_{beam,x} = m_0\langle v_{th,x,beam}^2\rangle = m_0\gamma_0^2\langle v_{th,x,lab}^2\rangle = m_0\gamma_0^2(\beta_0 c)^2\langle x_{th,x,lab}'^2\rangle, \\ = m_0(\gamma_0\beta_0 c)^2\gamma_x\varepsilon_{x,rms} = m_0\gamma_0\beta_0 c^2\gamma_x\varepsilon_{x,N}. \end{aligned} \tag{4.21}$$

By above equations, the equation of the normalized thermal electron momentum with respect to the normalized emittance and other parameters is written by

$$u_{th,x} = \gamma_0\frac{\sqrt{\langle v_{th,x,lab}^2\rangle}}{c} = \sqrt{\gamma_0\beta_0\gamma_x\varepsilon_{x,N}} \simeq \sqrt{\frac{\gamma_0\varepsilon_{x,N}}{\beta_x}}, \tag{4.22}$$

where $u_{th,x}$ is the normalized electron momentum from the transverse thermal kinetic energy.

4.5 Simulations of a long beam-driven plasma wakefields using WARP

In this section, we see that how the theories of self-modulation and hose instabilities show up with the PIC code WARP. Most of the beam parameters are from the Brookhaven National Laboratory Accelerator Test Facility (ATF), and in the last part, we see the self-modulation instability using the parameters of the Injector Test Facility (ITF) of Pohang Accelerator Laboratory (PAL).

Perturbation of beam slice's centroid of non-ideal axisymmetric smooth beam (Hose instability)

Without any seeding of self-modulation instability, the beam centroid evolution is dominant. The beam generates the asymmetric instability, so induced plasma wakefields are also asymmetric.

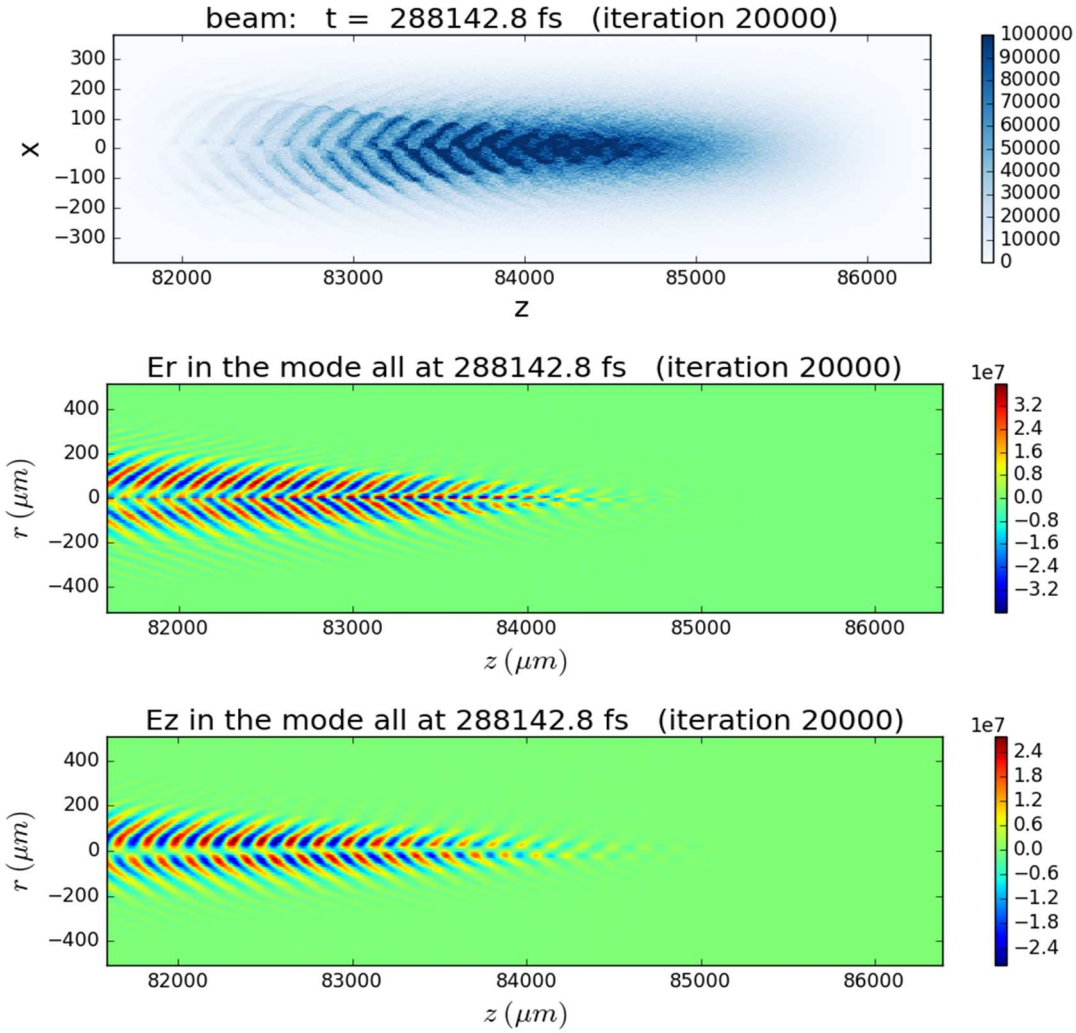

Fig. 4.4. The hose instability of smooth electron beam with ATF beam parameters: Here plasma electron density is $n_0 = 4.2e+22\ [m^{-3}]$, beam energy is 58 MeV ($\gamma_0 = 114$), rms transverse momentum spread is $\sqrt{\langle p_\perp^2 \rangle}/m_b c = 8.6\times10^{-3}$, transverse rms beam size is $\sigma_r = 120\ \mu m$, longitudinal rms beam size is $\sigma_z = 960\ \mu m$, beam density profile is $n_b = n_{b0}\left[1+\cos\left(\sqrt{\frac{\pi}{2}}\frac{z+\sigma_z\sqrt{2\pi}}{\sigma_z}\right)\right]e^{-\frac{r^2}{2\sigma_r^2}}$, initial beam density peak is $n_{b0} = 3.6e+18\ [m^{-3}]$, beam length is $L_b = 2\sigma_z\sqrt{2\pi}$, and total beam charge is $Q = 250\ pC$.

ULSAN NATIONAL INSTITUTE OF SCIENCE AND TECHNOLOGY

Perturbation of beam slice's radius of non-ideal axisymmetric half-cut electron beam (Self-modulation instability)

With the seeding of self-modulation instability, such as half-cut beam, the beam radius evolution is dominant. The beam generates the axisymmetric instability and wakefields. The wakefields are larger than those of the case in the hose instability.

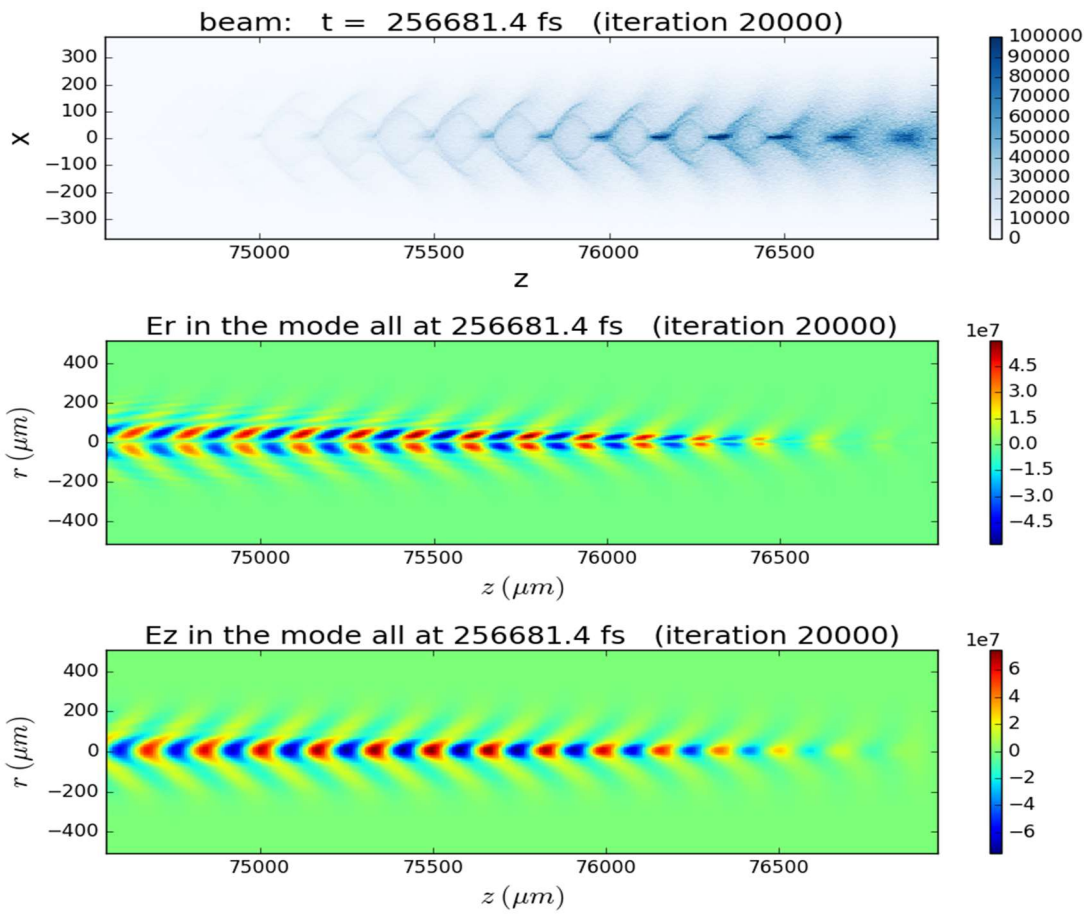

Fig. 4.5. The self-modulation instability of half-cut electron beam with ATF beam parameters: Here plasma electron density is $n_0 = 4.2e + 22\ [m^{-3}]$, beam energy is 58 MeV ($\gamma_0 = 114$), rms transverse momentum spread is $\sqrt{\langle p_\perp^2 \rangle}/m_b c = 8.6\times10^{-3}$, transverse rms beam size is $\sigma_r = 120\ \mu m$, longitudinal rms beam size is $\sigma_z = 960\ \mu m$, beam density profile is $n_b = n_{b0}\left[1 + \cos\left(\sqrt{\frac{\pi}{2}}\frac{z+\sigma_z\sqrt{2\pi}}{\sigma_z}\right)\right] e^{-\frac{r^2}{2\sigma_r^2}}$, initial beam density peak is $n_{b0} = 3.6e + 18\ [m^{-3}]$, beam length is $L_b = \sigma_z\sqrt{2\pi}$, and total beam charge is $Q = 125\ pC$.

Self-modulation instability with varying plasma densities

Because a long driving beam which excites the plasma waves along the beam propagation direction will be modulated into many micro-bunches whose lengths are in the order of λ_p. The number of modulated beam density peaks varies with plasma density. In the numerical examples presented here, the propagation distances of beams in plasmas are all about 10 cm.

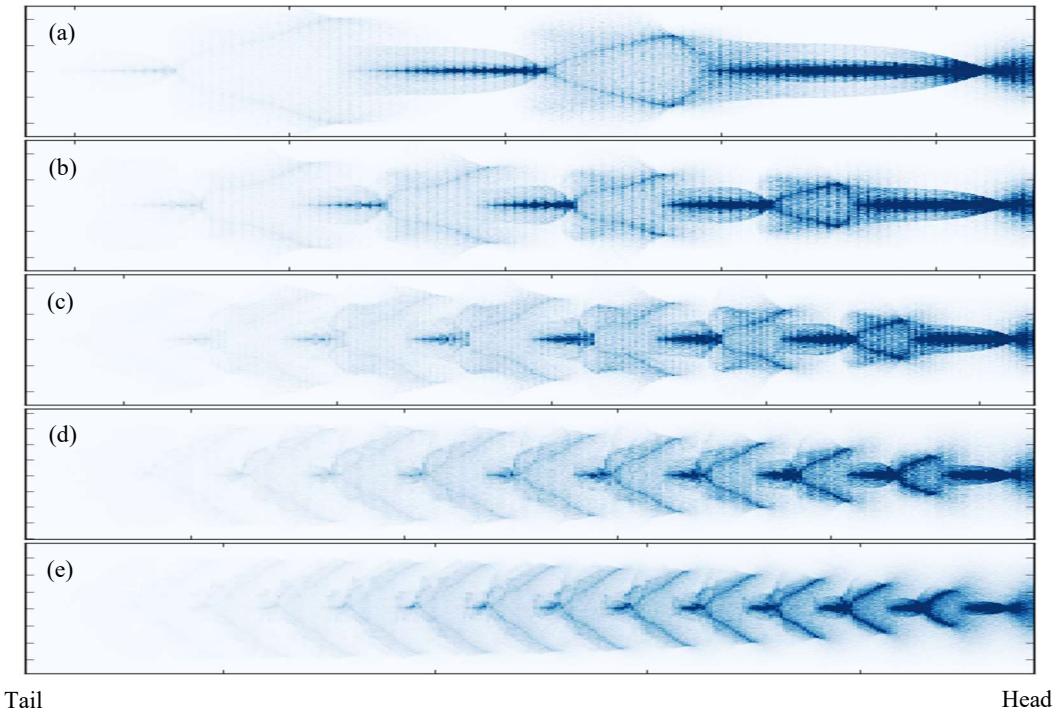

Fig. 4.6. The self-modulation instability of half-cut electron beam with ATF beam parameters in varying plasma densities: The number of modulated bunches increases as increasing plasma density. Here plasma electron density is $n_0 = 1.8e+21\ [m^{-3}] \sim 4.2e+22\ [m^{-3}]$, $\frac{L_b}{\lambda_{pe}} =$ (a) 3, (b) 6, (c) 9, (d) 12, (e) 15, beam energy is 58 MeV ($\gamma_0 = 114$), rms transverse momentum spread is $\sqrt{\langle p_\perp^2 \rangle}/m_b c = 8.6\times10^{-3}$, transverse rms beam size is $\sigma_r = 120\ \mu m$, longitudinal rms beam size is $\sigma_z = 960\ \mu m$, beam density profile is $n_b = n_{b0}\left[1+\cos\left(\sqrt{\frac{\pi}{2}}\frac{z+\sigma_z\sqrt{2\pi}}{\sigma_z}\right)\right]e^{-\frac{r^2}{2\sigma_r^2}}$, initial beam density peak is $n_{b0} = 3.6e+18\ [m^{-3}]$, beam length is $L_b = \sigma_z\sqrt{2\pi}$, and total beam charge is $Q = 125\ pC$.

ULSAN NATIONAL INSTITUTE OF SCIENCE AND TECHNOLOGY

Perturbation of beam slice's radius of non-ideal axisymmetric half-cut proton beam (Self-modulation instability)

According to Ref. [10], because the number of exponentiation of SMI is $\sim(n_{b0}\zeta z^2)^{\frac{1}{3}}(n_0 M_b \gamma_0)^{-\frac{1}{3}}$ and $m_p \approx 1836 m_e$, when other parameters were fixed, the proton beam propagating in plasma takes 43 times longer distance to get the exponentiation of the electron beam case. So, here using $\gamma_0 = 25$ is more useful. It is 0.22 times of the electron beam case of this study.

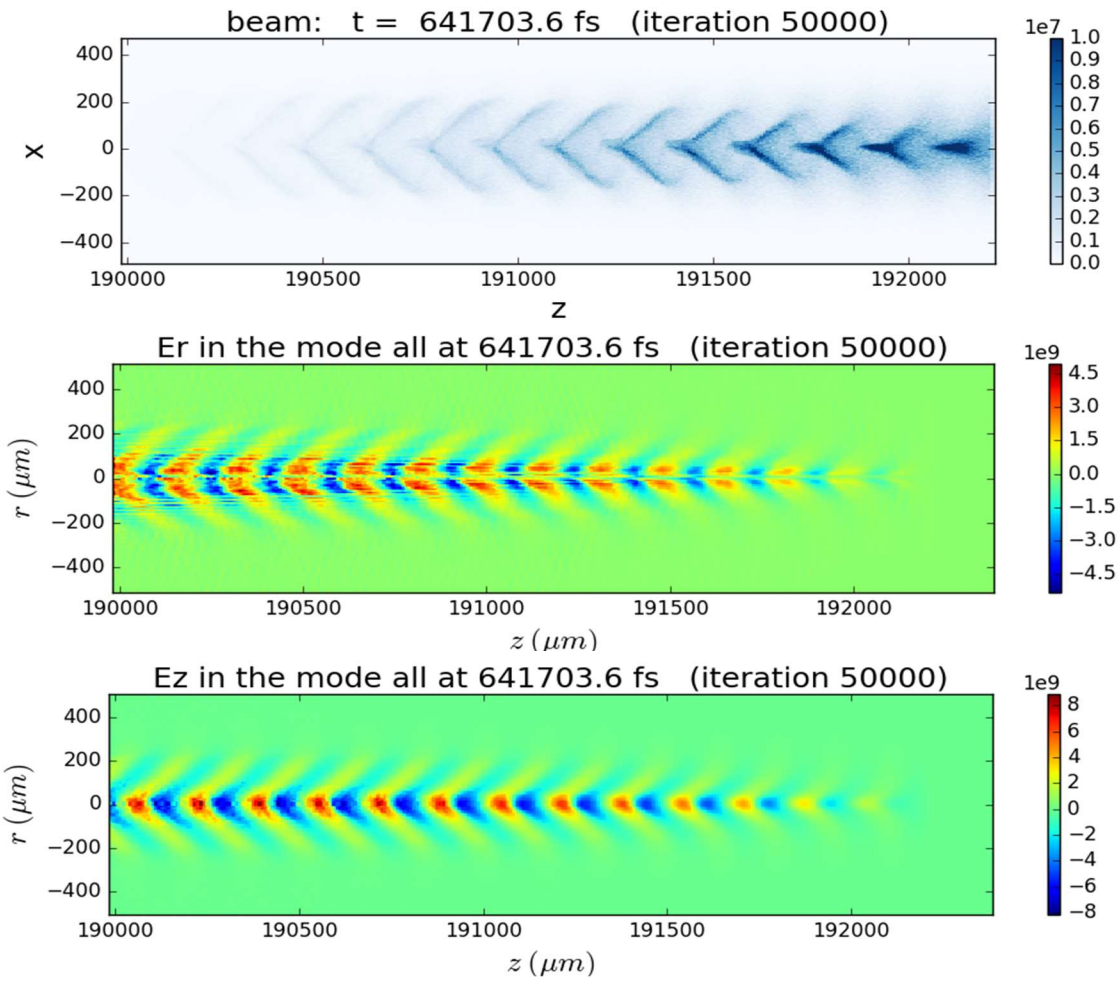

Fig. 4.7 The self-modulation instability of half-cut proton beam with ATF beam parameters: Here plasma electron density is $n_0 = 4.2e + 22\ [m^{-3}]$, beam energy is 24 GeV ($\gamma_0 = 25$), rms transverse momentum spread is $\sqrt{\langle p_\perp^2 \rangle}/m_b c = 4.5\times10^{-3}$, transverse rms beam size is $\sigma_r = 120\ \mu m$, longitudinal rms beam size is $\sigma_z = 960\ \mu m$, beam density profile is $n_b = n_{b0}\left[1 + \cos\left(\sqrt{\frac{\pi}{2}}\frac{z+\sigma_z\sqrt{2\pi}}{\sigma_z}\right)\right] e^{-\frac{r^2}{2\sigma_r^2}}$, initial beam density peak is $n_{b0} = 3.6e + 18\ [m^{-3}]$, beam length is $L_b = \sigma_z\sqrt{2\pi}$, and total beam charge is $Q = 125\ pC$.

ULSAN NATIONAL INSTITUTE OF SCIENCE AND TECHNOLOGY

The longitudinal accelerating and transverse focusing fields of Self-Modulated electron bunches (ATF)

The longitudinal accelerating and transverse focusing fields of the self-modulated electron bunches are depicted in Fig. 4.8. Here the red curve of the third graph in Fig. 4.8 is showing the density of plasma electrons and driving beam together. We see that at the places where perturbed plasma electron density has positive value, the electron beam is defocused and at the places where perturbed plasma electron density has negative value, the electron beam is focused. The instability grows up with wakefields in the direction from beam's head to tail.

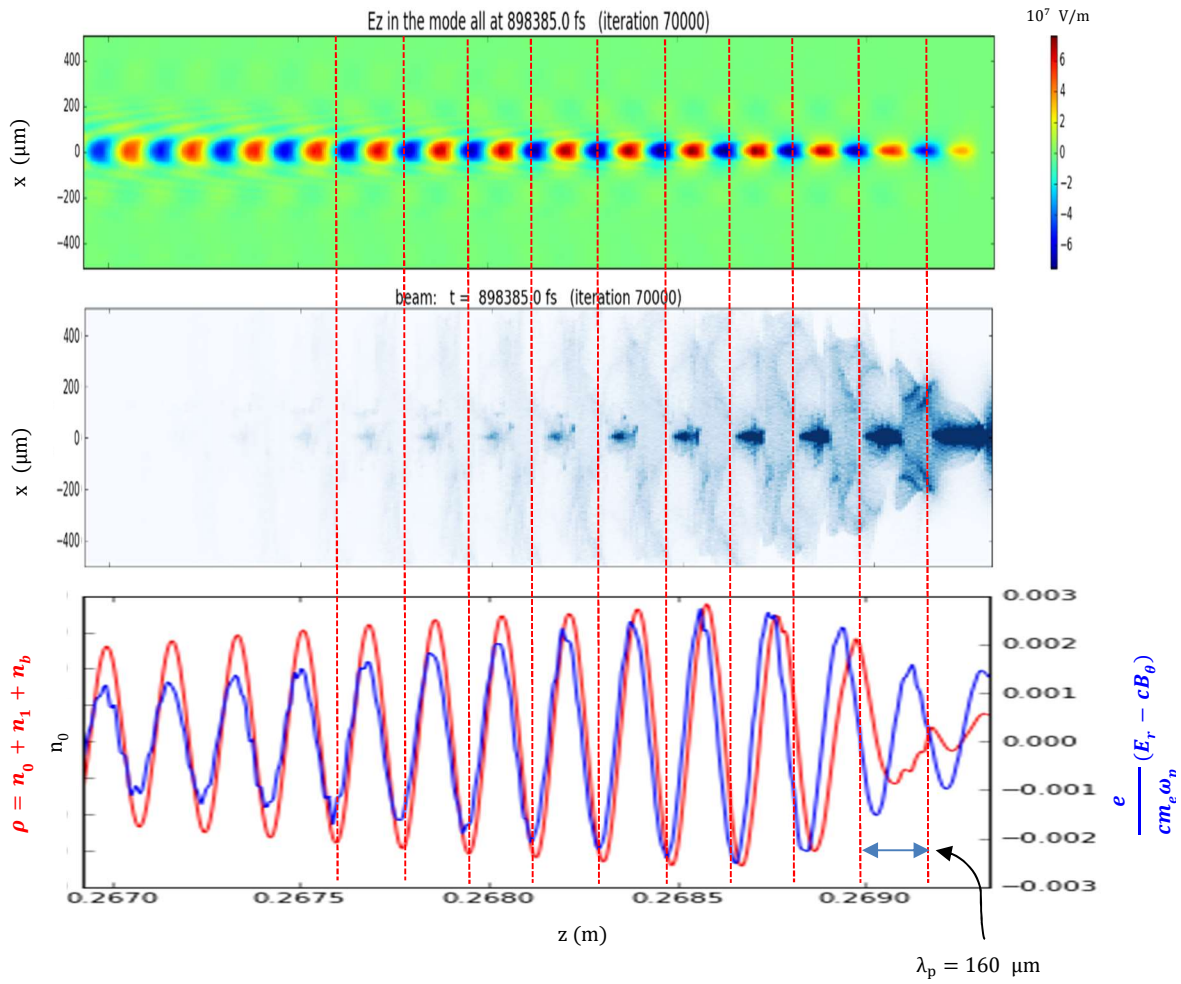

Fig. 4.8. The self-modulation instability of half-cut electron beam with ATF beam parameters: Here plasma electron density is $n_0 = 4.2e + 22\ [m^{-3}]$, beam energy is 58 MeV $(\gamma_0 = 114)$, rms transverse momentum spread is $\sqrt{\langle p_\perp^2 \rangle}/m_b c = 8.6\times10^{-3}$, transverse rms beam size is $\sigma_r = 120\ \mu m$, longitudinal rms beam size is $\sigma_z = 960\ \mu m$, beam density profile is $n_b = n_{b0}\left[1 + \cos\left(\sqrt{\frac{\pi}{2}}\frac{z+\sigma_z\sqrt{2\pi}}{\sigma_z}\right)\right] e^{-\frac{r^2}{2\sigma_r^2}}$, initial beam density peak is $n_{b0} = 3.6e + 18\ [m^{-3}]$, beam length is $L_b = \sigma_z\sqrt{2\pi}$, and total beam charge is $Q = 125$ pC.

Because the parameters of ITF beam are quite similar to those of the ATF, Ref. [13] is good reference for studying SMI with ITF beam parameters. So, we could build the experimental setup of SMI at PAL.

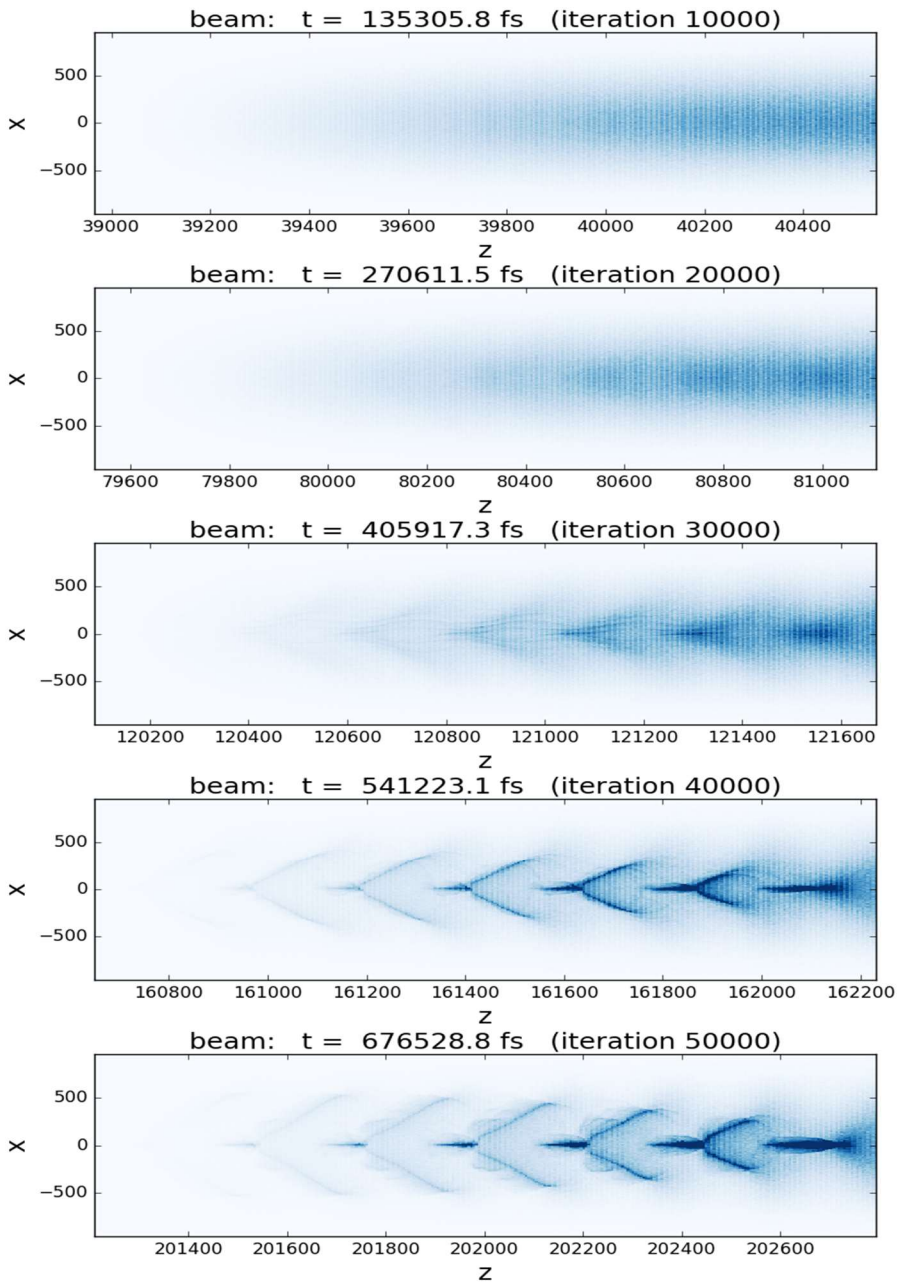

Fig. 4.9. The self-modulation instability of half-cut electron beam with ITF beam parameters: Here plasma electron density is $n_0 = 2.5e + 22\ [m^{-3}]$, beam energy is 60 MeV $(\gamma_0 = 114)$, rms transverse momentum spread is $\sqrt{\langle p_\perp^2 \rangle}/m_b c = 2.4\times10^{-3}$, transverse rms beam size is $\sigma_r = 318\ \mu m$, longitudinal rms beam size is $\sigma_z = 637\ \mu m$, beam density profile is $n_b = n_{b0}\left[1 + \cos\left(\sqrt{\frac{\pi}{2}}\frac{z+\sigma_z\sqrt{2\pi}}{\sigma_z}\right)\right] e^{-\frac{r^2}{2\sigma_r^2}}$, initial beam density peak is $n_{b0} = 3.6e + 18\ [m^{-3}]$, beam length is $L_b = \sigma_z\sqrt{2\pi}$, and total beam charge is $Q = 580\ pC$.

ULSAN NATIONAL INSTITUTE OF SCIENCE AND TECHNOLOGY

5. Summary and future works

In this thesis, the fundamental concepts of beam-driven plasma wakefield are introduced. So, the self-modulation instability of a long charged particle beam can be described. Here we use the PIC code WARP to check which the theories are properly described. Although in this thesis, any quantitative approaches are not covered explicitly, referring references especially for the simulation result from warp, we find out that the results are quite reasonable.

A beam bunch propagating through plasma excites the plasma wakefield at some conditions. The optimum wake is obtained for $k_p\sigma_z = 2^{\frac{1}{2}}$ and $k_p\sigma_r \leq 1$. Where k_p is plasma wave number and σ_z (or σ_r) is RMS beam length (or RMS beam radius). But we are interested in using CERN's long and high-energy proton beams. The CERN's proton beams are much longer (~ 12 cm) than the optimum driving beam length (in order of plasma wavelength λ_p). Here we focus on the instability which occurs based on the interaction between beam and plasma electrons. By this instability, the long driving beam is modulated along the propagation direction, so it makes the beam satisfy the optimum size for excitation of plasma waves. What we should know is that the plasma oscillation which is initially and axi-symmetrically excited by beam head seed self-modulation of driving beam. Evolution of beam envelope in time could result in beam centroid offset or radius pinching. Where the two phenomena, centroid offset and radius pinching of the beam in plasma are called 'Self-modulation instability' and 'Hose instability'. Those two instabilities compete each other. As the last step, the parameters of Injector Test Facility (ITF) at Pohang Accelerator Laboratory (PAL) was used to demonstrate the self-modulation instability.

But in this thesis, there are a few results and concepts to be studied in the quantitative ways more. i) How the beam mismatching of the beam in plasma would affect the instabilities and wakefields, ii) why the self-modulated long proton beam in plasma make wakefields stronger than those of electron beam case when only those beam particle species are different, and iii) the detailed organization of variation of growth rates with comparing the theories and the result of PIC code are those.

ULSAN NATIONAL INSTITUTE OF SCIENCE AND TECHNOLOGY

6. Appendix

6.1 Fundamental equations

Maxwell's equations

	Gaussian units	SI units
Gauss's law (macroscopic)	$\nabla \cdot \mathbf{D} = 4\pi\rho_f$	$\nabla \cdot \mathbf{D} = \rho_f$
Gauss's law (microscopic)	$\nabla \cdot \mathbf{E} = 4\pi\rho_f$	$\nabla \cdot \mathbf{E} = \frac{\rho_f}{\epsilon_0}$
Gauss's law for magnetism	$\nabla \cdot \mathbf{B} = 0$	$\nabla \cdot \mathbf{B} = 0$
Maxwell-Faraday equation	$\nabla \times \mathbf{E} = -\frac{1}{c}\frac{\partial \mathbf{B}}{\partial t}$	$\nabla \times \mathbf{E} = -\frac{\partial \mathbf{B}}{\partial t}$
Ampere-Maxwell equation (macroscopic)	$\nabla \times \mathbf{H} = \frac{4\pi}{c}\mathbf{J}_f + \frac{1}{c}\frac{\partial \mathbf{D}}{\partial t}$	$\nabla \times \mathbf{H} = \mathbf{J}_f + \frac{\partial \mathbf{D}}{\partial t}$
Ampere-Maxwell equation (microscopic)	$\nabla \times \mathbf{B} = \frac{4\pi}{c}\mathbf{J} + \frac{1}{c}\frac{\partial \mathbf{E}}{\partial t}$	$\nabla \times \mathbf{B} = \mu_0\mathbf{J} + \frac{1}{c^2}\frac{\partial \mathbf{E}}{\partial t}$

Basic laws of electromagnetism

	Gaussian units	SI units
Lorentz force	$\mathbf{F} = q\left(\mathbf{E} + \frac{1}{c}\mathbf{v} \times \mathbf{B}\right)$	$\mathbf{F} = q(\mathbf{E} + \mathbf{v} \times \mathbf{B})$
Coulomb's law	$\mathbf{F} = \frac{q_1 q_2}{r^2}\hat{\mathbf{r}}$	$\mathbf{F} = \frac{1}{4\pi\epsilon_0}\frac{q_1 q_2}{r^2}\hat{\mathbf{r}}$
Electric field of stationary point charge	$\mathbf{E} = \frac{q}{r^2}\hat{\mathbf{r}}$	$\mathbf{E} = \frac{1}{4\pi\epsilon_0}\frac{q}{r^2}\hat{\mathbf{r}}$
Biot-Savart law	$\mathbf{B} = \frac{1}{c}\oint \frac{I d\mathbf{l} \times \hat{\mathbf{r}}}{r^2}$	$\mathbf{B} = \frac{\mu_0}{4\pi}\oint \frac{I d\mathbf{l} \times \hat{\mathbf{r}}}{r^2}$

Vector and scalar potentials

	Gaussian units	SI units
Electric field (static)	$\mathbf{E} = -\nabla\phi$	$\mathbf{E} = -\nabla\phi$
Electric field (general)	$\mathbf{E} = -\nabla\phi - \frac{1}{c}\frac{\partial \mathbf{A}}{\partial t}$	$\mathbf{E} = -\nabla\phi - \frac{\partial \mathbf{A}}{\partial t}$
Magnetic field	$\mathbf{B} = \nabla \times \mathbf{A}$	$\mathbf{B} = \nabla \times \mathbf{A}$

ULSAN NATIONAL INSTITUTE OF SCIENCE AND TECHNOLOGY

6.2 Derivation and solving of differential equations from the body

A. 1

1.1

$$\partial_t n_{p1} + n_{p0}\boldsymbol{\nabla}\cdot\mathbf{v}_{p1} = 0$$
$$\partial_t \mathbf{v}_{p1} \simeq -\frac{e}{m}\left(\mathbf{E}_{p1} + \mathbf{E}_{b1}\right) = -\frac{e}{m}\mathbf{E}_1 \tag{A.1.1}$$

$$\rho(\mathbf{x}) = -e n_{p1}(\mathbf{x}) - Q\delta(\mathbf{x} - \mathbf{x_0}),$$
$$\vec{J}_1(\mathbf{x}) = -e n_{p0}\mathbf{v}_{p1}(\mathbf{x}) - Q\mathbf{v}_b\delta(\mathbf{x} - \mathbf{x}_0), \tag{A.1.2}$$

$$\nabla^2\phi_1 = -4\pi\rho_1$$
$$\nabla_\perp^2\mathbf{A}_1 - \frac{1}{c^2}\partial_t^2\mathbf{A}_1 = -\frac{4\pi}{c}\mathbf{J}_1 - \frac{1}{c}\boldsymbol{\nabla}\,\partial_t\phi_1 \tag{A.1.3}$$

$$\nabla^2\phi_1 = -4\pi\rho_1 = -4\pi\left(-e n_{p1}(\mathbf{x}) - Q\delta(\mathbf{x} - \mathbf{x}_0)\right)$$
$$\nabla^2\,\partial_\zeta^2\phi_1 = -4\pi\left(-e\,\partial_\zeta^2 n_{p1}(\mathbf{x}) - Q\,\partial^2\delta(\mathbf{x} - \mathbf{x}_0)\right)$$
$$4\pi e\,\partial_\zeta^2 n_{p1}(\mathbf{x}) = \frac{4\pi e}{v_b^2}\partial_t^2 n_{p1}(\mathbf{x}) = \frac{4\pi e}{v_b^2}\partial_t\left(-n_{p0}\boldsymbol{\nabla}\cdot\mathbf{v}_{p1}\right) = -\frac{4\pi e n_{p0}}{v_b^2}\boldsymbol{\nabla}\cdot\partial_t\mathbf{v}_{p1}$$
$$= -\frac{4\pi e n_{p0}}{v_b^2}\boldsymbol{\nabla}\cdot\left(-\frac{e}{m}\mathbf{E}_1\right) = \frac{4\pi e^2 n_{p0}}{m v_b^2}\boldsymbol{\nabla}\cdot\mathbf{E}_1 = \frac{4\pi e^2 n_{p0}}{m v_b^2}\boldsymbol{\nabla}\cdot(-\boldsymbol{\nabla}\phi) \tag{A.1.4}$$
$$k_p^2 = \frac{4\pi n_{p0} e^2}{m v_b^2}$$

$$\nabla^2\left(\partial_\zeta^2 + \frac{4\pi e^2 n_{p0}}{m v_b^2}\right)\phi = 4\pi Q\,\partial_\zeta^2\delta(\mathbf{x} - \mathbf{x}_i)$$
$$\nabla^2\left(\frac{1}{|\vec{x} - \vec{x}_i|}\right) = -4\pi\delta(\mathbf{x} - \mathbf{x}_i)$$
$$\nabla^2\left(\partial_\zeta^2 + \frac{4\pi e^2 n_{p0}}{m v_b^2}\right)\phi = -Q\,\partial_\zeta^2\nabla^2\left(\frac{1}{|\mathbf{x} - \mathbf{x}_i|}\right) \tag{A.1.5}$$
$$\nabla^2\left(\partial_\zeta^2 + k_p^2\right)\phi = -Q\,\partial_\zeta^2\nabla^2\left(\frac{1}{|\mathbf{x} - \mathbf{x}_i|}\right)$$
$$\left(\partial_\zeta^2 + k_p^2\right)\phi = -Q\,\partial_\zeta^2\left(\frac{1}{|\mathbf{x} - \mathbf{x}_i|}\right)$$

$$\phi_1(\zeta) = -\frac{2\pi Q}{\lambda_p}\left[\frac{1}{k_p|\zeta|} + k_p\int_\zeta^\infty d\zeta'\,\frac{\sin k_p(\zeta' - \zeta)}{k_p|\zeta'|}\right] \tag{A.1.6}$$

ULSAN NATIONAL INSTITUTE OF SCIENCE AND TECHNOLOGY

$$\nabla_\perp^2 \mathbf{A}_1 = -\frac{4\pi}{c}\mathbf{J}_1 - \beta_0 \boldsymbol{\nabla}\, \partial_\zeta \phi_1$$
$$\partial_t \mathbf{v}_{p1} = -\frac{e}{m}\mathbf{E}_1 = -v_b\, \partial_\zeta \mathbf{v}_{p1} \tag{A.1.7}$$

$$\partial_\zeta \mathbf{v}_{p1}(\vec{x}) = \frac{e}{mv_b}\mathbf{E}_1 = -\frac{e}{mv_b}\left(\frac{1}{c}\partial_t \mathbf{A}_1 + \boldsymbol{\nabla}\phi_1\right) = \frac{e}{mv_b}\left(\frac{1}{c}v_b\, \partial_\zeta \mathbf{A}_1 - \boldsymbol{\nabla}\phi_1\right)$$
$$\nabla_\perp^2 \mathbf{A}_1 = -\frac{4\pi}{c}\mathbf{J}_1 - \beta_0 \boldsymbol{\nabla}\, \partial_\zeta \phi_1 = -\frac{4\pi}{c}\left(-en_{p0}\mathbf{v}_{p1}(\mathbf{x}) - Q\mathbf{v}_b \delta(\mathbf{x}-\mathbf{x}_i)\right) - \beta_0 \boldsymbol{\nabla}\, \partial_\zeta \phi_1 \tag{A.1.8}$$
$$\partial_\zeta \nabla_\perp^2 \mathbf{A}_1 = \frac{4\pi}{c}\left(en_{p0}\, \partial_\zeta \mathbf{v}_{p1}(\mathbf{x}) + Q\mathbf{v}_b\, \partial_\zeta \delta(\mathbf{x}-\mathbf{x}_i)\right) - \beta_0\, \partial_\zeta \boldsymbol{\nabla}\, \partial_\zeta \phi_1$$

$$\partial_\zeta \nabla_\perp^2 \mathbf{A}_1 = \frac{4\pi}{c}\left[en_{p0}\frac{e}{mv_b}\left(\frac{1}{c}v_b\, \partial_\zeta \mathbf{A}_1 - \boldsymbol{\nabla}\phi_1\right) + Q\mathbf{v}_b\, \partial_\zeta \delta(\mathbf{x}-\mathbf{x}_i)\right] - \beta_0 \boldsymbol{\nabla}\, \partial_\zeta^2 \phi_1$$
$$\partial_\zeta \nabla_\perp^2 \mathbf{A}_1 - \partial_\zeta \frac{v_b^2}{c^2}\left(\frac{4\pi e^2 n_{p0}}{v_b^2 m}\right)\mathbf{A}_1 = -\beta_0 \boldsymbol{\nabla}\, \partial_\zeta^2 \phi_1 - \frac{v_b}{c}\frac{4\pi e^2 n_{p0}}{mv_b^2}\boldsymbol{\nabla}\phi_1 + \frac{\mathbf{v}_b}{c}4\pi Q\, \partial_\zeta \delta(\mathbf{x}-\mathbf{x}_i)$$
$$\partial_\zeta\left(\nabla_\perp^2 - \beta_0^2 k_p^2\right)\mathbf{A}_1 = -\beta_0 \boldsymbol{\nabla}\left(\partial_\zeta^2 + k_p^2\right)\phi + 4\pi\beta_0 Q\, \partial_\zeta \delta(\mathbf{x}-\mathbf{x}_i)$$
$$\partial_\zeta\left(\nabla_\perp^2 - \beta_0^2 k_p^2\right)\mathbf{A}_1 = Q\beta_0 \boldsymbol{\nabla}\, \partial_\zeta^2\left(\frac{1}{|\mathbf{x}-\mathbf{x}_i|}\right) + 4\pi\beta_0 Q\, \partial_\zeta \delta(\mathbf{x}-\mathbf{x}_i) \tag{A.1.9}$$
$$\left(\nabla_\perp^2 - \beta_0^2 k_p^2\right)\mathbf{A}_1 = Q\beta_0 \boldsymbol{\nabla}\, \partial_\zeta\left(\frac{1}{|\mathbf{x}-\mathbf{x}_i|}\right) + 4\pi\beta_0 Q\delta(\mathbf{x}-\mathbf{x}_i)$$
$$\left(\nabla_\perp^2 - \beta_0^2 k_p^2\right)A_{1z} = Q\beta_0\, \partial_\zeta^2\left(\frac{1}{|\mathbf{x}-\mathbf{x}_i|}\right) - \beta_0 Q\nabla^2\left(\frac{1}{|\mathbf{x}-\mathbf{x}_i|}\right) = -\beta_0 Q\nabla_\perp^2\left(\frac{1}{|\mathbf{x}-\mathbf{x}_i|}\right)$$

$$A_{1z}(\zeta) = -\frac{2\pi Q}{\lambda_p}\beta_0^2\int_0^\infty d\rho' K_1(\beta_0 k_p \rho')\frac{\rho'}{[\rho'^2+\zeta^2]^{\frac{3}{2}}} \tag{A.1.10}$$

ULSAN NATIONAL INSTITUTE OF SCIENCE AND TECHNOLOGY

A. 3

3.1.0 Wakefields of an axisymmetric beam driver

$$\frac{d^2R}{dr^2}+\frac{1}{r}\frac{dR}{dr}-k^2R=\begin{cases}\frac{8eNk}{a^2}\left(1-\frac{r^2}{a^2}\right), & r<a\\ 0 \quad , & r>a\end{cases} \tag{A.3.1}$$

Now we will find the solutions of given differential equation in two parts, $r<a$ and $r>a$.

3.1.1 Inside of the beam ($r<a$)

Let's assume $R_p(r)$ and $R_h(r)$ satisfying equations below.

$$\begin{gathered}\left(\frac{d^2}{dr^2}+\frac{1}{r}\frac{d}{dr}-k^2\right)R_h(r)=0,\\ \left(\frac{d^2}{dr^2}+\frac{1}{r}\frac{d}{dr}-k^2\right)R_p(r)=\frac{8eNk}{a^2}\left(1-\frac{r^2}{a^2}\right).\end{gathered} \tag{A.3.2}$$

Summing up two equations,

$$\left(\frac{d^2}{dr^2}+\frac{1}{r}\frac{d}{dr}-k^2\right)\left(R_p(r)+R_h(r)\right)=\frac{8eNk}{a^2}\left(1-\frac{r^2}{a^2}\right). \tag{A.3.3}$$

So, we obtain the form of $R(r)$ we will solve.

$$R(r)=R(r)_h+R(r)_p. \tag{A.3.4}$$

First of all, for the modified Bessel equation with azimuthal symmetry ($m=0$) in the left-hand side, the general solution is

$$R_h(r)=C_1K_0(kr)+C_2I_0(kr). \tag{A.3.5}$$

In the region, $r<a$, our homogeneous solution will be $R(r)_h=C_2I_0$ ($\because K_0(0)=\infty$ and $V(r=\infty,z)=R(\infty)Z(z)$=Finite). Then the rest of the work which we should do is to find the particular solution $R_p(r)$ satisfying our inhomogeneous differential equation.

$$\left(\frac{d^2}{dr^2}+\frac{1}{r}\frac{d}{dr}-k^2\right)R_p(r)=\frac{8eNk}{a^2}\left(1-\frac{r^2}{a^2}\right). \tag{A.3.6}$$

ULSAN NATIONAL INSTITUTE OF SCIENCE AND TECHNOLOGY

Assuming power series in r,

$$R(r) = \sum_{n}^{\infty} a_n r^n. \tag{A.3.7}$$

Our differential equation will be

$$\sum_{n}^{\infty} [a_n n(n-1) r^{n-2} + a_n n r^{n-2} - k^2 a_n r^n] = \frac{8eNk}{a^2}\left(1 - \frac{r^2}{a^2}\right). \tag{A.3.8}$$

To hold for all $r > 0$, each coefficient of r^n in both sides should be equal for all n. Therefore, only zeroth and second order of r remain.

$$[-k^2 a_0 + 4a_2 - k^2 a_2 r^2] = \frac{8eNk}{a^2}\left(1 - \frac{r^2}{a^2}\right). \tag{A.3.9}$$

Separating it into two parts,

$$\begin{aligned} &\text{For the zeroth order,} \quad -k^2 a_0 + 4a_2 = \frac{8eNk}{a^2}, \\ &\text{For the seconde order,} \quad k^2 a_2 = \frac{8eNk}{a^2}\frac{1}{a^2}. \end{aligned} \tag{A.3.10}$$

As results,

$$\begin{aligned} a_0 &= \frac{8eN}{k^2 a^2}\left(\frac{4}{ka^2} - k\right), \\ a_2 &= \frac{8eN}{ka^4}. \end{aligned} \tag{A.3.11}$$

Then, the particular solution is

$$R(r)_p = a_0 + a_2 r^2. \tag{A.3.12}$$

Then, we obtain the result below.

$$R(r) = R(r)_h + R(r)_p = C_2 I_0(kr) + a_0 + a_2 r^2, \qquad r < a. \tag{A.3.13}$$

We will decide the coefficient of the first term in right hand side using boundary condition later.

3.1.2 Outside of the beam ($r > a$)

The homogeneous solution in this region will be $R(r) = R(r)_h = C_1 K_0(kr)$ due to $I_0(0) = \infty$.

ULSAN NATIONAL INSTITUTE OF SCIENCE AND TECHNOLOGY

3.1.3 Remaining boundary conditions, continuity of potential and electric field

The potential $V(r,z) = R(r)Z(z)$ and its partial derivative $\partial_r V(r,z)$ should be continuous at $r = a$.

$$\begin{gathered} R_-(a_-) = C_2 I_0(ka) + a_0 + a_2 a^2 = C_1 K_0(ka) = R_+(a_+), \\ \partial_r R_-(r)|_{r=a_-} = C_2 \partial_r I_0(kr)|_{r=a} + 2a_2 a = C_1 \partial_r K_0(kr)|_{r=a} = \partial_r R_+(r)|_{r=a_+}. \end{gathered} \tag{A.3.14}$$

Here it is used that the modified Bessel function I_0 and K_0 are already continuous.

$$C_1 = -\frac{(a_0 + a_2 a^2)\partial_r I_0(kr)|_{r=a} - 2a_2 a I_0(ka)}{K_0(ka)\partial_r I_0(kr)|_{r=a} - I_0(ka)\partial_r K_0(kr)|_{r=a}} \tag{A.3.15}$$

and

$$C_2 = -\frac{(a_0 + a_2 a^2)\partial_r K_0(kr)|_{r=a} - 2a_2 a K_0(ka)}{K_0(ka)\partial_r I_0(kr)|_{r=a} - I_0(ka)\partial_r K_0(kr)|_{r=a}}. \tag{A.3.16}$$

From the properties of modified Bessel functions, Wronskian and recurrence relations of the modified Bessel equation [11] lead us to three equations below,

$$\frac{1}{K_0(ka)\partial_r I_0(kr)|_{r=a} - I_0(ka)\partial_r K_0(kr)|_{r=a}} = a \tag{A.3.17}$$

and

$$\partial_r K_0(kr)|_{r=a} = \frac{k^2 a}{2}[K_0(ka) - k_2(ka)] \tag{A.3.18}$$

and

$$\partial_r I_0(kr)|_{r=a} = \frac{k^2 a}{2}[I_0(ka) - I_2(ka)]. \tag{A.3.19}$$

Using listed equations above, we get final result.

$$R(r) = \frac{16eN}{ka^2}\begin{cases} K_2(ka)I_0(kr) + \frac{1}{2} - \frac{2}{(ka)^2} - \frac{r^2}{2a^2}, & r < a \\ I_2(ka)K_0(kr) \quad , & r > a \end{cases} \tag{A.3.20}$$

ULSAN NATIONAL INSTITUTE OF SCIENCE AND TECHNOLOGY

3.2 Nonlinear one dimensional relativistic plasma oscillation

3.2.0 Here we introduce a very famous work of the general investigation of the nonlinear wave motions of the plasma electrons by Akhizer and Polovin in 1956 [5]. In different way from the linear case, we will not ignore the higher order terms. We reconsider the Maxwell's equations and equation of motion in plasma electrons.

$$\begin{aligned}
\nabla\cdot\mathbf{E} &= 4\pi e(n-n_0),\\
\nabla\times\mathbf{E} &= -\frac{1}{c}\frac{\partial\mathbf{H}}{\partial t},\\
\nabla\cdot\mathbf{H} &= 0,\\
\nabla\times\mathbf{H} &= \frac{1}{c}\frac{\partial\mathbf{E}}{\partial t}+\frac{4\pi}{c}ne\mathbf{v},\\
\frac{\partial\mathbf{p}}{\partial t}+(\mathbf{v}\cdot\nabla)\mathbf{p} &= e\mathbf{E}+\frac{e}{c}\mathbf{v}\times\mathbf{H}.
\end{aligned} \tag{A.3.21}$$

Where n_0 is the equilibrium electron density. Where the whole system is approximately neutral. $\mathbf{p}$ is the electron momentum, equal to $[1-\beta^2]^{-\frac{1}{2}}m\mathbf{v}$. β is normalized phase velocity. All the equations above are functions of $(\hat{\mathbf{i}}\cdot\mathbf{r}-Vt)$, which is one of the properties in the general wave motions of the plasma. Rewriting above equations,

$$\hat{\mathbf{i}}\times\mathbf{E}' = \beta\mathbf{H}', \tag{A.3.22}$$

$$\hat{\mathbf{i}}\times\mathbf{H}' = -\beta\mathbf{E}'+\frac{4\pi}{c}en\mathbf{v}, \tag{A.3.23}$$

$$\hat{\mathbf{i}}\cdot\mathbf{H}' = 0, \tag{A.3.24}$$

$$\hat{\mathbf{i}}\cdot\mathbf{E}' = 4\pi e(n-n_0), \tag{A.3.25}$$

$$(\hat{\mathbf{i}}\cdot\mathbf{v}-V)\mathbf{p}' = e\mathbf{E}+\frac{e}{c}\mathbf{v}\times\mathbf{H}. \tag{A.3.26}$$

By integrating Eq. (A.3.22), we obtain

$$\mathbf{H} = \frac{1}{\beta}\hat{\mathbf{i}}\times\mathbf{E}+\mathbf{H}_0 \tag{A.3.27}$$

3.2.1 The density of the background plasma electrons n is, combining Eqs. (A.3.23) and (A.3.25),

$$\begin{aligned}
\hat{\mathbf{i}}\cdot(\hat{\mathbf{i}}\times\mathbf{H}') = \mathbf{H}'\cdot(\hat{\mathbf{i}}\times\hat{\mathbf{i}}) = 0 &= -\beta\hat{\mathbf{i}}\cdot\mathbf{E}'+\frac{4\pi}{c}en\hat{\mathbf{i}}\cdot\mathbf{v}\\
-\beta 4\pi e(n-n_0)+\frac{4\pi}{c}en\hat{\mathbf{i}}\cdot\mathbf{v} &= 0\\
n &= \frac{n_0V}{V-\hat{\mathbf{i}}\cdot\mathbf{v}}
\end{aligned} \tag{A.3.28}$$

ULSAN NATIONAL INSTITUTE OF SCIENCE AND TECHNOLOGY

3.2.2 We multiply Eq. (A.3.26) on the left vectorially by $\hat{\mathbf{i}}$ and use Eq. (A.3.27). Then, we obtain the equation of the magnetic field.

$$(\hat{\mathbf{i}}\cdot\mathbf{v}-V)\hat{\mathbf{i}}\times\mathbf{p}' = e\hat{\mathbf{i}}\times\mathbf{E}+\frac{e}{c}\hat{\mathbf{i}}\times(\mathbf{v}\times\mathbf{H}),$$

$$= e\beta(\mathbf{H}-\mathbf{H}_0)+\frac{e}{c}[\mathbf{v}(\hat{\mathbf{i}}\cdot\mathbf{H})-\mathbf{H}(\hat{\mathbf{i}}\cdot\mathbf{v})] = \frac{e}{c}\mathbf{H}(V-\hat{\mathbf{i}}\cdot\mathbf{v})-\frac{e}{c}[V\mathbf{H}_0-\mathbf{v}(\hat{\mathbf{i}}\cdot\mathbf{H})], \tag{A.3.29}$$

$$\mathbf{H} = -\frac{c}{e}(\hat{\mathbf{i}}\times\mathbf{p}')+\frac{V\mathbf{H}_0-\mathbf{v}(\hat{\mathbf{i}}\cdot\mathbf{H}_0)}{V-\hat{\mathbf{i}}\cdot\mathbf{v}}.$$

Here it was used that $\hat{\mathbf{i}}\cdot\mathbf{H}=\hat{\mathbf{i}}\cdot\mathbf{H}_0$.

3.2.3 We want to make the equation of motion in the parameters we can control. Taking the scalar product $\hat{\mathbf{i}}$ on Eq. (A.3.26) and using Eq. (A.3.29) and Eq. (A.3.25),

$$(\hat{\mathbf{i}}\cdot\mathbf{v}-V)\hat{\mathbf{i}}\cdot\mathbf{p}' = e\hat{\mathbf{i}}\cdot\mathbf{E}+\frac{e}{c}\hat{\mathbf{i}}\cdot(\mathbf{v}\times\mathbf{H}) = e\hat{\mathbf{i}}\cdot\mathbf{E}+\frac{e}{c}\hat{\mathbf{i}}\cdot\left(\mathbf{v}\times\left(-\frac{c}{e}(\hat{\mathbf{i}}\times\mathbf{p}')+\frac{V\mathbf{H}_0-\mathbf{v}(\hat{\mathbf{i}}\cdot\mathbf{H}_0)}{V-\hat{\mathbf{i}}\cdot\mathbf{v}}\right)\right),$$

$$(\hat{\mathbf{i}}\cdot\mathbf{v}-V)\hat{\mathbf{i}}\cdot\mathbf{p}'+\hat{\mathbf{i}}\cdot\mathbf{v}\times(\hat{\mathbf{i}}\times\mathbf{p}')-e\beta\frac{\hat{\mathbf{i}}\cdot(\mathbf{v}\times\mathbf{H}_0)}{V-\hat{\mathbf{i}}\cdot\mathbf{v}} = e\hat{\mathbf{i}}\cdot\mathbf{E}, \tag{A.3.26}$$

$$\left[(\hat{\mathbf{i}}\cdot\mathbf{v}-V)\hat{\mathbf{i}}\cdot\mathbf{p}'+\hat{\mathbf{i}}\cdot\mathbf{v}\times(\hat{\mathbf{i}}\times\mathbf{p}')-e\beta\frac{\hat{\mathbf{i}}\cdot(\mathbf{v}\times\mathbf{H}_0)}{V-\hat{\mathbf{i}}\cdot\mathbf{v}}\right]' = e\hat{\mathbf{i}}\cdot\mathbf{E}' = 4\pi e^2(n-n_0).$$

3.2.4 Taking the vector $\hat{\mathbf{i}}$ in the z direction and introducing normalized momentum $\boldsymbol{\rho}=\mathbf{p}/mc$ and the normalized velocity $\mathbf{u}=\mathbf{v}/c$ and using Eq. (A.3.28), we get the general form of the differential equation of longitudinal, nonlinear and relativistic plasma oscillation. Where $\tau = t-(\hat{\mathbf{i}}\cdot\mathbf{r}/V)$, $\omega_0^2 = 4\pi e^2 n_0/m$, and $\Omega = e\mathbf{H}_0/mc$.

$$\frac{d}{d\tau}\left\{(u_z-\beta)\frac{d\rho_z}{d\tau}+u_x\frac{d\rho_x}{d\tau}+u_y\frac{d\rho_y}{d\tau}+\frac{\beta}{\beta-u_z}\left(u_x\Omega_y-u_y\Omega_x\right)\right\} = \omega_0^2\frac{\beta^2 u_z}{\beta-u_z}. \tag{A.3.27}$$

When the external magnetic field $\mathbf{H}_0$ is not applied and especially only we want to consider longitudinal one-dimensional cases, $u_x = u_y = 0$. In general, the plasma wave motions in large amplitudes are only analytically solvable when it is treated longitudinally in one-dimensional cases. Then we get another form of this equation by rewriting the normalized plasma electron momentum ρ_z in terms of the normalized plasma electron velocity $u = u_z$. Using the fact that

$$u_z\frac{d}{d\tau}\left(\frac{u_z}{\sqrt{1-u_z^2}}\right) = \frac{d}{d\tau}\left(\frac{1}{\sqrt{1-u_z^2}}\right), \tag{A.3.28}$$

the one-dimensional nonlinear plasma oscillation in absence of the driving beam is

$$\frac{d^2}{d\tau^2}\left(\frac{1-\beta u_z}{\sqrt{1-u_z^2}}\right) = \omega_0^2\frac{\beta^2 u_z}{\beta-u_z}. \tag{A.3.29}$$

ULSAN NATIONAL INSTITUTE OF SCIENCE AND TECHNOLOGY

3.2.5 To obtain the longitudinal electric field by the modulation of the plasma electrons, we use again Eq. (A.3.26).

$$\mathbf{E} = \frac{1}{e}(\hat{\mathbf{i}} \cdot \mathbf{v} - V)\mathbf{p}' - \frac{1}{c}(\mathbf{v} \times \mathbf{H}). \tag{A.3.30}$$

Where $v_x = v_y = 0$ and there exist only z-component. Checking it, we know the second term of left-hand side should be zero. Taking $\hat{\imath}$ in z (longitudinal) direction and introducing a new variable defined by $\tau = \omega_p(t - \hat{\mathbf{i}} \cdot \mathbf{r}/V)$ following Ref. [6], the result we want is

$$\begin{aligned} E_z &= \frac{mc\omega_p}{eV}(V - v_z)\frac{p_z'}{mc} = \frac{mc\omega_p}{e\beta_{ph}}(\beta_{ph} - \beta_z)\frac{d\rho_z}{d\tau} \simeq \frac{mc\omega_p}{e}(1 - \beta_z)\frac{d}{d\tau}\left(\frac{\beta_z}{\sqrt{1 - \beta_z^2}}\right) \\ &= \frac{mc\omega_p}{e}\frac{d}{d\tau}\left(\frac{\beta_z}{\sqrt{1 - \beta_z^2}} - \frac{1}{\sqrt{1 - \beta_z^2}}\right) = \frac{mc\omega_p}{e}\frac{d}{d\tau}\left(\frac{1 - \beta_z}{1 + \beta_z}\right)^{\frac{1}{2}}. \end{aligned} \tag{A.3.31}$$

Where V/c and v_z/c were written by β_{ph} and β_z.

3.2.6 The first integral of our differential equation is obtained by the procedure below, using the initial conditions which are $x(0) = 1,\ x'(0) = 0$.

$$\begin{aligned} \frac{d^2x}{d\tau^2} &= \frac{1}{2}\left(\frac{1}{x^2} - 1 + 2\alpha\right), \\ 2\frac{dx}{d\tau}\frac{d}{d\tau}\left(\frac{dx}{d\tau}\right) &= \frac{dx}{d\tau}\left(\frac{1}{x^2} - 1 + 2\alpha\right), \\ \frac{d}{d\tau}\left(\frac{dx}{d\tau}\right)^2 &= \frac{d}{d\tau}\left(-\frac{1}{x} - x + 2\alpha x\right), \\ \int_{\tau'=0}^{\tau'=\tau} d\left(\frac{dx}{d\tau'}\right)^2 &= \int_{\tau'=0}^{\tau'=\tau} d\left(-\frac{1}{x} - x + 2\alpha x\right). \end{aligned} \tag{A.3.32}$$

$$\left(\frac{dx}{d\tau}\right)^2 = 2(1 - \alpha) - \frac{1}{x} - (1 - 2\alpha)x.$$

ULSAN NATIONAL INSTITUTE OF SCIENCE AND TECHNOLOGY

3.2.7 The perturbed plasma electron densities corresponding to turning points of oscillation are from $x(\beta)$ and plasma electron density n.

$$n = \frac{n_0 V}{V - \hat{\mathbf{i}} \cdot \mathbf{v}} \equiv \frac{n_0 \beta_{ph}}{\beta_{ph} - \beta} \simeq \frac{n_0}{1 - \beta},$$
$$x(\tau, \beta_1) = 1 = \left(\frac{1 - \beta_1}{1 + \beta_1}\right)^{\frac{1}{2}}, \qquad x(\tau, \beta_2) = \frac{1}{1 - 2\alpha} = \left(\frac{1 - \beta_2}{1 + \beta_2}\right)^{\frac{1}{2}}. \tag{A.3.33}$$

For τ_1,

$$\beta_1 = 0,$$
$$n - n_0 = 0. \tag{A.3.34}$$

For τ_2,

$$\beta_2 = \frac{-2\alpha + 2\alpha^2}{1 - 2\alpha + 2\alpha^2},$$
$$n - n_0 = -2n_b(1 - \alpha). \tag{A.3.35}$$

ULSAN NATIONAL INSTITUTE OF SCIENCE AND TECHNOLOGY

A.4

4.1 Using Leibnitz's rule, we obtain a second-order differential equation coupled to the beam-envelope equation.

$$\frac{d}{dx}\int_A^B f(x,t)dt = \int_A^B \frac{\partial f(x,t)}{\partial x}dt + f(x,B)\left(\frac{dB}{dx}\right) - f(x,A)\left(\frac{dA}{dx}\right) \tag{A.4.1}$$

So, we get two simultaneous second-order differential equations.

$$\begin{gathered}\frac{\partial^2 r_b(\xi,\tau)}{\partial\tau^2} - \frac{1}{r_b^3(\xi,\tau)} = -y(\xi,\tau) \\ \frac{d^2 y(\xi,\tau)}{d\xi^2} + y(\xi,\tau) = r_b(\xi,\tau)\end{gathered} \tag{A.4.2}$$

4.2 Assuming the beam radius perturbation is enough small compared with the beam radius,

$$y = \frac{1}{r_b^3} - \frac{\partial^2 r_b}{\partial\tau^2} = \frac{1}{(1+\delta r_b)^3} - \frac{\partial^2 \delta r_b}{\partial\tau^2} \approx 1 - 3\delta r_b - \frac{\partial^2 \delta r_b}{\partial\tau^2} \tag{A.4.3}$$

and substituting y into the new equation we got,

$$\begin{gathered}\frac{\partial^2}{\partial\xi^2}\left(1 - 3\delta r_b - \frac{\partial^2 \delta r_b}{\partial\tau^2}\right) + 1 - 3\delta r_b - \frac{\partial^2 \delta r_b}{\partial\tau^2} = 1 + \delta r_b \\ \frac{\partial^2}{\partial\xi^2}\frac{\partial^2 \delta r_b}{\partial\tau^2} + 3\frac{\partial^2 \delta r_b}{\partial\xi^2} + \frac{\partial^2 \delta r_b}{\partial\tau^2} + 3\delta r_b = -\delta r_b\end{gathered} \tag{A.4.1}$$

We obtain a new equation of $\delta\hat{r}_b$.

$$\left(\partial_\xi^2 + 1\right)(\partial_\tau^2 + 3)\delta\hat{r}_b = -\delta\hat{r}_b \tag{A.4.1}$$

4.3 Dispersion relation of the wave in the beam is

$$\begin{gathered}\frac{\partial^2}{\partial\xi^2}\frac{\partial^2}{\partial\tau^2}\exp(i\delta\omega\tau - ik\xi) + 3\frac{\partial^2}{\partial\xi^2}\exp(i\delta\omega\tau - ik\xi) + \frac{\partial^2}{\partial\tau^2}\exp(i\delta\omega\tau - ik\xi) + 3\exp(i\delta\omega\tau - ik\xi) \\ = -\exp(i\delta\omega\tau - ik\xi) \\ (-\delta\omega^2)(-k^2) + 3(-k^2) + (-\delta\omega^2) + 3 = -1 \\ D \equiv (k^2 - 1)(\delta\omega^2 - \Delta) = -1, \qquad \Delta \equiv 3\end{gathered} \tag{A.4.4}$$

ULSAN NATIONAL INSTITUTE OF SCIENCE AND TECHNOLOGY

4.4 Finding $k = k_r + ik_i$ with respect to $\delta\omega = \delta\omega_r + i\delta\omega_i$, dispersion relation of the instability is

$$k^2 = \frac{\delta\omega^2 - 4}{\delta\omega^2 - 3}. \tag{A.4.1}$$

With respect to the complex variables of k and $\delta\omega$,

$$\begin{aligned} k_r^2 + 2ik_rk_i - k_i^2 &= \frac{\delta\omega_r^2 + i2\delta\omega_r\delta\omega_i - \delta\omega_i^2 - 4}{\delta\omega_r^2 + i2\delta\omega_r\delta\omega_i - \delta\omega_i^2 - 3} \\ &= \frac{\delta\omega_r^4 + 2\delta\omega_r^2\delta\omega_i^2 - 7\delta\omega_r^2 + 2i\delta\omega_r\delta\omega_i + \delta\omega_i^4 + 7\delta\omega_i^2 + 12}{\delta\omega_r^4 + 2\delta\omega_r^2\delta\omega_i^2 - 6\delta\omega_r^2 + \delta\omega_i^4 + 6\delta\omega_i^2 + 9}, \end{aligned} \tag{A.4.1}$$

Defining $A \equiv \delta\omega_r^4 + 2\delta\omega_r^2\delta\omega_i^2 - 6\delta\omega_r^2 + \delta\omega_i^4 + 6\delta\omega_i^2 + 9,$ (A.4.1)

Real part is

$$k_r^2 - k_i^2 = \frac{A - \delta\omega_r^2 + \delta\omega_i^2 + 3}{A}. \tag{A.4.1}$$

Imaginary part is

$$k_rk_i = \frac{\delta\omega_r\delta\omega_i}{A}. \tag{A.4.1}$$

So, complex k in complex plane of $\delta\omega$ will be calculated from two equations

$$k_r^4 - \frac{A - \delta\omega_r^2 + \delta\omega_i^2 + 3}{A}k_r^2 - \left(\frac{\delta\omega_r\delta\omega_i}{A}\right)^2 = 0 \tag{A.4.1}$$

and

$$k_i^4 + \frac{A - \delta\omega_r^2 + \delta\omega_i^2 + 3}{A}k_i^2 - \left(\frac{\delta\omega_r\delta\omega_i}{A}\right)^2 = 0. \tag{A.4.1}$$

6. 3 Script of WARP for plasma wakefield acceleration

```
"""
This is a typical input script that runs a simulation of laser-wakefield acceleration using Warp in 2D / Circ / 3D.

Usage
-----------------------------------------------------------------------------------------------------------------------
- Modify the parameters below to suit your needs
- Type "python -i lpa_script.py" in a terminal
- When the simulation finishes, the python session will *not* quit. Therefore the simulation can be continued by
running step(). Otherwise, one can just type exit()
"""
# Import warp-specific packages
from warp.init_tools import *

# -----------------------------------------------------------------------------------------------------------------------
# Parameters (Modify the values below to suit your needs)
# -----------------------------------------------------------------------------------------------------------------------

# General parameters

# Dimension of simulation ("3d", "circ", "2d", "1d")
dim = "circ"
# Number of azimuthal modes beyond m=0, for "circ" (not used for "2d" and "3d")
circ_m = 1
# Total number of timesteps in the simulation
N_steps = 200000
# Whether to run the simulation interactively (0:off, 1:on)
interactive = 0

# Simulation box

# Number of grid cells in the longitudinal direction
Nz = 240
# Number of grid cells in transverse direction (represents Nr in "circ")
Nx = 50
# Number of grid cells in the 3rd dimension (not used for "2d" and "circ")
Ny = 50
# Dimension of the box in longitudinal direction (meters)
zmin = -1.5*sqrt(2*pi)*637.e-6
```

ULSAN NATIONAL INSTITUTE OF SCIENCE AND TECHNOLOGY

```
zmax = 0.
# Dimension of the box in transverse direction (box ranges from -xmax to xmax)
xmax = 4.2*120.e-6
# Dimension of the box in 3rd direction (not used for "2d" and "circ")
ymax = 4.2*120.e-6
# Field boundary conditions (longitudinal and transverse respectively)
f_boundz    = openbc
f_boundxy = openbc
if dim == "circ":
    f_boundxy = dirichlet
# Particles boundary conditions (longitudinal and transverse respectively)
p_boundz    = absorb
p_boundxy = absorb
# Moving window (0:off, 1:on)
use_moving_window = 1
# Speed of the moving window (ignored if use_moving_window = 0)
v_moving_window = clight

# Diagnostics

# Period of diagnostics (in number of timesteps)
diag_period = 10000
# Whether to write the fields
write_fields = 1
# Whether to write the particles
write_particles = 1
# Whether to write the diagnostics in parallel
parallel_output = False

# Numerical parameters

# Field solver (0:Yee, 1:Karkkainen on EF,B, 3:Lehe)
stencil = 0
# Particle shape (1:linear, 2:quadratic, 3:cubic)
depos_order = 1
# Gathering mode (1:from cell centers, 4:from Yee mesh)
efetch = 1

# Particle pusher (0:Boris, 1:Vay)
particle_pusher = 1
```

ULSAN NATIONAL INSTITUTE OF SCIENCE AND TECHNOLOGY

```
# Current smoothing parameters

# Turn current smoothing on or off (0:off; 1:on)
use_smooth = 1
# Number of passes of smoother and compensator in each direction (x, y, z)
npass_smooth = array([[ 0 , 0 ], [ 0 , 0 ], [ 1 , 1 ]])
# Smoothing coefficients in each direction (x, y, z)
alpha_smooth = array([[ 0.5, 3.], [ 0.5, 3.], [0.5, 3./2]])
# Stride in each direction (x, y, z)
stride_smooth = array([[ 1 , 1 ], [ 1 , 1 ], [ 1 , 1 ]])

# Plasma macroparticles

# Initialize some preexisting plasmas electrons (0:off, 1:on)
# (Can be used in order to neutralize pre-ionized ions, if any,
# or in order to simulate a plasma without having to initialize ions)
use_preexisting_electrons = 1
# Initialize plasma ions (0:off, 1:on)
use_ions = 0
# Number of macroparticles per cell in each direction
# In Circ, nppcelly is the number of particles along the
# azimuthal direction. Use a multiple of 4*circ_m
plasma_nx = 2
plasma_ny = 4
plasma_nz = 3

# Plasma content and profile

# Reference plasma density (in number of particles per m^3)
n_plasma = 2.8e22
# Relative density of the preexisting electrons (relative to n_plasma)
rel_dens_preexisting_electrons = 1.
# The different elements used. (Only used if use_ions is different than 0.)
# relative_density is the density relative to n_plasma.
# q_start is the ionization state of the ions at the beginning of the simulation
# q_max is the maximum ionization state

# If q_start is not equal to q_max, ionization between states will be computed.
ion_states = { 'Hydrogen': {'relative_density':1., 'q_start':1, 'q_max':1 },
```

ULSAN NATIONAL INSTITUTE OF SCIENCE AND TECHNOLOGY

```
                    'Helium': {'relative_density':0.25, 'q_start':0, 'q_max':2 } }
# Positions between which the plasma is initialized
# (Transversally, the plasma is initialized between -plasma_xmax and
# plasma_xmax, along x, and -plasma_ymax and plasma_ymax along y)
plasma_zmin = 1.e-6
plasma_zmax = 1.
plasma_xmax = xmax
plasma_ymax = ymax
# Define your own profile and profile parameters below
ramp_start = plasma_zmin
ramp_length = plasma_zmin*10
ramp_plateau = plasma_zmax

def plasma_dens_func( x, y, z ):
    """
    User-defined function: density profile of the plasma

    It should return the relative density with respect to n_plasma,
    at the position x, y, z (i.e. return a number between 0 and 1)

    Parameters
    ----------------------------------------------------------------------------------------------------
    x, y, z: 1darrays of floats
        Arrays with one element per macroparticle
    Returns
    ----------------------------------------------------------------------------------------------------
    n : 1d array of floats
        Array of relative density, with one element per macroparticles
    """
    # Allocate relative density
    n = ones_like(z)
    # Make linear ramp
    n = where( z<ramp_start+ramp_length, (z-ramp_start)/ramp_length, n )
    # Supress density before the ramp
    n = where( z<ramp_start, 0., n )
    # Reduce density by half after the ramp
    n = where( z> ramp_start+ramp_length+ramp_plateau, 0.5*n, n )

# Put the density to 0 later
    n = where( z> ramp_start+ramp_length+2*ramp_plateau, 0., n )
```

ULSAN NATIONAL INSTITUTE OF SCIENCE AND TECHNOLOGY

```
    return(n)

# Relativistic beam

# Initialize beam electrons (0:off, 1:on)
# (Please be aware that initializing a beam in 2D geometry makes very little
# physical sense, because of the long range of its space-charge fields)
use_beam = 1
# Longitudinal momentum of the beam
beam_uz = 113.5
beam_uxth = 0.0086
beam_uyth = 0.0086
beam_uzth = 0.01*113.5
# Beam density
n_beam = 3.6e18
# Number of macroparticles per cell in each direction
beam_nx = 2*plasma_nx
beam_ny = 2*plasma_ny
beam_nz = 2*plasma_nz
# Positions between which the beam is initialized
# (Transversally, the plasma is initialized between -plasma_xmax and
# plasma_xmax, along x, and -plasma_ymax and plasma_ymax along y)
beam_zmin = -sqrt(2*pi)*960.e-6
beam_zmax = 0.
beam_xmax = 3*120.e-6
beam_ymax = 3*120.e-6

# Define your own profile and profile parameters below
beam_rmax = beam_xmax

def beam_dens_func(x, y, z):
    """
    User-defined function: density profile of the beam

    It should return the relative density with respect to n_beam,
    at the position x, y, z (i.e. return a number between 0 and 1)

    Parameters
```

ULSAN NATIONAL INSTITUTE OF SCIENCE AND TECHNOLOGY

```
    x, y, z: 1darrays of floats
        Arrays with one element per macroparticle
    Returns
-------------------------------------------------------------------------------------------------------------------------------
    n : 1d array of floats
        Array of relative density, with one element per macroparticles
    """
    # Allocate relative density

    sigz = 960.e-6
    sigr = 120.e-6

    n = ones_like(z)
    n = n*(1+cos(sqrt(pi/2)*(z/sigz)))
    r = sqrt(x**2 + y**2)
    n = n*exp(-r**2/(2*(sigr**2)))
    n[r > beam_rmax] = 0.

    return(n)

# -------------------------------------------------------------------------------------------------------------------------------
# Initialization of the simulation (Normal users should not modify this part.)
# -------------------------------------------------------------------------------------------------------------------------------

# Set some general options for warp
set_diagnostics( interactive )
set_boundary_conditions( f_boundz, f_boundxy, p_boundz, p_boundxy )
set_simulation_box( Nz, Nx, Ny, zmin, zmax, xmax, ymax, dim )
set_moving_window( use_moving_window, v_moving_window )

# See smoothing.py
set_smoothing_parameters( use_smooth, dim, npass_smooth,
                          alpha_smooth, stride_smooth )
# Creation of the species
elec = None
ions = None
elec_from_ions = None
beam = None
# Create the plasma species
# Reference weight for plasma species
```

ULSAN NATIONAL INSTITUTE OF SCIENCE AND TECHNOLOGY

```
plasma_weight = prepare_weights( n_plasma, plasma_nx, plasma_ny,
                                 plasma_nz, dim, circ_m )
if use_preexisting_electrons:
    elec_weight = rel_dens_preexisting_electrons * plasma_weight
    elec = Species(type=Electron, weight=elec_weight, name='electrons')
if use_ions:
    ions, elec_from_ions = initialize_ion_dict( ion_states, plasma_weight,
                                                group_elec_by_element=True )
# Create the beam
if use_beam:
    beam_weight = prepare_weights( n_beam, beam_nx, beam_ny,
                                   beam_nz, dim, circ_m )
    beam = Species(type=Proton, weight=beam_weight, name='beam')
# Set the numerical parameters only now: they affect the newly created species
set_numerics( depos_order, efetch, particle_pusher, dim)

# Setup the field solver object
em = initialize_em_solver( stencil, dim,
    npass_smooth, alpha_smooth, stride_smooth,
    circ_m = (dim =="circ")*circ_m )
registersolver(em)

# Introduce the laser
if use_laser==1:
    add_laser( em, dim, laser_a0, laser_w0, laser_ctau, laser_z0,
        zf=laser_zfoc, theta_pol=laser_polangle, source_z=laser_source_z,
        laser_file=laser_file, laser_file_energy=laser_file_energy )

# Introduce the beam
# Load the beam
if use_beam:
    PlasmaInjector( beam, None, w3d, top, dim, beam_nx, beam_ny, beam_nz,
                    beam_zmin, beam_zmax, beam_xmax, beam_ymax,
                    dens_func = beam_dens_func, uz_m=beam_uz, ux_th=beam_uxth,
                    uy_th=beam_uyth, uz_th=beam_uzth )
    initialize_beam_fields( em, dim, beam, w3d, top )


# Introduce the plasma
# Create an object to store the information about plasma injection
```

ULSAN NATIONAL INSTITUTE OF SCIENCE AND TECHNOLOGY

```
plasma_injector = PlasmaInjector( elec, ions, w3d, top, dim,
            plasma_nx, plasma_ny, plasma_nz, plasma_zmin,
            plasma_zmax, plasma_xmax, plasma_ymax, plasma_dens_func )
# Continuously inject the plasma, if the moving window is on
if use_moving_window :
    installuserinjection( plasma_injector.continuous_injection )

# Setup the diagnostics
remove_existing_directory( ['diags'] )
if write_fields == 1:
    diag1 = FieldDiagnostic( period=diag_period, top=top, w3d=w3d, em=em,
                    comm_world=comm_world, lparallel_output=parallel_output )
    installafterstep( diag1.write )
if write_particles == 1:
    diag2 = ParticleDiagnostic( period=diag_period, top=top, w3d=w3d,
                species={ species.name : species for species in listofallspecies },
                comm_world=comm_world, lparallel_output=parallel_output )
    installafterstep( diag2.write )

print('\nInitialization complete\n')

# ------------------------------------------------------------------------------------------------------------------------
# Simulation loop (Normal users should not modify this part either.)
# ------------------------------------------------------------------------------------------------------------------------

# Non-interactive mode
if interactive==0:
    n_stepped=0
    while n_stepped < N_steps:
        step(10)
        n_stepped = n_stepped + 10

    dump()
    printtimers()

# Interactive mode
elif interactive==1:
    print '<<< To execute n steps, type "step(n)" at the prompt >>>'
```

ULSAN NATIONAL INSTITUTE OF SCIENCE AND TECHNOLOGY

7. References

[1] A. Caldwell, K. Lotov, A. Pukhov, and F. Simon, “Proton-driven plasma-wakefield acceleration,” Nature Phys. 5, 363 (2009).

[2] E. Esarey, P. Sprangle, J. Krall, and A. Ting, “Overview of Plasma Accelerator Concepts,” IEEE Trans. Plasma Sci. 24, 252 (1996).

[3] P. Chen, J. M. Dawson, R. W. Huff, and T. Katsouleas, “Acceleration of electrons by the interaction of a bunched electron beam with a plasma,” Phys. Rev. Lett. 54, 693 (1985).

[4] R. D. Ruth, A. W. Chao, P. L. Morton, and P. B. Wilson, “A plasma wakefield accelerators,” Part. Accel. 17, 171 (1985).

[5] A. I. Akhiezer and R. V. Polovin, “Theory of Wave Motion of an Electron Plasma,” JETP 3, 696 (1956).

[6] J. B. Rosenzweig, “Nonlinear Plasma Dynamics in the Plasma Wakefield Accelerator,” IEEE Trans. Plasma Sci. PS-15. 186 (1987).

[7] W. Lu, C. Huan, M. M. Zhou, W. B. Mori, and T. Katsouleas, “Limits of linear plasma wakefield theory for electron or positron beams,” Phys. Plasmas 12, 063101 (2005).

[8] N. Kumar, A. Pukhov, and K. Lotov, “Self-Modulation Instability of a Long Proton Bunch in Plasmas,” Phys. Rev. Lett. 104, 255003 (2010).

[9] C. B. Schroeder, C. Benedetti, E. Esarey, F. J. Grüner, and W. P. Leemans, “Coupled beam hose and self-modulation instabilities in overdense plasma,” Phys. Rev. E. 86, 026402 (2012).

[10] C. B. Schroeder, C. Benedetti, E. Esarey, F. J. Grüner, and W. P. Leemans, “Growth and Phase velocity of Self-Modulated Beam-Driven Plasma Waves,” Phys. Rev. Lett. 107, 145002 (2011).

[11] J. Krall and G. Joyce, “Transverse equilibrium and stability of the primary beam in the plasma wake-field accelerator,” Phys. Plasmas 2, 1326 (1995).

[12] M. Reiser, “Theory and Design of Charged Particle Beams,” Wiley-VCH, second ed.

[13] Y. Fang, V. E. Yakimenko, M. Babzien, M. Fedurin, K. P. Kusche, R. Malone, J. Vieira, W. B. mori, and P. Muggli, “Seeding of Self-Modulation Instability of a Long Electron Bunch in a Plasma,” Phys. Rev. Lett. 112, 045001 (2014).

[14] G. B. Arfken, H. J. Weber, “MATHEMATICAL METHODS FOR PHYSICISTS,” Elsevier, sixth ed.

[15] R. Keinigs and M. E. Jones, “Two-dimensional dynamics of the plasma wakefield accelerator,” Phys. Fluids 30, 252 (1987).

[16] E. P. Lee and R. K. Cooper, “GENERAL ENVELOPE EQUATION FOR CYLINDRICALLY SYMMETRIC CHARGED-PARTICLE BEAMS,” Part. Accel. 7, 83 (1976).

[17] A. Friedman, R. H. Cohen, D. P. Grote, S. M. Lund, W. M. Sharp, J.-L. Vay, I. Haber, and R. A. Kishek, "Computational Methods in the Warp Code Framework for Kinetic Simulations of Particle Beams and Plasmas," IEEE Trans. Plasma Sci. 42, 1321 (2014).

[18] Yee, K. (1966), “Numerical solution of initial boundary value problems involving maxwell’s equations in isotropic media,” IEEE Trans. Antennas Propag. 14, 302 (1966).